INTERACTIONS BETWEEN AGING AND CHRONIC KIDNEY DISEASE ON THE

SKELETON

Samantha P. Tippen

Submitted to the faculty of the University Graduate School
in partial fulfillment of the requirements
for the degree
Doctor of Philosophy
in the Department of Anatomy and Cell Biology,
Indiana University

May 2023

Accepted by the Graduate Faculty of Indiana University, in partial
fulfillment of the requirements for the degree of Doctor of Philosophy.

Doctoral Committee

_____
Matthew R. Allen, PhD, Chair

_____
Kenneth E. White, PhD

March 20, 2023

_____
Sharon M. Moe, MD

_____
Joseph M. Wallace, PhD

DEDICATION

I would like to dedicate my dissertation to the Chickasaw Nation, one of the federally recognized Native American tribes headquartered in Ada, Oklahoma. My paternal grandmother was of Chickasaw descent, and while at a powwow, she was asked whether she had any grandchildren. As a result of this interaction, I was able to register with the Chickasaw Nation and receive funding through my entire educational journey while pursuing undergraduate, graduate, and doctoral degrees. As one of few Chickasaw students to pursue a PhD, I am very driven to represent and honor my Native American heritage through a long and successful career. This is the beginning of that career. Thank you all for your unwavering support.

ACKNOWLEDGEMENT

My educational journey has been quite a winding road, but I wouldn't change a single thing. Entering the IBMG program in the fall of 2018, I was then certain that I wanted to be a PI, but the experiences I have had over the last 5 years dramatically changed my career trajectory.

First, I want to thank my mentor, Dr. Matt Allen, for his continued support and guidance. I didn't realize the importance of having a kind and supportive mentor when I was doing my lab rotations, but I knew there was something special about your approach to mentoring and research when I met you. Over the years, I've seen you allow each of your mentees to pursue passions outside of the lab, and I am eternally grateful for that opportunity. Your willingness to allow me time to pursue teaching (to the point where 80-90% of my time is spent in scrubs or studying anatomical materials) gave me the knowledge and experience to have an amazing job lined up before I graduate. Even though my career plan is now different than when I started, the skills I have learned in the past years and the example you have set have been invaluable and will continue to influence me throughout my career. I am so grateful for the opportunity I had to work with you.

Second, I want to thank the rest of my committee. Dr. Sharon Moe – it has been such a pleasure being part of the greater collaborative research group at IUSM, which gave me the opportunity to gain wisdom from you and your team as well as a valuable clinical perspective for the duration of my PhD. Dr. Ken White – I will always remember how you clearly explained CRISPR to me during my IBMG interview, a time when teaching me something was not necessary, but you took the time to do I which I appreciated. Additionally, collaborating with you and your team was the first step in this series of studies. Dr. Joey Wallace – it's been such a privilege to work with your lab over these years and I especially appreciate the help from you and your team, which enabled us to generate novel data in these studies.

Third, I can't forget about the amazingly fun and often silly lab where I've spent the last five years. Although lab members have come and gone, one person has been constant during my entire journey. Corinne, I looked up to you from the beginning, with your easily ability to talk to

anyone who came in the door and the breadth of knowledge that you so easily speak about. But now, I see you like the sister I never had and can thank you for bringing sarcasm and Star Wars into my life. I'm so proud of both of our journeys and can't wait to see what comes next.

Fourth, I can't forget about several other faculty members that aren't on my committee but have played a major role in my life – Drs. Joe Bidwell, Jess Byram, & Margaret McNulty. Joe, being your student during my first semester and then transitioning to and staying your TA for four years has been a journey to say the least. Over that time, you've become my second dad (you will always be referred to as "Dad #2" in our family), even down to your struggles with technology and your take-no-BS attitude. Jess, you've been an example of the kind of educator I want to be – kind and understanding while creating an environment that allows everyone to feel comfortable. You've given me so many opportunities to teach and expand my knowledge and experience, and it's been a pleasure to work with you. I'm going to miss having a colleague who loves histology and embryology as much as you do. And Margaret, you were the first person that gave me an opportunity to teach in gross anatomy, and that experience changed my life as I found something that I loved to do and loved to teach. You've also been so supportive in offering me other opportunities and putting on your mentor hat when I needed it.

I can't forget to thank all the students that I've taught over the past three years. If I could keep you all with me so I had positive comments when I'm doubting myself, I totally would. I will always remember being told that it was clear that I would be an amazing teacher and I would be a great educator like Dr. Byram one day. I wish all of you the best on your career journeys – just know that each of you made a major impact on mine.

And last, I must thank my family. Moving 15 hours away from my parents, especially being an only child, was challenging but we made it work. Dad, thanks for always being a call away when I needed to make sure the mechanic wasn't taking advantage of me or when I wanted to check in on you after my grandmother developed dementia and passed away. Mom, thank you for always being my best friend, being open to hearing about my experimental struggles and the crazy things

Samantha P. Tippen

INTERACTIONS BETWEEN AGING AND CHRONIC KIDNEY DISEASE ON THE

SKELETON

In the US, 15% of adults have chronic kidney disease (CKD). While CKD occurs across all ages, the prevalence is highest in the aged, with ~40% of individuals over age 65 having some form of CKD. CKD and aging are each independently associated with higher fracture risk, and thus overlaying CKD in the aging population presents an additive fracture risk. Cortical porosity is a central tenet underlying skeletal fragility and occurs in CKD and aging. Previous research on cortical porosity has focused on preventing pore formation, while research on pore reversal (infilling) is lacking. Pore infilling is dependent on proper osteoblast function, and previous research has shown that infilling is possible in young mice. However, it is unclear whether infilling is possible in aging mice due to aging-associated osteoblast dysfunction. Therefore, we proposed that aging animals with CKD may require both suppression of CKD-induced elevations in parathyroid hormone (PTH) and anabolic therapy to infill cortical pores. Romosozumab, a humanized monoclonal sclerostin antibody, uses PTH-independent mechanisms to increase osteoblast activity, making it an attractive therapeutic for CKD. CKD was induced by feeding aging (78-week) male mice 0.2% adenine for six weeks followed by two weeks of maintenance on control diet for a total study duration of eight weeks of CKD; mice were then treated with calcium water, romosozumab, or the combination and their effectiveness in improving skeletal quantity and quality was evaluated. Romosozumab treatment was associated with higher trabecular bone volume, lower cortical porosity, and higher mechanical properties compared to control animals. Combination treatment also resulted in benefits to trabecular bone volume and mechanical properties. These results demonstrate that both romosozumab alone and when combined with PTH suppression can be effective at improving bone microarchitecture and mechanical properties in aged individuals with CKD who are at high risk of fracture.

Matthew R. Allen, PhD, Chair

Kenneth E. White, PhD

Sharon M. Moe, MD

Joseph M. Wallace, PhD

TABLE OF CONTENTS

LIST OF TABLES

LIST OF FIGURES

INTRODUCTION

Bone is an active structure that is continuously undergoing adaptation.

Bone is a highly dynamic organ that plays multiple roles:

1. The skeleton supports and protects the organs and allows for movement;

2. Bones are able to withstand mechanical loads and respond to and redirect stresses that are placed on the body;

3. The bone marrow supports hematopoiesis;

4. The cells found within the bone secrete factors key for paracrine and endocrine signaling, including sclerostin and FGF23; and

5. The bone provides a site for storage and release of key minerals, including calcium[1].

To maintain these roles, bone is organized into a complex structure, which plays a critical role in its mechanical function. Bone is divided into two primary compartments: an outer cortical shell and an inner region containing lattice-like trabecular bone interspersed with blood vessels and bone marrow (**Figure 1**). Trabecular bone is most often found in the metaphysis of long bones, vertebrae, ribs, and the iliac crest. Cortical bone is the primary component of the diaphysis of long bones and thus is primarily responsible for the mechanical properties of the bone.
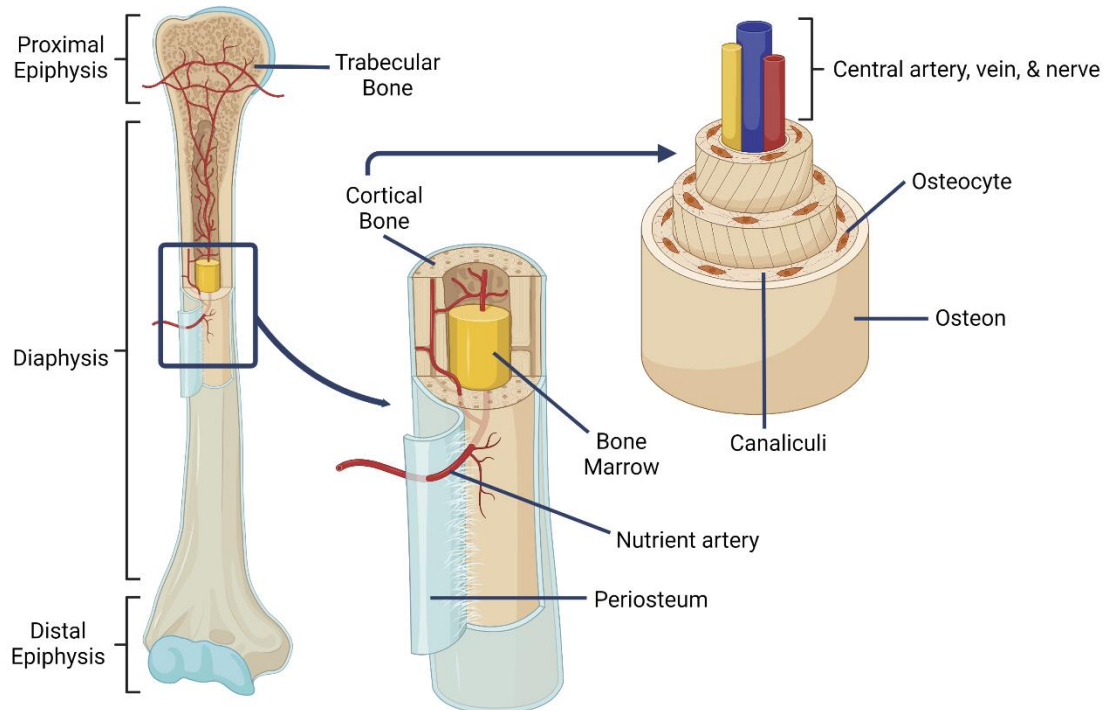
Figure 1: General structure of bone.

The skeleton is constantly regenerating itself, which means that each of us has a completely new skeleton about every 10 years. Although bones are initially formed through a process known as modeling, renewal occurs through another process known as remodeling. Bone remodeling involves a coupling of osteoblast and osteoclast activity on a given surface. Specifically, there is sequential osteoclast-mediated bone resorption followed by osteoblast-mediated bone formation on the same surface[2]. This process allows for the regeneration of the skeleton as a whole but is also responsible for repairing local defects, such as areas of microdamage or sites with apoptotic osteocytes. A variety of disease states cause alterations to the bone remodeling cycle by impacting the activity of osteoblasts and/or osteoclasts, resulting in net gain or loss of bone.

Declines in bone mass are associated with multiple factors.

Rapid bone growth occurs during the first two decades of life with peak bone mass being reached during the third decade[3] (**Figure 2**). In both men and women, increasing age is associated with a steady rate of bone loss shortly after reaching peak bone mass. Additionally in women, loss of estrogen during menopause accelerates bone loss, thereby producing a sharper decline in bone mass.
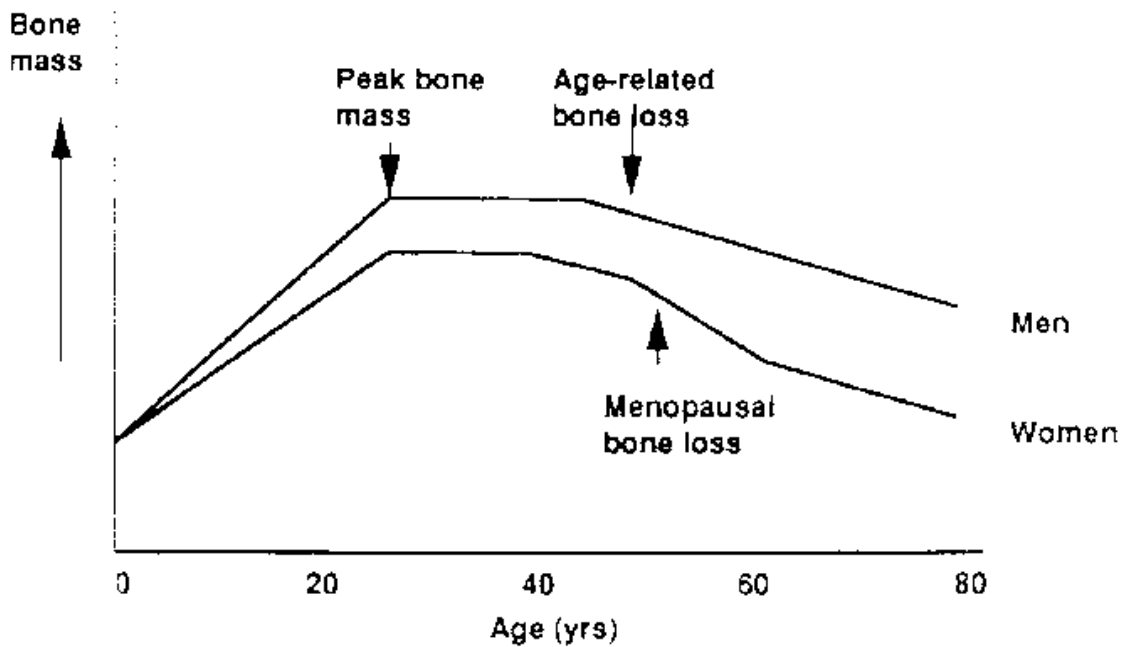
Figure 2: Peak bone mass is reached during the third decade of life, and bone mass begins to decline during the fourth and fifth decades. Two factors that contribute to loss of bone mass include age and menopause[3].

Most often, bone mass is evaluated clinically utilizing dual energy x-ray absorptiometry (DEXA), a method that determines the amount of mineralized tissue relative to the projection area (i.e., femoral neck, lumbar spine); to determine whether an individual has normal bone mass, osteopenia (low bone mass), or osteoporosis, the individual's bone mineral density (BMD) is compared to that of a young adult female[4]. Low bone mass is characterized as the BMD at either the femoral neck

or lumbar spine or both being between 1 and 2.5SD below the mean BMD of a young adult female, while osteoporosis is characterized as a BMD that is 2.5SD below the mean BMD of a young adult female[5,6]. Low bone mass predisposes individuals to osteoporosis and increases risk of fracture. In 2018, the prevalence of low bone mass at either the femoral neck or lumbar spine was 43.1%, while the prevalence of osteoporosis at either site was 12.6%[7].

Increasing age is associated with reduced efficiency of osteoblasts, which leads to less bone formation overall. Because the remodeling cycle involves coupling of bone resorption and formation, the osteoblasts rarely bring the bone surface of a remodeling unit back to the starting point, meaning that there is a net deficit of bone following each remodeling cycle[8]. This is the reason for declines in bone mass with age, which may eventually lead to osteoporosis. In addition to low bone mass, osteoporosis is characterized by deterioration of bone microarchitecture and fragility fractures. Alterations to bone remodeling result in changes to both the trabecular and cortical bone: there is thinning and loss of connectivity between trabeculae and thinning and porosity within cortical bone[8].

Aging is commonly associated with osteoporosis, which is recognized as the most common skeletal disorder in the world.

The National Osteoporosis Foundation has estimated that 10.2 million Americans have osteoporosis, and an additional 43.4 million Americans suffer from low bone mass[9]. From 2007 to 2018, the age-adjusted prevalence of osteoporosis in women increased from 14% to 20%[7]. It is also estimated that, by 2030, 71 million Americans will suffer from low bone mass or osteoporosis[9]. Fifty percent of women and 20% of men over the age of 50 are likely to experience an osteoporosis-related fracture[10]. It is believed that osteoporosis is underdiagnosed and thus undertreated in individuals over the age of 75, a population with the potential to greatly benefit from treatment. Additionally, our society is living longer, meaning that the number of people living with

osteoporosis will exponentially increase over the next several decades. These factors underlie the critical importance of managing and ideally preventing skeletal fractures.

Declines in bone properties are common in the aging population.

Changes in multiple factors including mineral metabolism and sex steroid deficiency cause reductions in bone mass due to age[11,12]. Bone loss occurs due to a reduction in osteoblast-mediated bone formation and an increase in osteoclast-mediated bone resorption. Additionally, there is also a loss in lacunar density, which means there is decreased communication with canaliculi and therefore decreased ability to sense mechanical loads[13]. The reduction in bone mass and increased brittleness of the tissue each contribute to a significantly elevated fracture risk[14,15]. The risk of hip fracture rises 1000-fold for people over 60 years of age compared to younger individuals[16]. Adding to the significance of the problem is that aged individuals are more than 70% more likely to die from fracture-related complications compared to those of younger age[17,18]. Bone fragility in the aging population significantly contributes to morbidity and mortality.

It is well established that aging is associated with altered bone remodeling and loss of trabecular microarchitecture, but aging is also associated with defective repair of microdamage and poor intrinsic material bone properties are also observed[19]. Declines in bone mass, density, and microarchitecture only explain approximately 75% of the fracture risk, and new research has shown that the remaining 25% could be, at least partially, explained by changes in bone hydration[20]. Bone water is found in four functional compartments – free water, loosely bound water, tightly bound water, and structural water – that can be viewed overall as total bone water. Bound water is critical for maintenance of bone toughness and strength, and decreases in bound water and toughness have been observed in aging specimens. Elderly cadaveric specimens had ~40% lower bound water compared to young specimens, which explained approximately 70% of the decrease in bone toughness between ages[21]. Additionally, 20-month-old BALB-c mice exhibited decreased bound

water, femoral toughness, and fracture toughness compared to six-month-old mice[22]. Taken together, aging causes a wide variety of changes in bone properties, including decreased structural and material properties and decreased bone hydration.

Aging individuals are at high risk of developing chronic kidney disease, which itself increases the risk of fracture and fracture-related mortality.

Nearly 40% of individuals in the United States over the age of 65 have some form of chronic kidney disease (CKD)[23]. CKD is a disease of progressive renal decline that often results in a triad of symptoms known as chronic kidney disease – mineral bone disorder (CKD-MBD): biochemical abnormalities (including changes in calcium, phosphorus, and parathyroid hormone), vascular calcifications, and bone deterioration (**Figure 3**)[24]. As CKD progresses and renal function continues to decline, patients proceed through five stages, with symptoms normally appearing during stage 3. Stage 5 CKD represents end-stage renal disease (ESRD) where dialysis is required.
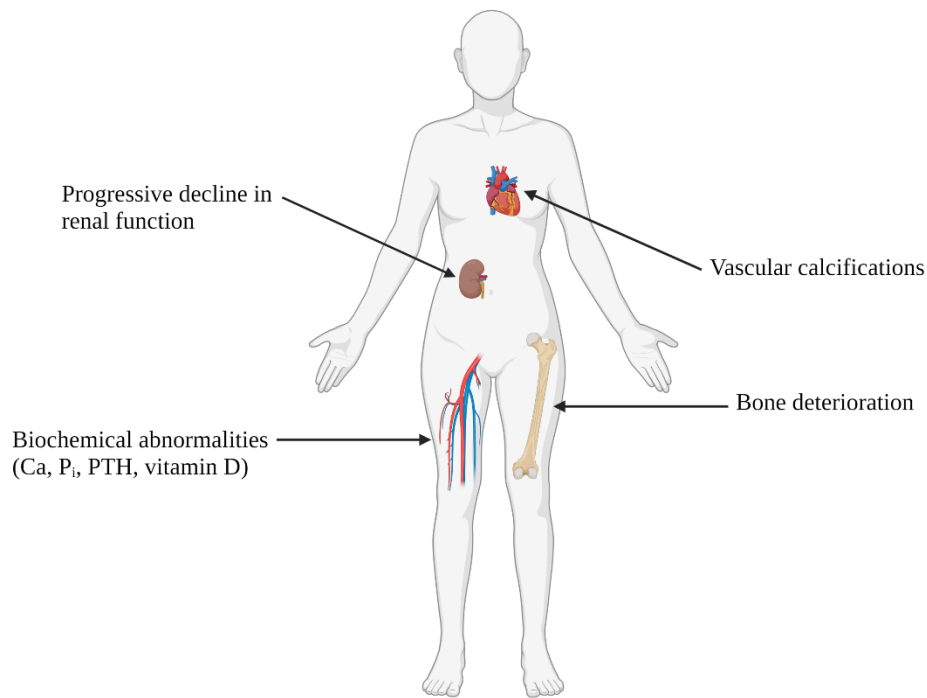
Figure 3: Consequences of disturbed mineral metabolism associated with CKD.

CKD, independent of aging, increases the risk of fracture. The rate of hip fracture is four times higher in end-stage CKD than the age-matched general population[25,26] (**Figure 4**). In the setting of dialysis, hip fracture rates are as much as 13 times higher than in the age-matched general population[27,28]. Fractures in CKD patients lead to longer hospitalization, higher costs, and higher mortality rates than patients without CKD who fracture[29]. The skeletal consequences of CKD are devastating and appear to interact with aging to further compound the issue[30].
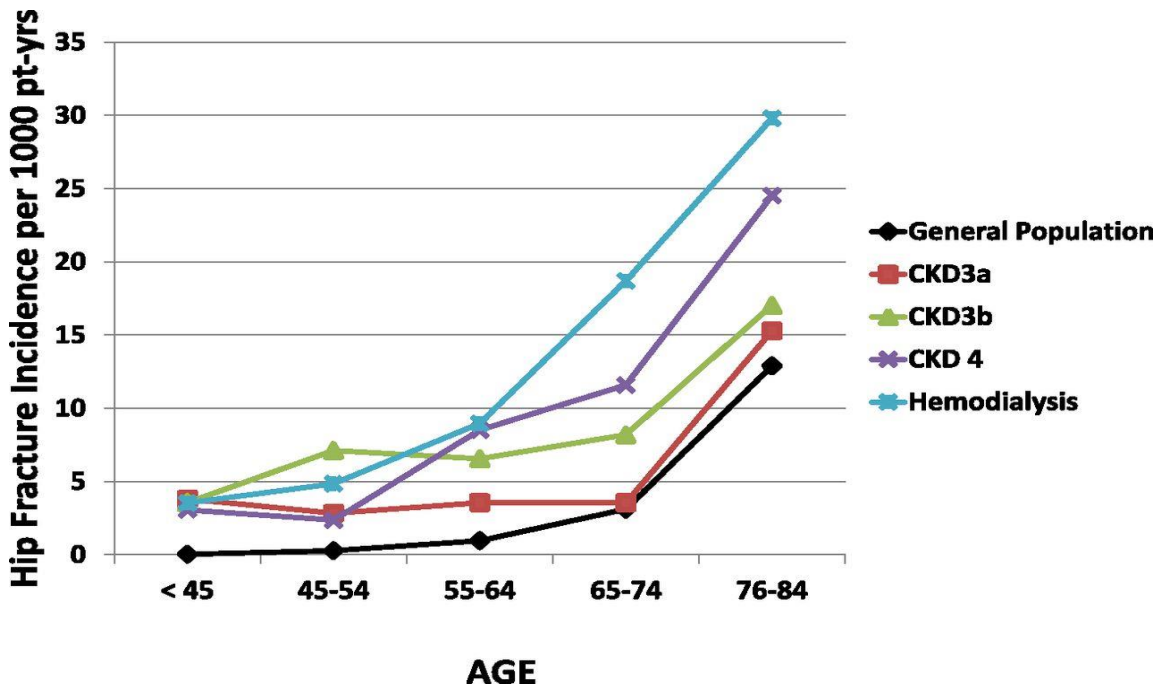
Figure 4: Across ages, the risk of fracture is higher in patients with CKD compared to the general population. A person with CKD at age 45 has the same risk as a non-CKD person at 65, while a person aged 65+ with CKD has a fracture risk 3-4 times higher than the general population[31].

Because CKD and aging are often comorbid diseases, it is often challenging to study them separately. Most studies focus on either disease alone rather than using a combination model. Realistically, it makes the most sense to study these two diseases together due to the high incidence of CKD in aging patients. However, no clinical trials and very few animal studies have looked at the intersection of aging and CKD. Data from the ARCH and FRAME studies, both focused on understanding and treating fractures in osteoporosis, have been utilized to look at the efficacy of pharmaceuticals in patients with differing kidney function. This type of analysis is helpful in determining the safety of these drugs in populations with declining kidney function, such as patients with CKD. However, more research is necessary before these pharmaceuticals could be standard in a clinical setting.

Bone loss in CKD is largely driven by cortical porosity, which can be recapitulated in various pre-clinical models.

Bone loss in CKD primarily impacts cortical bone (**Figure 5**), the bone that is most responsible for the mechanical properties of bone[32]. Cortical porosity also occurs with aging, although to a lesser degree than is typically noted in CKD. Numerous studies have demonstrated that cortical porosity is a central tenet that underlies the skeletal fragility found in CKD[33–37].
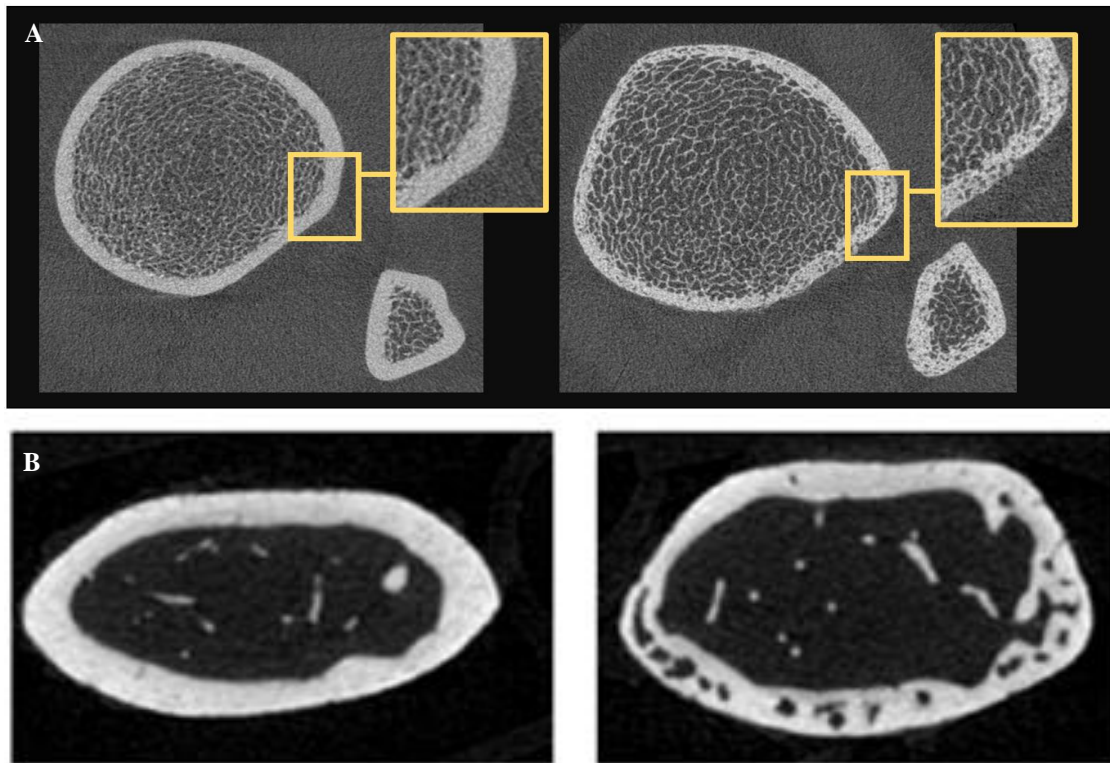
Figure 5: CKD-induced cortical porosity from (A) human HR-pQCT scans of the tibia and fibula (healthy on left, CKD on right) and (B) mouse adenine model (control on left, CKD on right).

With progression of CKD, the level of cortical porosity increases as does fracture risk[33,34,38,39]. Studies focused on assessing the molecular/cellular/tissue mechanisms underlying cortical porosity in CKD have employed various animal models. The adenine-induced nephropathy model utilizes oral dosing of adenine, which leads to crystal formation in the kidneys, causing decreased kidney function, hyperparathyroidism, and cortical porosity (**Figure 5**), all of which are hallmarks of

clinical CKD[40]. Other CKD models, such as 5/6 nephrectomy, produce an immediate loss of kidney function, while the adenine model, when given in lower doses over an extended period of time, produces a progressive loss of kidney function that is more characteristic of human CKD. Additionally, the progressive Cy/+ animal model, while useful for studying CKD, has limitations for assessing the aging-CKD interaction due to severe disease development prior to reaching old age[41].

Cortical porosity is associated with elevated parathyroid hormone.

Initiation of cortical porosity development requires recruitment of osteoclasts to begin resorbing bone[40]. Increased resorption has been hypothesized to be related to CKD-induced secondary hyperparathyroidism as PTH directly stimulates receptor activator of nuclear factor kappa-B ligand (RANKL) production, a key osteoclastogenesis regulator[42,43]. To date, most preclinical studies have focused on preventing cortical porosity development primarily through mechanisms that suppress PTH[44–48]. The current work focuses on a different paradigm, reversal (infilling) of cortical porosity (**Figure 6**).
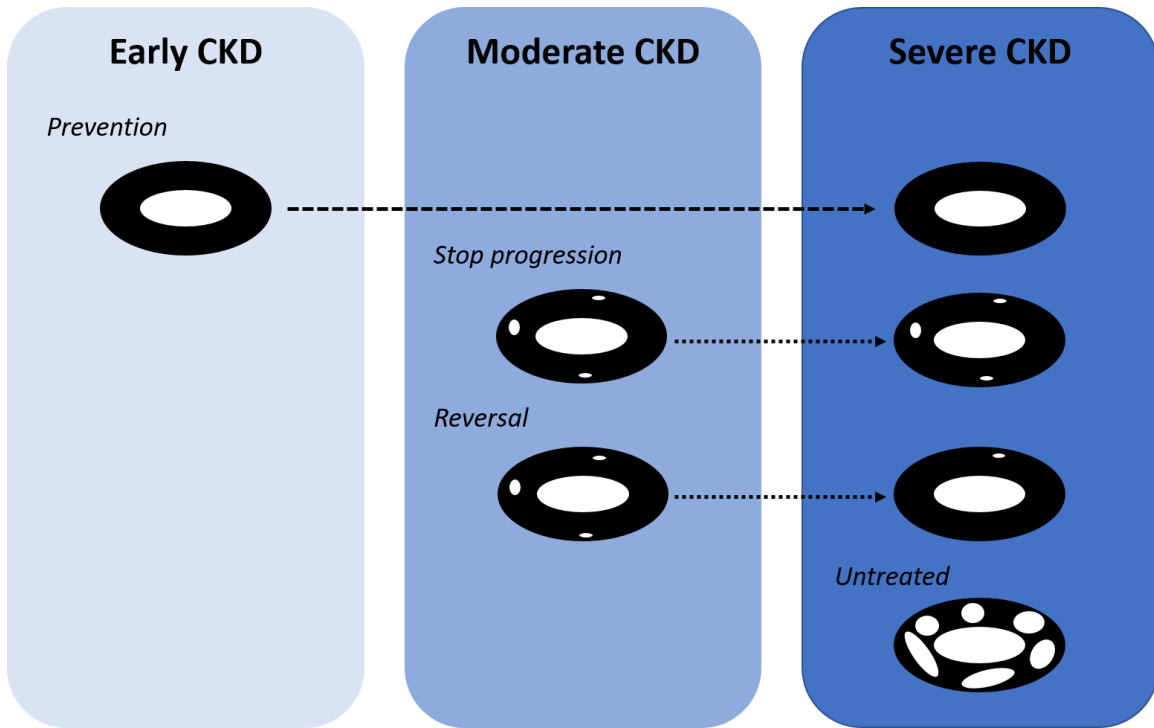
Figure 6: Schematic of timing and treatment goals for cortical porosity in CKD.

Previously, our lab has shown that cortical porosity can be reduced in skeletally mature animals through potent PTH suppression with calcium water supplementation (**Figure 7**); these data illustrate that, in skeletally mature animals, filling of cortical pores is possible. A key focus of this work is to explore the potential of combination treatment to not only suppress new pores from forming (through suppression of PTH) but also infill existing pores (through stimulation of anabolic bone formation).
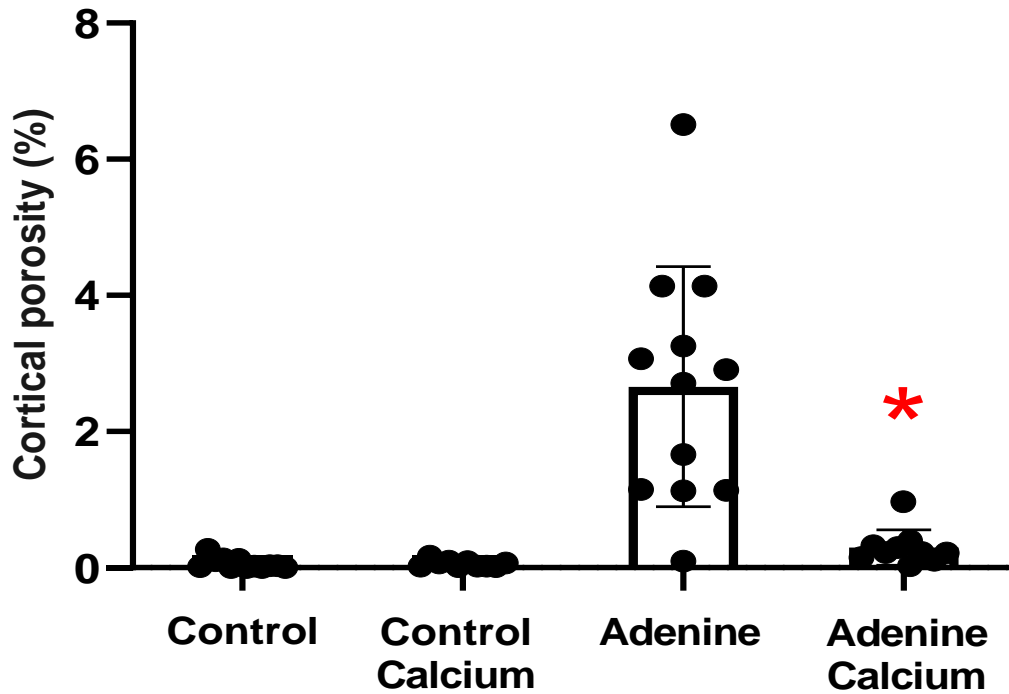
Figure 7: Cortical porosity is reversed in the young adenine model of CKD. Male mice were fed either control or adenine diet for six weeks at which time they were supplemented with calcium water (n=8-10/group). *p<0.05 compared to adenine controls.

Treatment of CKD-related bone deterioration is challenging.

The bone-related consequences of CKD can include "abnormalities in bone turnover, mineralization, volume, linear growth, or strength" as defined by KDIGO[49]. Because hyperparathyroidism is a strong driver of the observed bone deficits, most treatment options are aimed at reducing PTH levels. As a result, physicians use common markers of disordered mineral metabolism, such as calcium, phosphate, PTH, and 25-hydroxyvitamin D, to define potential treatment regimens. Patients with early-stage CKD can be given phosphate binders or calcimimetics, such as cinacalcet, to control and prevent worsening of the disease[50]. Cinacalcet was found to reduce clinical fracture risk in patients on hemodialysis (stage 5 CKD) as compared to placebo, with aging patients at a higher risk of fracture than young patients[51]. More recently, iron-

based phosphate binders, such as ferric citrate, have been effective at lowering serum phosphate in CKD patients[52].

During early-stage CKD, increased fracture risk is treated in an identical manner to those patients with osteoporosis; however, once a patient moves into later stages, there is a large spectrum of bone phenotypes, which makes identifying generalized therapeutic options difficult[53]. One commonly used approved anabolic bone therapy, teriparatide, utilizes intermittent PTH. Teriparatide has been shown to increase bone mineral density, reduce vertebral and non-vertebral fractures, and improve quality of life (through reductions in back pain) in an aging population[54]. However, in patients where PTH is already high, this treatment regimen could be detrimental, and thus administration of teriparatide to late-stage CKD patients should be approached with caution. Denosumab, another clinically approved bone therapeutic, is a monoclonal antibody that targets RANKL and thus inhibits osteoclast-mediated bone resorption. Denosumab is currently used as an osteoporosis therapy, but its efficacy in patients with low kidney function was previously unknown. Evaluation of data from the FREEDOM study (osteoporotic women aged 60-90 years) showed that patients had consistent gains in BMD and low incidence of fractures regardless of kidney function[55]. Another class of osteoporosis therapies, anti-resorptive bisphosphonates, are contraindicated in patients with reduced renal function[56]. Post-hoc analyses of the CPRD and SIDIAP cohorts (CKD stage 3b-5) have shown that bisphosphonate use is associated with a moderate risk of CKD progression compared to non-users, with 1 in every 10 patients experiencing progression[57]. Thus, more clinical trials for later-stage CKD-related bone loss are still needed.

Romosozumab is an enticing pharmaceutical option for treatment of CKD-related bone deterioration in aging patients.

Due to reduced bone formation during aging, we propose that treatment with an anabolic agent may be needed to infill cortical pores when CKD is overlaid on aging biology. Romosozumab, a

humanized monoclonal sclerostin antibody that was approved for use in osteoporosis in 2019[58], uses PTH-independent mechanisms to increase osteoblast activity, making it an attractive therapeutic for CKD. The Wnt pathway was first characterized in the 1980s but its role in bone formation and regeneration was not a focus until much later. In bone, Wnt ligands (Wnts) interact with proteins, such as Lrp5/6 and Frizzled, to upregulate bone formation[59]. After studying diseases resulting in excessive bone formation such as van Buchem disease, researchers found that inhibition of sclerostin caused excessive bone formation, leading to the thought that sclerostin could be a potential therapeutic target for disorders of low bone mass. Sclerostin is an osteocyte-derived protein that acts as an inhibitor of osteoblast-derived bone formation[60]; therefore, romosozumab increases bone formation by removing the inhibitory effect of sclerostin. Phase I clinical trials utilizing romosozumab have shown stimulation of bone formation and inhibition of bone resorption in healthy men and postmenopausal women[61]. Phase II clinical trials demonstrated that postmenopausal women treated with romosozumab had larger gains in bone mineral density than treatment with alendronate, an anti-resorptive bisphosphonate, or teriparatide[60]. Phase III clinical trials in men with osteoporosis showed increased bone mineral density after 1-year of treatment with romosozumab, indicating that romosozumab is an effective osteoporosis treatment in both men and women[62].

Patients with low kidney function are often excluded from osteoporosis clinical trials. However, researchers have performed post-hoc analyses on the ARCH and FRAME studies to assess the efficacy of romosozumab across mild and moderate levels of decreased renal function. Patients across all levels of renal function were found to have increased bone mineral density and lower risk of vertebral fractures, both of which are promising for aging, CKD patients (**Figure 8**)[58].
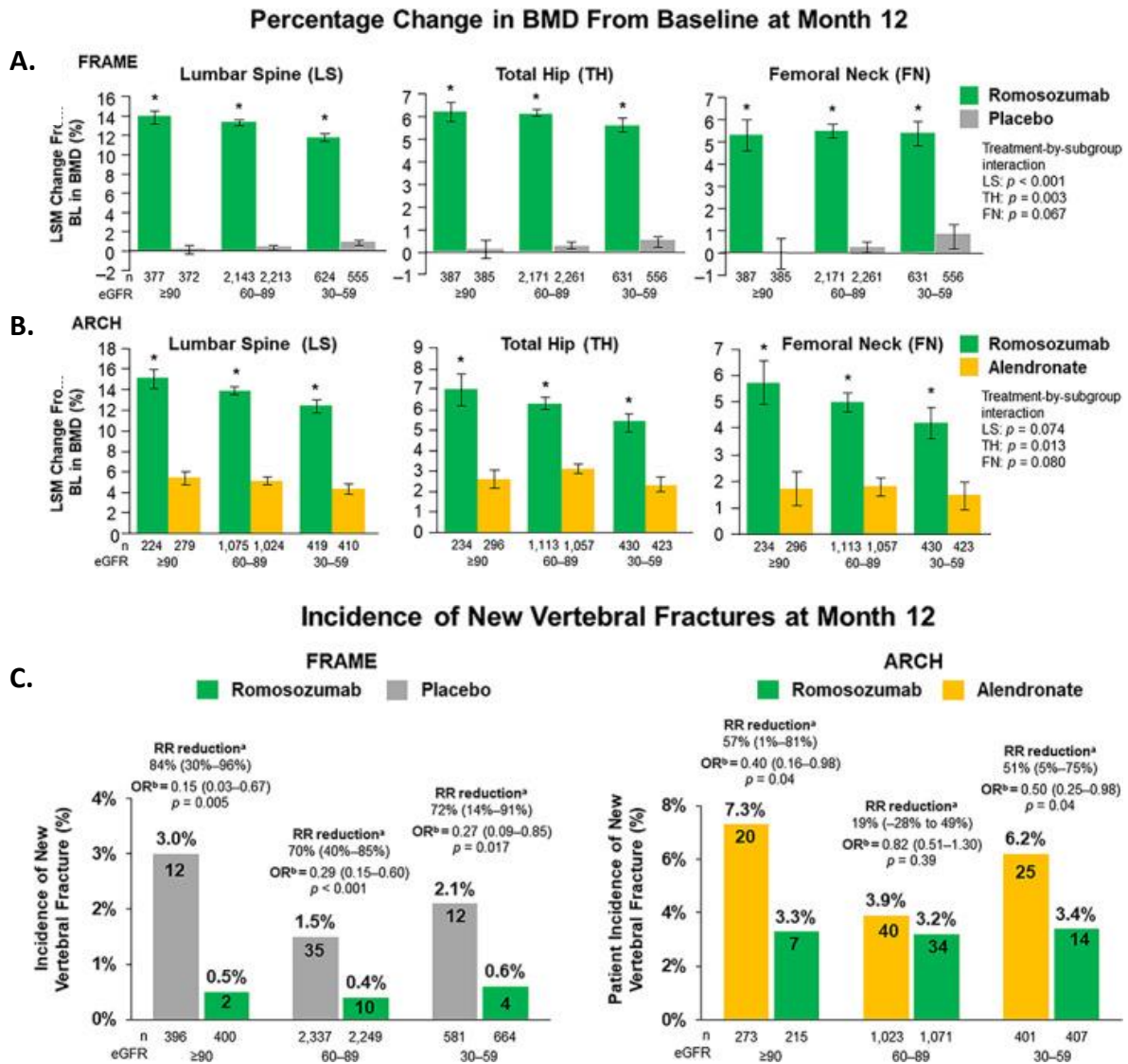
Figure 8: Romosozumab treatment improved bone mineral density (BMD) and reduced incidence of vertebral fractures across mild and moderate levels of decreased kidney function in the ARCH and FRAME studies[58].

The clinical significance of this dissertation work – exploring the interaction of aging and CKD.

While CKD occurs in patients of all ages, the prevalence is highest in aging individuals, with nearly 40% of those over age 65 having some form of CKD[23]. Independent of CKD, the aging population has decreased bone density and increased risk of fracture[63,64], meaning that overlaying CKD in the aging population presents an additive fracture risk[31]. However, little research has focused on the

15

interaction between aging and CKD and the effects on the skeleton. Due to prevalent secondary hyperparathyroidism in CKD, we previously demonstrated that calcium supplementation through calcium water is an effective method of reducing parathyroid hormone in the adenine-induced CKD mouse model[65]. Additionally, aging individuals have decreased osteoblast function alluding to the potential need to increase osteoblastic activity with a therapeutic like romosozumab to improve bone in this population. It is unknown whether a combination therapy including PTH suppression and anabolic therapy could represent a potential treatment option for aging CKD patients. **Based on this, and the above established scientific premise, the goal of the present series of studies was to test the hypothesis that preventing the deterioration of cortical bone, through the management of hyperparathyroidism and utilization of anabolic therapy, could mitigate cortical porosity and improve bone mechanical properties in aging CKD.**

CHAPTER 2

AGE AND SEX EFFECTS ON FGF23-MEDIATED RESPONSE TO MILD PHOSPHATE

CHALLENGE

2.1 Introduction

Control of phosphorus homeostasis is mediated by the actions of the osteocyte-produced hormone Fibroblast growth factor-23 (FGF23). FGF23 acts in concert with its co-receptor, Klotho (KL), and fibroblast growth factor receptors (FGFRs), which form a heteromeric signaling complex[66]. Circulating concentrations of phosphorus are regulated through altering reabsorption by the kidneys[67–69]. FGF23 acts in the kidney to downregulate the sodium-dependent phosphate transporters (NPT2a and NPT2c) to reduce phosphate reabsorption[70,71]. In parallel, FGF23 reduces the expression of the anabolic vitamin-D metabolizing enzyme 25-OH vitamin D 1α-hydroxylase and upregulates the catabolic 1,25-OH vitamin D 24-hydroxylase to lower circulating $1,25(OH)_2$ vitamin D (1,25D)[72].

As people age, a variety of physiological changes occur, including reduced cardiac function, muscle wasting, bone loss, and cognitive impairment. Many of these features have been recapitulated in $Fgf23^{-/-}$ and $Kl^{-/-}$ mice with premature aging phenotypes that are associated with the perturbation of phosphate homeostasis, causing hyperphosphatemia[73]. Studies have established that FGF23 levels increase while KL may decrease with age[74–77]. However, little is known about whether cellular mechanisms differ between young and old individuals and whether mild phosphate challenges induced through the consumption of a Western diet (higher than normal phosphate) further alter mineral metabolism.

Around age 45, females begin to maintain higher basal phosphate and FGF23 levels compared to males, which persists into old age[78]. Limited studies have focused on the mechanisms underlying these age-related sex effects. Given that the divergence in phosphate/FGF23 response between males and females is around the time of menopause, a role of estrogen seems likely. Indeed,

estrogen depletion results in increased reabsorption and thus higher systemic phosphate levels, and estrogen is associated with increased FGF23 and KL *in vivo*[79–81]. Further, women receiving estrogen therapy had lower phosphate levels compared to untreated women but comparable levels to age-matched men[82], suggesting a role of estrogen in this bone-kidney regulatory axis.

Chronic elevations of FGF23 lead to several adverse physiological changes including increased risk of fracture and cardiovascular disease, both associated with higher mortality[74,83]. For example, patients with CKD undergoing dialysis are at 4-13 times higher risk of hip fractures than the general population, and elevated FGF23 is associated with six-fold higher odds for death in this patient population[27,28]. How conditions with which chronic elevations in FGF23 are impacted by sex and age is not fully understood, however.

The aim of the present study was to test the hypothesis that advanced age leads to divergent effects with respect to sex on FGF23, its regulatory pathways, and bone in response to a phosphate challenge, which may mimic what occurs in the elderly population.

2.2 Materials & Methods

2.2.1 *Animal Studies*: Animal studies were approved by and performed according to the Institutional Animal Care and Use Committee (IACUC) at the Indiana University School of Medicine and comply with the NIH guidelines for the use of animals in research. Sixteen- and seventy-eight-week-old C57BL/6 wild-type male and female mice (n=6-8/age/sex) were purchased (JAX stock #000664, Bar Harbor, ME, USA) and acclimated prior to all studies. After one-week acclimatization to our facility, mice were placed on either a standard grain-based rodent diet (0.7% total phosphate and 0.4% non-phytate phosphorus, 2018SX, Harlan Teklad = Ch) or a casein-based rodent diet[84] (0.9% highly bioavailable phosphate and 0.6% calcium, TD.150303 Envigo; Madison, WI = Ca) for eight weeks (group sizes of 6-8). Diets and water were provided ad libitum throughout the study. Blood samples were collected from mice by facial vein bleed at days 0, 14, 28, and

42 of the study. Mice were euthanized by CO_2 inhalation followed by cervical dislocation, and blood was collected via cardiac puncture for endpoint serum and plasma biochemistries.

2.2.2 *Serum Biochemistries*: Routine serum biochemistries were tested by the Core facility of the Clinical and Translational Sciences Institute (CTSI) of the Indiana University School of Medicine using an automated COBAS MIRA Plus Chemistry Analyzer (Roche Diagnostics; Indianapolis, IN). Serum iFGF23, cFGF23, intact PTH, and 17β-estradiol concentrations were assessed using commercial ELISAs for mouse/rat (Quidel, Inc.; San Diego, CA and Abcam; Cambridge, UK).

2.2.3 *RNA Preparation and Quantitative RT-PCR (qPCR)*: Kidney, liver, bone, and flushed bone marrow from long bones were harvested and homogenized in 1mL of Trizol reagent (Invitrogen/Life Technologies, Inc.; Grand Island, NY) according to the manufacturer's protocol using a Bullet Blender (Next Advance, Inc.; Troy, NY), then further purified using the RNeasy Kit (Qiagen, Inc.; Germantown, MD). RNA samples were tested with intron-spanning primers (Applied Biosystems/Life Technologies, Inc.; Grand Island, NY) specific for fibroblast growth factor 23 (Fgf23), klotho, vitamin D 24-hydroxylase (Cyp24a1), 1α-hydroxylase (Cyp27b1), IL-1β, IL-6, TNFα, estrogen receptor α (Esr1), estrogen receptor β (Esr2), and androgen receptor (AR) mRNAs (primers were purchased as pre-optimized reagents (Applied Biosystems/Life Technologies, Inc.; Grand Island, NY); mouse actin was used as an internal control (IDT, Coralville, IA). The Taqman One-Step RT-PCR kit was used to perform qPCR. PCR conditions for all experiments were: 30min 48˚C, 10min 95˚C, followed by 40 cycles of 15s 95˚C and 1min 60˚C. The data were collected and analyzed by a StepOne Plus system (Applied Biosystems/Life Technologies, Inc.; Grand

Island, NY). The expression levels of mRNA were calculated relative to the appropriate controls, and the $2^{-\Delta\Delta CT}$ method was used to analyze the data[85].

2.2.4   *Aortic Calcification Assay*: Segments of the aortic arch were isolated and incubated in 0.6N HCl for 48h, the supernatant was analyzed for calcium using the o-cresolphthalein complex 1 method (Pointe Scientific, Canton, MI), and the data was normalized by tissue dry weight as previously described[86].

2.2.5   *Bone Microarchitecture*: The distal third of the femur was scanned using the Skyscan 1172 μCT (Bruker, Billerica, MA) using an isotropic voxel size of 8μm. Trabecular parameters were obtained by taking a 1mm sized region of interest (ROI) just proximal to the distal growth plate. Trabecular bone volume per tissue volume (BV/TV), trabecular thickness (Tb.Th), trabecular separation (Tb.Sp), and trabecular number (Tb.N) were measured. Cortical parameters (porosity and thickness, Ct.Th) were obtained as the average of five consecutive slices from a region located ~2mm proximal to the most proximal region of the trabecular bone ROI. All analyses and nomenclature were in accordance with recommended protocols[87].

2.2.6   *Bone Mechanics*: Tibial midshafts were scanned using the Skyscan 1176 μCT (Bruker, Billerica, MA) using an isotropic voxel size of 9μm. The total length and the medial-lateral diameter were measured with calipers. Bones were thawed and hydrated with saline, and tibiae were tested by four-point bending (ElectroForce, New Castle, DE) with the medial and lateral surfaces in compression and tension, respectively. Testing was carried out at a displacement rate of 0.025mm/sec. After the samples were tested until failure, the length of the distal fragment was measured to determine the site of fracture for later use in geometric calculations to determine material-level mechanical properties. A custom

MATLAB code was used to generate geometric information, and a second MATLAB code was used for data collection[88]. Structural parameters include ultimate force, stiffness, displacement, and work; material parameters include stress, strain, modulus, and toughness. These properties were estimated using standardized equations that convert force and displacement into stress and strain, respectively, by accounting for bone geometry[89]. All mechanical parameters are presented using standard nomenclature[90].

2.2.7 *In Vitro Studies*: MPC2 (mesenchymal stem cells that can be induced to osteocytes) cells were cultured in complete media (α-MEM supplemented with 10% FBS, 25mM L-glutamine, and 25mM penicillin/streptomycin) at 33˚C until 80% confluent[91]. The cells were then transferred to osteogenic media (complete media supplemented with 4mM beta-glycerophosphate and 50µg/mL ascorbic acid) and differentiated at 37˚C for 3 or 3.5 weeks. Cells were treated with either 0.01mM or 0.1mM estradiol (doses according to[80,92]) (Sigma-Aldrich, Burlington, MA) for 24h with and without 10nM $1,25(OH)_2D$ (Millipore Sigma, Cleveland, OH) for 24h. The cells were then harvested for RNA using the RNeasy Kit (Qiagen, Inc.; Germantown, MD) according to the manufacturer's protocol for cells.

2.2.8 *Statistical Analysis*: Murine data were analyzed as a 2x2 factorial ANOVA (diet-by-age) with main effects of diet, age, and diet-by-age interactions noted as well as effect sizes (ES); male and female data were analyzed separately. Effect sizes were used to compare and quantify the difference between males and females for respective categories. If the model 2x2 ANOVA was statistically significant ($p<0.05$), an all-groups Duncan post-hoc analysis was applied to determine differences between groups. Intact FGF23 analysis was performed by repeated measures ANOVA followed by a Tukey post-hoc test. In vitro data was analyzed as a one-way ANOVA; if the ANOVA was statistically significant ($p<0.05$), a Dunnett post-hoc analysis was applied to determine differences between vehicle and each

respective group (SPSS Statistics 25, IBM, Armonk NY, USA). All data are presented as mean ± standard deviation (SD).

2.3 Results

2.3.1 *Under phosphate challenge, aging mice maintain normal biochemical regulation*

To assess the influence of dietary phosphate, young and aging male and female mice were placed on either a control (chow) or a casein-based diet that has higher phosphate bioavailability and thus mimics higher phosphate intake. At the end of the study, neither female nor male mice had differences in serum phosphate when assessed by age (young vs. old) and diet (chow vs. casein) (2x2 ANOVA p=0.177 and p=0.207, respectively, **Figure 9A**). For both sexes, the age/diet effects for serum calcium and creatinine were not different (**Table 1**), suggesting minimal changes in kidney function in the aging mice despite additional phosphate load.
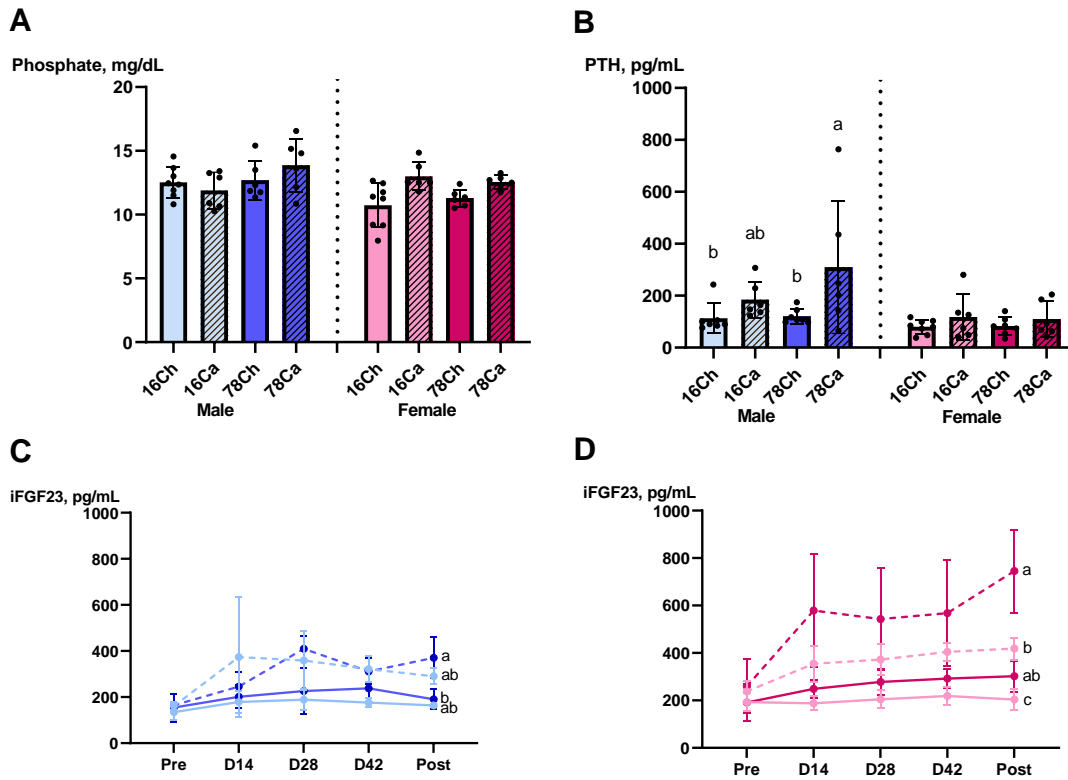
Figure 9: Measures of chronic kidney disease (phosphate and parathyroid hormone (PTH), and intact FGF23 (iFGF23). **a** Serum phosphate was not statistically different in male or female mice (p=0.177 and p=0.207, respectively). **b** PTH was elevated in older, male animals on casein diet as compared to those on the chow diet (diet p=0.019, ES=0.226) but there was no difference in female mice (p=0.541). **c** iFGF23 in male mice was elevated in aging animals and further elevated in those on casein diet (diet p=0.014, ES=0.265). **d** iFGF23 in female mice was higher overall as compared to male mice, with older animals on casein diet having the highest levels (diet p<0.0001, ES=0.788; age p<0.0001, ES=0.599; interaction p=0.004, ES=0.309). Group sizes of 6-8. Data plotted as mean and standard deviation with point plots representing individual animal data. Bars not sharing the same letter are statistically different.

Table 1: Biochemical parameters.

	Male				Female			
	16Ch (n=8)	**16Ca (n=6)**	**78Ch (n=6)**	**78Ca (n=6)**	**16Ch (n=8)**	**16Ca (n=6)**	**78Ch (n=7)**	**78Ca (n=6)**
Phosphate (mg/dL)	12.53±1.2	11.89±1.44	12.69±1.52	13.85±2.09	10.73±1.73	12.99±1.11	12.53±3.35	12.55±0.52
Calcium (mg/dL)	13.27±1.2	12.96±0.92	13.13±1.28	13.6±1.3	11.99±1.1	13.23±0.63	13.69±2.63	13.26±1.1
Alkaline Phosphatase (mg/dL)	67±5[b]	65±8[b]	78±33[ab]	100±23[a]	94±11	166±109	126±34	133±65
BUN (mg/dL)	21.61±4.77	25.53±3.1	23.53±3.56	24.34±3.81	25.21±3.38[a]	26.18±6.62[a]	22.77±7.83[a]	13.21±1.2[b]
Creatinine (mg/dL)	0.32±0.14	0.34±0.16	0.35±0.06	0.32±0.17	0.4±0.1	0.5±0.3	0.35±0.1	0.41±0.1
Serum Iron (mmol/L)	25.3±9.4[a]	16.8±3.7[b]	16±2.8[b]	14.8±7.7[b]	24.3±4.1	26.9±7.5	23.5±9.9	30.3±8.8
cFGF23 (pg/mL)	27.02±17.47	50.83±30.19	40.66±13.83	66.37±16.84	65.43±43.27	109.55±20.83	80.16±19.06	142.58±143.44
Serum PTH (pg/mL)	91.13±10.62[b]	184.24±70.56[ab]	120.46±28.73[b]	309.44±254.9[a]	80.14±27.18	117.8±88.51	82.68±34.54	109.52±68.48
Serum 17β-estradiol (pg/mL)	50.28±11.50	41.23±8.28	64.88±28.55	49.03±23.09	75.92±7.82	58.99±8.80	77.30±9.25	73.07±21.59

Ch – chow diet, Ca – casein diet. Data provided as mean and standard deviation. Columns not sharing the same letter are statistically significant (males and females analyzed separately).

2.3.2   *Sex is a critical factor in determining maintenance of mineral metabolism following phosphate challenge in aging mice*

We next tested the hormones critical for maintaining phosphate homeostasis via the bone-kidney axis. There was a main effect of time for both male and female iFGF23 levels over the course of the study ($p<0.0001$) (**Figure 9C and 9D**). In both sexes, older mice fed the casein diet had higher levels of plasma iFGF23. Older females had higher iFGF23 (old > young, $p<0.0001$) with effect of diet (casein > chow, $p<0.0001$) and an age-by-diet interaction ($p=0.004$). Male mice fed the casein diet had higher iFGF23 (casein > chow, $p=0.014$, ES=0.265) without effect of age ($p=0.065$) or an interaction ($p=0.095$). FGF23 can also be processed into proteolytic fragments, therefore the '*C*-terminal' or 'total' FGF23 ELISA was also used. There were no differences in final cFGF23 between groups for either females or males (**Table 1**). Females fed the casein diet had higher bone FGF23 mRNA expression (casein > chow, $p=0.027$, ES=0.221) without effect of age or an interaction (Table 2). There were no differences across groups for male mice. For marrow FGF23 mRNA expression, female and male mice showed no differences across groups (**Table 2**). Thus, with phosphate diet challenge, FGF23 was differentially increased in aging female mice.

Diet had a significant effect on PTH levels in male mice ($p=0.019$, ES=0.226) but no effect of age and no age-by-diet interaction (**Figure 9B**). Older male mice fed the casein diet had higher PTH compared to both young and old mice receiving the chow diet. Female mice had no differences in serum PTH across groups (**Figure 9B**). There were no differences in calcium levels across groups in female or male mice (2x2 ANOVA $p=0.078$ and $p=0.813$, respectively) (**Table 1**).

To begin exploring potential mechanisms underlying the biochemical findings, gene expression was assessed in several tissues. In older females fed the casein diet, elevated FGF23 mRNA expression was associated with elevated kidney KL, kidney Cyp24a1, and kidney Cyp27b1 mRNA expression (**Table 2**).

Table 2: Mineral metabolism gene expression data.

	Male				Female			
	16Ch (n=8)	**16Ca (n=6)**	**78Ch (n=6)**	**78Ca (n=6)**	**16Ch (n=8)**	**16Ca (n=6)**	**78Ch (n=7)**	**78Ca (n=6)**
Bone Fgf23	1.199±0.72	1.045±0.72	2.125±1.58	1.045±0.59	1.105±0.49[b]	1.222±0.59[b]	1.374±0.84[b]	2.852±1.18[a]
Marrow Fgf23	1.259±0.94	0.523±0.45	1.046±0.68	0.800±0.97	1.189±0.82	1.282±0.71	2.125±2.59	2.426±2.46
Kidney Klotho	1.008±0.14	1.030±0.08	1.609±1.04	1.578±1.13	1.011±0.15[a]	0.773±0.06[ab]	0.677±0.10[ab]	0.530±0.12[b]
Kidney Cyp24a1	1.067±0.43	2.011±1.53	0.788±0.55	1.328±0.84	1.069±0.42[b]	0.848±0.56[b]	1.080±0.51[b]	1.933±0.72[a]
Kidney Cyp27b1	1.245±0.89	1.188±0.54	1.965±1.29	1.962±1.51	1.112±0.56[b]	3.028±1.90[ab]	2.933±2.23[ab]	5.130±2.52[a]

Ch – chow diet, Ca – casein diet. Data provided as mean and standard deviation. Columns not sharing the same letter are statistically significant (males and females analyzed separately).

Older females exhibited increased kidney KL mRNA expression (old > young, $p<0.0001$, ES=0.643) with an effect of diet (casein > chow, $p<0.0001$, ES=0.444) but no age-by-diet interaction. Older females also exhibited increased kidney Cyp24a1 mRNA expression (old > young, $p=0.02$, ES=0.222) with no effect of diet ($p=0.164$) but an interaction ($p=0.023$, ES=0.215); kidney Cyp27b1 mRNA expression was also higher in older females (old > young, $p=0.02$, ES=0.233) with an effect of diet (casein > chow, $p=0.015$, ES=0.25) but no interaction effect (**Table 2**). There were no differences between groups in male mice for kidney KL, Cyp24a1, or Cyp27b1 mRNA expression (**Table 2**).

In addition to transcriptional changes in genes involved in mineral metabolism, increased phosphate intake can also be linked to markers of tissue inflammation and calcification. Indeed, the kidney showed increased IL-6 and TNF mRNAs, and the liver showed increased IL-1 mRNA expression (**Supplementary Table 1**). Older mice had the highest levels of aortic calcification, but mild phosphate challenge did not contribute to worsening calcification over the time course tested (**Supplementary Table 1**).

2.3.3   *Aging mice exhibit reduced trabecular bone volume, increased cortical porosity, and altered bone mechanical properties, which are independent of phosphate challenge*
To determine whether phosphate challenge influenced bone properties over the time course tested, several static and functional parameters were tested.
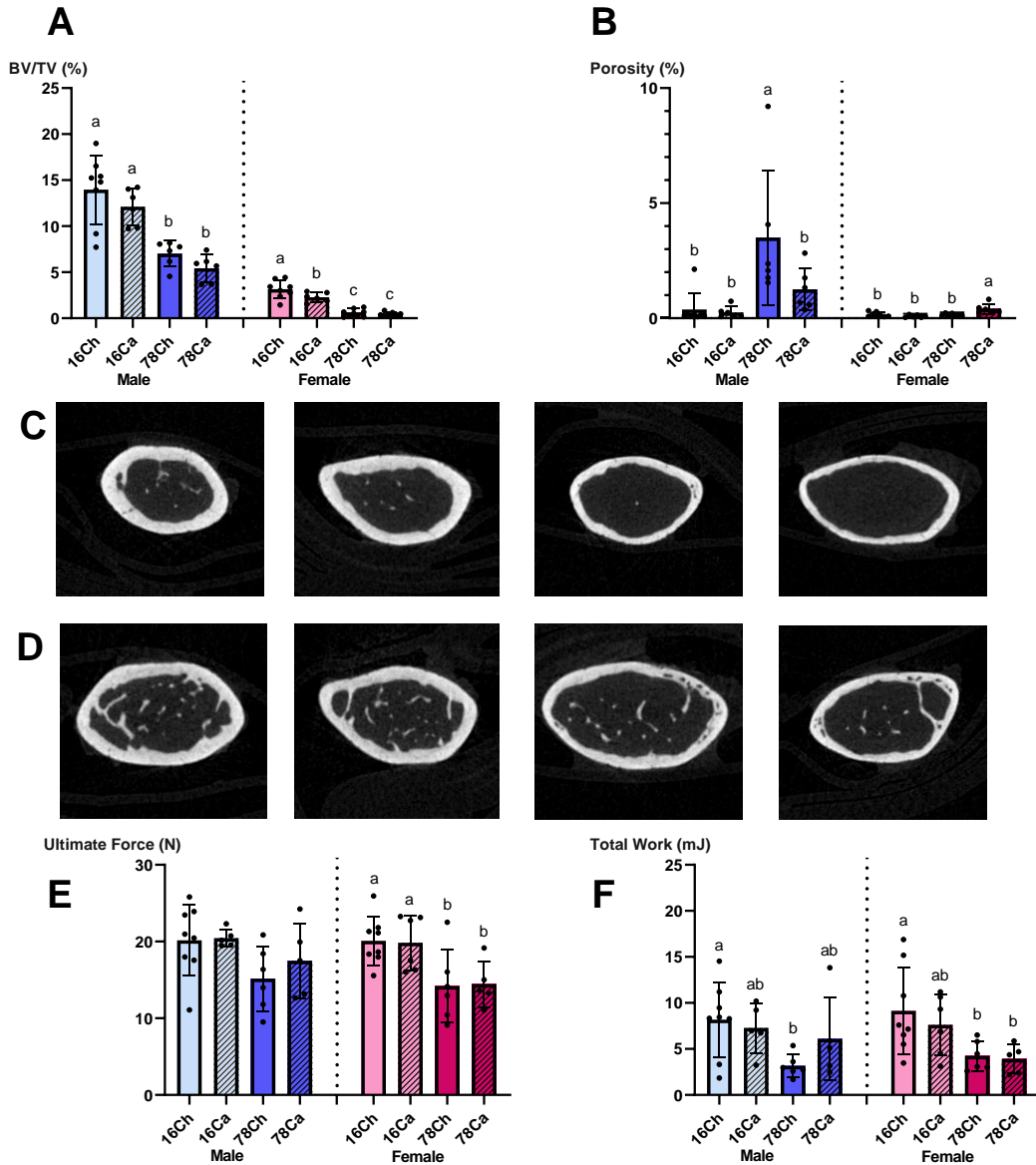
Figure 10: Bone parameters and mechanical properties. **a** Bone volume significantly decreased with age in both male and female mice (p<0.0001, ES=0.683 and p<0.0001, ES=0.767, respectively). **b** Cortical porosity increased significantly with age in both male and female mice (p=0.002, ES=0.348 and p=0.003, ES=0.319, respectively). **c** Representative μCT images of female (top – 16Ch, 16Ca, 78Ch, 78Ca) mouse femurs. **d** Representative μCT images of male (bottom – 16Ch, 16Ca, 78Ch, 78Ca) mouse femurs. **e** Ultimate force significantly decreased with age in female mice (p=0.001, ES=0.406), but there were no differences in male mice. **f** Total work was

significantly different with age in both male and female mice (p=0.041, ES=0.192 and p=0.005, ES=0.323). Group sizes of 6-8. Data plotted as mean and standard deviation with point plots representing individual animal data. Bars not sharing the same letter are statistically different.

Trabecular bone volume and cortical bone thickness were higher in young mice regardless of sex. In this regard, young female mice had higher trabecular bone volume (young > old, p<0.0001, ES=0.767) without effect of diet and an interaction effect; young male mice also had higher trabecular bone volume (young > old, p<0.0001, ES=0.683) without effect of diet or an interaction effect (**Figure 10A**). There were no differences in trabecular thickness between groups of female and male mice (**Supplementary Table 2**). Female mice fed the casein diet exhibited greater trabecular separation (casein > chow, p=0.001, ES=0.394) without effect of age or an interaction; older male mice had greater trabecular separation (old > young, p<0.0001, ES=0.854) without effect of diet or an interaction (**Supplementary Table 2**). Female mice fed the casein diet had higher trabecular number (casein > chow, p=0.001, ES=0.394) without effect of age or an interaction; older male mice had higher trabecular number (old > young, p<0.0001, ES=0.696) without effect of diet or an interaction effect (**Supplementary Table 2**).

Older males had increased cortical porosity (old > young, p=0.002, ES=0.348) without effect of diet or an interaction (**Figure 10B**). In female mice, increased porosity was affected by age (old > young, p=0.003, ES=0.319) and diet (casein > chow, p=0.048, ES=0.16) with a strong interaction between the variables (p=0.002, ES=0.347) (**Figure 10B**). Older female mice receiving the casein diet exhibited the highest levels of porosity of all the female groups.

To determine the bone mechanical properties across groups, 4-point bending of the tibia was performed. Young females had higher ultimate force (young > old, p=0.001, ES=0.406) without effects of diet or interaction; there were no differences in ultimate force between groups in male mice (**Figure 10E**). Young female mice exhibited higher total work (young > old, p=0.005, ES=0.323) without effect of diet or an interaction; young male mice also exhibited higher total work (young > old, p=0.041, ES=0.192) but no effect of diet or an interaction (**Figure 10F**). Young females had higher ultimate stress (young > old, p=0.002, ES=0.368) and resilience (young > old, p=0.007, ES=0.297), but ultimate stress and resilience were not different between groups of male mice. For female and male mice, there were no differences in total displacement, stiffness, or total strain (**Supplementary Table 2**). Thus, natural aging negatively influences normal bone properties, with females performing slightly worse than males.

2.3.4 *Administration of exogenous estradiol upregulates Fgf23 and estrogen receptor levels in vitro*

We next tested potential differences in sex steroids across sexes. There were no differences in plasma 17β-estradiol concentration between groups in male and female mice (2x2 ANOVA p=0.256 and p=0.07, respectively), consistent with reports across all ages in humans[93] (**Table 1**). There were no differences across groups in male or female mice for bone mRNA expression of *Esr1*, *Esr2*, or *AR* (**Supplementary Table 3**).
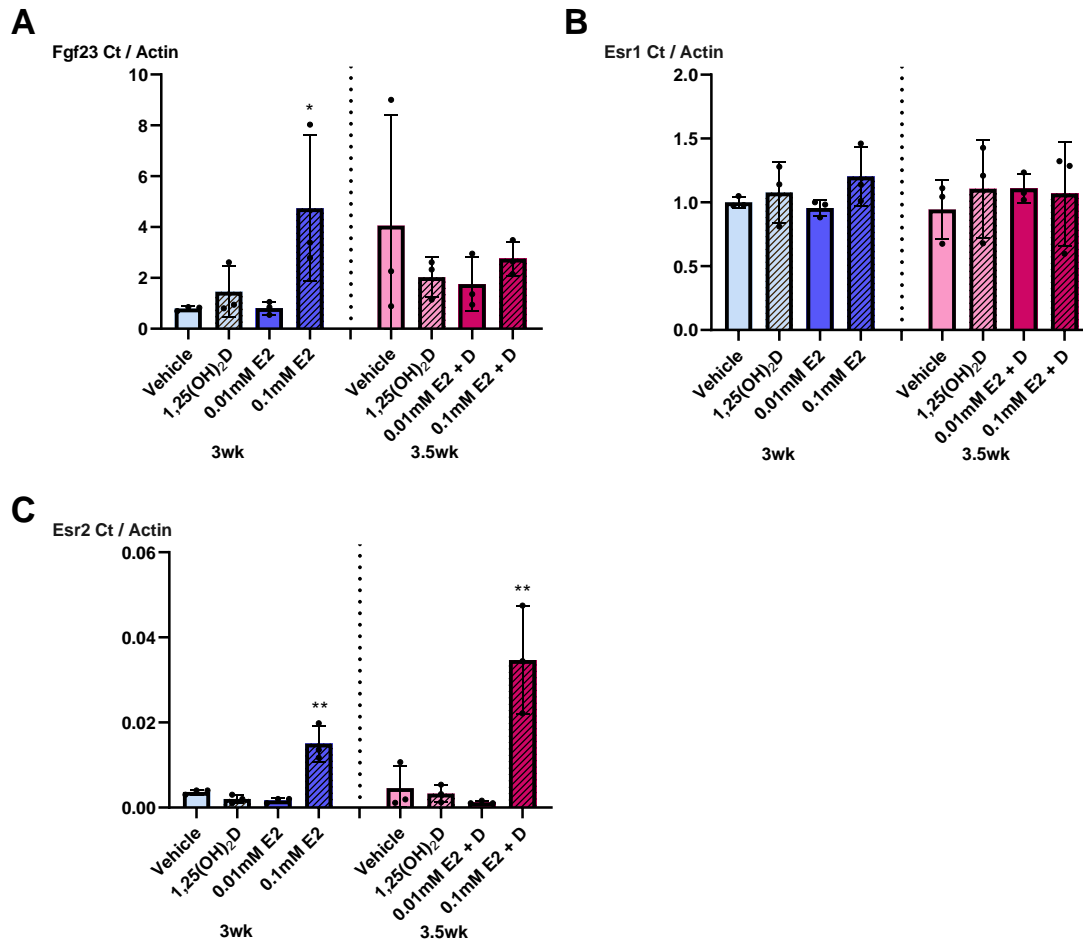
Figure 11: *In vitro* gene expression with estradiol treatment in osteoblast/osteocyte mesenchymal stem cell line. **a** FGF23 expression was significantly increased with 0.1mM estradiol treatment as compared to vehicle (p=0.033). Addition of 1,25-vitamin D did not produce any additional effect. **b** Esr1 expression was no different with any concentration of estradiol or 1,25-vitamin D treatment. **c** Esr2 expression was significantly increased with 0.1mM estradiol (p=0.001) and 0.1mM + 1,25-vitamin D treatment (p=0.002). Data plotted as mean and standard deviation with point plots representing individual animal data (n=3 for all treatments). *statistically different from all other groups (p<0.05).

To examine mechanistic effects of estradiol in isolation on bone cells, we used a novel MSC line that can be differentiated into osteocytes[91], like primary MSCs[94]. The cells were treated at two stages of differentiation (3 and 3.5 weeks) with estradiol and/or 1,25(OH)$_2$D, hormones that potentially influence *Fgf23* transcription. After 24h, there was a main effect of estradiol treatment on *Fgf23* mRNA expression between groups at 3 weeks of differentiation (p=0.038, ES=0.631) (**Figure 11A**). Cells treated with the higher estradiol dose (0.1mM) alone exhibited statistically higher *Fgf23* expression as compared to the vehicle (p=0.033); there were no differences in cells treated with 1,25(OH)$_2$D or the lower estradiol dose (0.01mM). For *Esr1* mRNA expression, there were no differences between groups (**Figure 11B**). For *Esr2* expression, there was a main effect of treatment between groups (p<0.0001, ES=0.898) (**Figure 11C**); cells treated with the higher estradiol dose alone exhibited statistically higher *Esr2* expression as compared to the vehicle (p=0.01). At 3.5 weeks of differentiation, there was no effect of treatment on *Fgf23* expression or Esr1 expression; however, there was a main effect of treatment on *Esr2* mRNA between groups (p=0.001, ES=0.855). Cells treated with the higher estradiol dose exhibited significantly higher *Esr2* expression as compared to the vehicle (p=0.002) (**Figure 11C**).

In summary, our results show that there are sex- and age-specific effects of moderate phosphate loading in mice. These collective data support that aging females employ mechanisms, potentially through the presence of estradiol, to increases FGF23 to maintain effective FGF23-KL signaling and thus normal serum phosphate concentrations, whereas male mice maintain KL expression. These changes may provide insight into differential mechanisms and regulation that are increasingly important during aging when phosphate clearance is reduced.

2.4 Discussion

Our study highlights sex, age, and diet differences in the management of phosphate metabolism. Both age and diet influenced iFGF23 in female mice, with older females fed the casein diet expressing the highest levels of iFGF23; although aging males fed the casein diet also expressed the highest iFGF23, the level was two-fold higher in older female mice. KL is widely reputed as the "anti-aging gene," because its expression has been shown to decrease with age[75–77] and KL overexpression is associated with extended lifespan in both male and female mice[95]. Coincidentally, KL levels decreased with age and diet only in females, whereas levels in male mice increased with age. Previous studies performed in human cohorts demonstrating elevations in kidney KL expression in both sexes may have been potentially confounded by combining male and female results[96,97] and/or normal versus various stages of CKD[98]. Considering that males and females may acquire CKD and proceed through the stages toward ESRD at different rates, gender variation in KL expression is especially interesting. Since males express less serum iFGF23 than females, it is plausible that KL expression is higher to facilitate more efficient FGF23-KL signaling. These results could indicate that older females use protective mechanisms, such as increasing FGF23 production, to maintain serum phosphate in the normal range, thus preventing mineral dysregulation. Although males upregulated kidney KL mRNA, these protective mechanisms may be somewhat compromised in older males. Although additional clinical studies are certainly required, the changes in KL could, in part, explain why males exhibit more severe kidney damage than females during progressive renal disease[99].

FGF23 is well-established as a hormone known to control phosphate metabolism with an effect on the kidneys following its secretion from osteocytes. Indeed, disturbances in the FGF23-KL axis can lead to significant pathological consequences. The MrOS study found that when eGFR is below 60mL/min/1.73m^2 and renal function is considered poor, elevated FGF23 correlates

with fracture risk in elderly men[100]. In our study, serum creatinine and BUN were not significantly elevated, supporting that there was not a major decline in kidney function following mild phosphate challenge, yet this did produce differential FGF23 expression to maintain similar phosphate levels. A previous study that evaluated biochemical parameters in an elderly population demonstrated that serum phosphate did not increase exponentially until eGFR dropped below 47mL/min/1.72m^2. This finding potentially illustrates that the mice in the current study maintained generally normal renal function, thus the observed patterns in FGF23 production and KL mRNA expression observed in human patients are likely due to other mechanisms, such as sex steroids, inflammation, or oxidative stress[101]. Indeed, we found that older female mice with normal renal function were able to respond to increased phosphate load by elevating FGF23.

Alterations in sex steroid signaling could be considered a likely mechanism for the observed gender differences in phosphate-sensitive responses, therefore *in vivo* and *in vitro* assays were performed. Estradiol was higher in females of each age and diet group as has been shown clinically, but older females did not exhibit the age-related drop in estrogens that are associated with human menopause. This could be due to difficulties in simulating human menopause as a result of a large proportion of female mice (60-70%) entering a state of constant estrus that can last for up to 100 days; in these cases, older female mice expressed stable estradiol levels, similar to observations in our study[102,103]. A previous study also found that administration of high amounts of estradiol caused increased *Fgf23* and *KL* mRNA expression both in rats that had undergone ovariectomy and in UMR-106 rat osteosarcoma cells, respectively[80]. Our results recapitulated the increased *Fgf23* mRNA expression with estradiol treatment in a novel mouse mesenchymal cell line as well as expansion into examining changes in estradiol receptor expression. This previous study did not investigate the downstream signaling effects of FGF23

upregulation and how this was influenced by sex differences, a notable strength of the present study.

There are several limitations to our study. First, the grain-based chow diet and the purified casein diet are not completely comparable. Although grain-based diets are relatively rich in phosphorus (0.7% in chow diet), the phosphorus is bound in the form of inositolphosphoric acids (phytate, "myo-inositol hexaphosphate"); previous studies have demonstrated that very little of the phosphorus is absorbed by the GI tract and is thus less bioavailable[104–107]. It is estimated that 0.4% may be bioavailable. In contrast, the casein diet contains casein-based protein and no phytate, so the phosphorus is almost completely bioavailable[41,108]. The two diets also utilize different protein sources/amounts of protein and amounts of fiber/different types of fiber. A future study could address diets with varied phosphorus availability as the sole difference between diets. Second, we did not measure glomerular filtration rate (GFR) in our mice, and thus minor changes in renal function may not have been identified. However, BUN was not different across groups, thus there were no signs of even mild CKD. Third, we did not utilize charcoal-stripped fetal bovine serum in our *in vitro* studies. Thus, estradiol was likely present in the culture media. Our experiments did use similar estradiol concentrations as those reported as activating concentrations in bone cells, but we cannot rule out that our effects were seen at the highest doses due to the presence of physiological levels of this hormone. Indeed, a future study could be performed with MPC2 cells and charcoal-stripped serum. Key strengths of our study included paired sex and aged animals, and the fact that a slight increase in bioavailable phosphate through the casein diet did not induce CKD but rather mimicked potential increases in phosphate in an aging model. Further, the ability to test hormonal effects in a new *in vitro* system of cultured osteocytes that produce FGF23 demonstrated isolated effects of estrogen.

In conclusion, this study is the first to examine how sex and age contribute to crossover effects on FGF23 and phosphate regulatory pathways. Aging with associated with increased aortic calcification, decreased trabecular bone mass, and increased cortical porosity, all of which are common signs of the aging process but were not FGF23-dependent. More importantly, our results show that the expression of *KL* mRNA differs between male and female mice, with males upregulating *KL* expression in aging compared to females. This observation could indicate that the sexes employ different mechanisms to maintain effective FGF23-KL signaling. Finally, controlling phosphate intake throughout aging could have modifiable outcomes for FGF23-related phenotypes.

CONFLICT OF INTEREST

KEW receives royalties from Kyowa-Hakko-Kirin Pharmaceuticals, Inc. for licensing the FGF23 gene through Indiana University.

2.5 Supplementary Tables

Supplementary Table 1: Heart calcification and inflammation gene expression data.

	Male				Female			
	16Ch (n=8)	**16Ca (n=6)**	**78Ch (n=6)**	**78Ca (n=6)**	**16Ch (n=8)**	**16Ca (n=6)**	**78Ch (n=7)**	**78Ca (n=6)**
Aortic Calcification (mmol/mg)	2.44±.084[b]	2.83±0.93[b]	4.12±0.87[a]	3.80±0.59[a]	2.75±1.03[b]	2.07±1.19[b]	4.69±0.99[a]	4.09±0.72[a]
Kidney IL-1β	1.094±0.46	1.891±0.97	2.527±1.87	1.073±0.87	1.028±0.26	1.271±0.86	1.215±0.47	1.900±1.06
Kidney IL-6	1.113±0.55[b]	1.268±1.05[b]	4.762±4.15[a]	1.417±1.07[b]	1.036±0.29[b]	1.267±0.85[b]	5.253±5.12[ab]	8.126±5.32[a]
Kidney TNF	2.324±2.71	1.018±0.55	1.971±0.72	0.968±0.48	1.524±1.65[b]	1.321±1.47[b]	1.869±2.26[b]	4.599±2.82[a]
Liver IL-1β	1.070±0.42	1.410±1.00	0.722±0.45	1.951±1.60	1.056±0.35[ab]	0.928±0.32[b]	0.899±0.26[b]	1.442±0.38[a]
Liver IL-6	1.364±1.12	1.709±1.23	0.956±0.93	1.641±1.44	1.052±0.32	0.995±0.52	1.333±0.63	0.669±0.46
Liver TNF	1.684±1.77	2.127±2.21	2.252±2.14	4.606±3.64	1.275±1.07	1.366±0.76	2.913±3.63	4.675±4.81

Ch – chow diet, Ca – casein diet. Data provided as mean and standard deviation. Columns not sharing the same letter are statistically significant (males and females analyzed separately).

Supplementary Table 2: Bone geometry and mechanical properties.

	Male				Female			
	16Ch (n=8)	**16Ca (n=6)**	**78Ch (n=6)**	**78Ca (n=6)**	**16Ch (n=8)**	**16Ca (n=6)**	**78Ch (n=7)**	**78Ca (n=6)**
BV/TV (%)	13.975±3.74[a]	12.121±2.01[b]	7.004±1.40[c]	5.425±1.48[c]	3.150±0.98[a]	2.275±0.52[b]	0.627±0.42[c]	0.511±0.18[c]
Tb.Th (mm)	0.060±0.004	0.059±0.003	0.058±0.007	0.058±0.006	0.049±0.006	0.047±0.008	0.051±0.019	0.055±0.015
Tb.Sp (mm)	0.233±0.018[b]	0.230±0.009[b]	0.321±0.029[a]	0.334±0.026[a]	0.330±0.023[c]	0.343±0.016[a]	0.556±0.470[bc]	0.609±0.570[ab]
Tb.N (1/mm)	2.328±0.58[a]	2.060±0.26[ab]	1.203±0.24[b]	0.953±0.31[b]	0.641±0.16[c]	0.481±0.09[a]	0.116±0.07[bc]	0.095±0.03[ab]
Porosity (%)	0.378±0.71b	0.254±0.25[b]	3.503±2.93[a]	1.258±0.93[b]	0.153±0.10[b]	0.086±0.05[b]	0.143±0.22[b]	0.378±0.71[a]
Cs.Th (mm)	0.154±0.005[a]	0.145±0.005[a]	0.108±0.016[c]	0.120±0.008[b]	0.188±0.008[a]	0.171±0.008[b]	0.154±0.009[c]	0.145±0.017[c]
Ultimate Force (N)	20.16±4.65	15.16±4.21	20.44±1.16	17.50±4.85	20.09±3.15[a]	19.83±3.56[a]	14.20±4.78[b]	14.43±3.01[b]
Total Displacement (μm)	616.4±237.4	321.3±92.8	554.3±222.9	515.2±281.7	762.6±429.5	601±257.5	421.1±225.5	455±197.8
Stiffness (N/mm)	107.55±19.30	89.06±18.22	99.11±23.44	101.59±10.02	85.03±28.40	99.91±14.61	86.47±14.99	70.97±13.91
Total Work (mJ)	8.18±4.05[a]	3.16±1.24[ab]	7.27±2.70[b]	6.09±4.54[ab]	9.14±4.75[a]	7.62±3.31[ab]	4.24±1.62[b]	3.90±1.57[b]
Ultimate Stress (MPa)	125.1±38.4	110.2±41.8	173.4±48.2	118.1±40.3	185.3±36.9[ab]	204.5±45.7[a]	125.4±30.7[c]	150.2±49.3[bc]
Total Strain (με)	59494±26082	27528±6474	50273±17444	40442±21578	63320±41885	48469±21999	33115±19616	37364±16326
Resilience (MPa)	1.08±0.81	0.88±0.74	1.46±0.88	0.79±0.46	2.00±0.88[a]	1.89±0.71[a]	0.93±0.47[b]	1.26±0.56[ab]
Toughness (MPa)	4.69±2.34[a]	1.86±0.39[a]	5.76±2.66[b]	3.22±2.41[ab]	7.40±5.12	6.35±3.16	3.05±1.44	3.31±1.46

Ch – chow diet, Ca – casein diet. Data provided as mean and standard deviation. Columns not sharing the same letter are statistically significant (males and females analyzed separately).

Supplementary Table 3: *In vivo* sex steroid signaling gene expression data.

	Male				Female			
	16Ch (n=8)	**16Ca (n=6)**	**78Ch (n=6)**	**78Ca (n=6)**	**16Ch (n=8)**	**16Ca (n=6)**	**78Ch (n=7)**	**78Ca (n=6)**
Bone Esr1	1.114±0.42	0.884±0.81	0.998±0.80	0.840±0.61	1.432±0.79	1.366±0.72	1.846±0.49	2.202±1.37
Bone Esr2	1.610±1.23	0.910±0.94	1.552±1.45	1.336±1.25	1.781±0.92	1.427±0.90	1.415±0.69	1.351±1.05
Bone AR	1.095±0.41	1.162±0.89	0.675±0.48	0.756±0.42	1.680±1.10	1.213±0.64	1.776±0.45	2.063±1.22

Ch – chow diet, Ca – casein diet. Data provided as mean and standard deviation.

CHAPTER 3

THE COMBINATION OF AGING AND CHRONIC KIDNEY DISEASE LEADS TO AN

EXACERBATED CORTICAL POROSITY PHENOTYPE

3.1 Introduction

Chronic kidney disease (CKD) and aging are each independently associated with higher risk of fracture. Although ~38% of the U.S. population of 65+ years has CKD[23], the interaction between aging and CKD with respect to bone structure and mechanics is not well understood. Skeletal fragility associated with CKD is primarily due to deterioration of cortical bone and development of holes within the cortical bone (cortical porosity), the region that principally determines the mechanical properties of the bone[33]. Often due to unbalanced remodeling, cortical porosity also occurs in aging, although to a lesser degree than in CKD[109]. Interactions between CKD and aging are important to understand in order to frame efficacy of future treatments for the aging CKD population.

Despite osteonal remodeling not being a normal part of rodent physiology, we previously have shown robust cortical porosity development in rodents with CKD[23,33,109], indicating the potential for overlapping mechanisms of porosity development in rodents and humans. We have shown that mice with adenine-induced CKD have a skeletal phenotype that includes cortical porosity and thinning[110]. Additionally, we and others have documented age-induced cortical porosity in male mice without impaired renal function[111]. The goal of this study was to compare the individual and combined effects of aging and CKD on cortical porosity and mechanical properties utilizing the adenine-induced CKD model in young, skeletally mature and aging mice. We hypothesized that interactions would exist between CKD and aging for cortical porosity and whole-bone mechanical properties.

41

3.2 Materials & Methods

3.2.1 *Animals*: Male C57Bl/6J mice were obtained from Jackson Laboratories (JAX stock #000-664, Bar Harbor, ME, USA) at 15- and 77- weeks of age (n=16/age) and group housed at an institutionally approved animal facility with 12h light/dark cycles. After one week of acclimation, all mice were switched to a casein diet with adjusted calcium and phosphorus (0.9% P, 0.6% Ca). Half of the mice were given the same casein-based diet with 0.2% adenine (AD; Envigo-Teklad Diets, Madison, WI, USA) to induce CKD while the remaining mice served as age-matched controls (CON; n=8/group). After six weeks on the adenine diet, the AD mice were switched to the casein diet for an additional two weeks to produce an eight-week total timeline. Body weight was measured weekly, and animals were monitored for health daily. Animals were euthanized via exsanguination under isoflurane anesthesia, and blood was collected from the heart for biochemical analyses. One femur was fixed in 10% neutral buffered formalin, and one tibia was placed in saline-soaked gauze and frozen. All animal procedures were approved by the Indiana University School of Medicine Institutional Animal Care and Use Committee prior to the initiation of experimental protocols, and methods were carried out in accordance with relevant guidelines and regulations.

3.2.2 *Serum Biochemistries*: Cardiac blood collected at time of termination was used to measure serum calcium and phosphorus (Pointe Scientific, Canton, MI, USA) and blood urea nitrogen (BUN) (BioAssay Systems, Hayward, CA, USA) via colorimetric assays. Serum parathyroid hormone (PTH) was measured via ELISA (Immutopics Quidel, San Diego, CA, USA) as previously described[40].

3.2.3   *Ex Vivo Micro-Computed Tomography of the Femur*: Distal femora were scanned on a SkyScan 1172 system (Bruker, Billerica, MA, USA) using a custom holder that allows scanning of 3 bones at a time[112] with the following settings: 60kV, medium camera, 0.5 aluminum filter, frame averaging of 2, 0.7 rotation step, and 8µm voxel size. Trabecular bone architecture was analyzed from a 1mm region of interest (ROI) just proximal to the distal growth plate. Measures of trabecular bone included bone volume fraction/total volume, trabecular thickness, trabecular number, and trabecular spacing. Cortical bone geometry was analyzed from five consecutive slices ~2.5mm proximal to the distal growth plate in a region proximal to the trabecular bone of the distal femur. Measures of cortical bone included cortical bone area, cortical thickness, and cortical porosity. Cortical porosity was determined by assessing void area between the periosteal and endosteal surfaces, presented as a percentage of overall cortical bone area. ROIs were hand-drawn with a binary threshold of 100 – 255. All nomenclature followed standard recommendations[87]. A visual interpretation of our analysis process can be found in **Supplemental Figure 1**.
Tibial midshafts were group-scanned using the SkyScan 1172 system (Bruker, Billerica, MA, USA) with a 0.5 aluminum filter and a 9µm voxel size to assess geometric properties for stress/strain calculations following mechanical testing. Cortical bone geometry was analyzed from five consecutive slices selected at the location of the proximal tibiofibular joint (TFJ); measures of cortical bone included cortical bone area, cortical thickness, and cortical porosity.

3.2.4   *Four-Point Bending of the Tibia*: Tibiae underwent four-point bending (TA Instruments, New Castle, DE, USA) as previously described[111]. Briefly, bones were thawed to room temperature soaked in PBS. The anterior surface was placed on two metal supports located ±9mm from the mid-diaphysis testing site, and the upper supports were centered on the bone with a span of ±4mm. Specimens were loaded to failure at a rate of 0.025mm/sec,

producing a force-displacement curve for each sample. Structural mechanical properties (yield/ultimate load, stiffness, pre-yield/post-yield/total displacement, and pre-yield/post-yield/total energy to failure) were obtained directly from the curves using a MATLAB code, while estimated material properties (ultimate stress, elastic modulus, strain, resilience, total toughness) were derived from force-displacement curves and geometric properties noted above using standard beam-bending equations for four-point bending.

3.2.5 *Statistical Analysis*: Statistical analyses were completed in SPSS Statistics 25 (IBM, Armonk, NY, USA). Data were analyzed as a 2x2 factorial ANOVA (age-by-disease) with main effects of disease (CKD versus control), age (young versus aging), and disease-by-age interactions noted. When the 2x2 ANOVA was statistically significant ($p<0.05$), an all-groups Duncan post-hoc analysis was applied to determine individual group differences. Linear regressions were performed to assess the relationships between cortical porosity, PTH, and select mechanical properties. All data are presented as mean ± standard deviation.

3.3 Results

Due to low body condition scoring, one young adenine fed mouse was euthanized at week 5, and one aging adenine fed mouse was euthanized at week 7. Two aging adenine fed mice died of unknown causes at week 1 and week 7; one aging control mouse died of unknown causes prior to the start of the study. This resulted in group sizes of young control (n=8), young adenine (n=7), aging control (n=7), and aging adenine (n=5).

3.3.1 *Ingestion of adenine resulted in reduced food intake and body weight in both ages.*

There was an age-by-disease interaction for endpoint body weight ($p<0.0001$). Both young (-37%) and aging (-29%) AD mice had significantly lower values than their age-matched controls (**Figure 12B**). Body weight differences were consistent with altered food intake. While on the adenine diet, young mice consumed 54% and aging mice consumed 55% of the total food consumed by age-matched mice on the control diet; with resumption of the control diet at week 7, food intake increased in both young (+62%) and aging (+67%) mice.
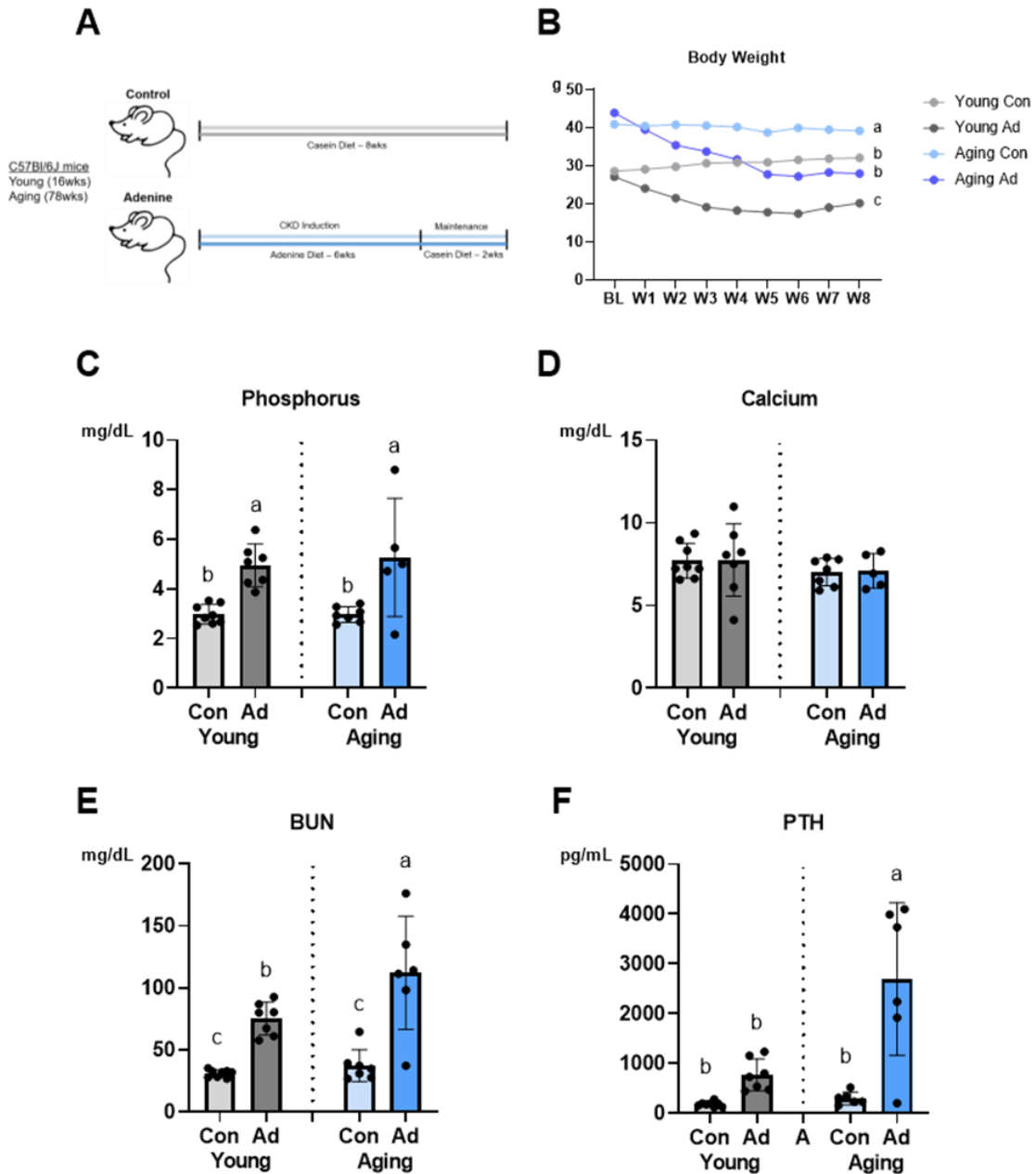
Figure 12: Biochemical parameters reveal interactions between aging and CKD. **A** Schematic of study design (n=6-8 per group). **B** Both adenine-fed groups (AD) had lower endpoint body weight (p<0.0001) compared to control (Con) with an effect of age (p=0.002) and an age-by-disease interaction (p<0.0001). **C** Serum phosphorus was highest in adenine-fed groups (p<0.0001), although there was no age-by-disease interaction effect. **D** There were no differences in serum

calcium across groups. **E** Blood urea nitrogen (BUN) was highest in aging AD mice (p=0.02) with an effect of disease (p<0.0001) and an age-by-disease interaction (p<0.0001). **F** Parathyroid hormone (PTH) was highest in aging AD mice (p=0.002) with an effect of disease (p<0.0001) and an interaction effect (p<0.0001). Data are presented as mean ± standard deviation. Bars with different letter notations are statistically different from each other (p<0.05).

3.3.2   Biochemical indices were influenced by both age and disease.

Although there was no age-by-disease interaction for serum phosphorus, both young (+40%) and aging (+44%) AD mice had significantly higher values than their age-matched controls (**Figure 12C**). There were no differences in serum calcium across the four groups (**Figure 12D**). There was an age-by-disease interaction for serum BUN (p<0.0001) and serum PTH (p<0.0001). While there was no difference between young and aging CON mice, both young (+59%) and aging (+67%) AD mice had significantly higher values than their age-matched controls. Aging AD mice had BUN levels significantly higher than young AD animals (+33%) (**Figure 12E**). Young and aging control mice had no differences in PTH. Aging AD mice had PTH levels that were nine-fold higher than their age-matched controls (p<0.05). The young AD group had four-fold higher PTH than the young CON group, but this did not reach statistical significance (**Figure 12F**).

3.3.3   Cortical bone structure was compromised by both age and disease.

There was an age-by-disease interaction for femoral cortical porosity (p=0.001). Aging AD mice had +78% higher femoral porosity than young AD mice and +63% higher femoral porosity than age-matched controls (**Figure 13A**). The young AD group exhibited three-fold higher femoral porosity than the young CON group (p<0.0001). From linear regression analysis, PTH levels predicted ~35% of femoral cortical porosity across this dataset.

Although there were effects of age (p=0.014) and disease (p=0.004) on tibial midshaft cortical porosity, the age-by-disease interaction did not reach significance (p=0.051). Aging AD mice had +76% higher tibial cortical porosity than young AD mice and +86% higher tibial cortical porosity than age-matched counterparts (**Figure 13B**).

A Femoral Cortical Porosity

B Tibial Cortical Porosity

C Femoral Cortical Area

D Tibial Cortical Area

E Femoral Cortical Thickness

F Tibial Cortical Thickness

G

Young   Aging

Con

Ad - closest to mean

Ad - highest porosity
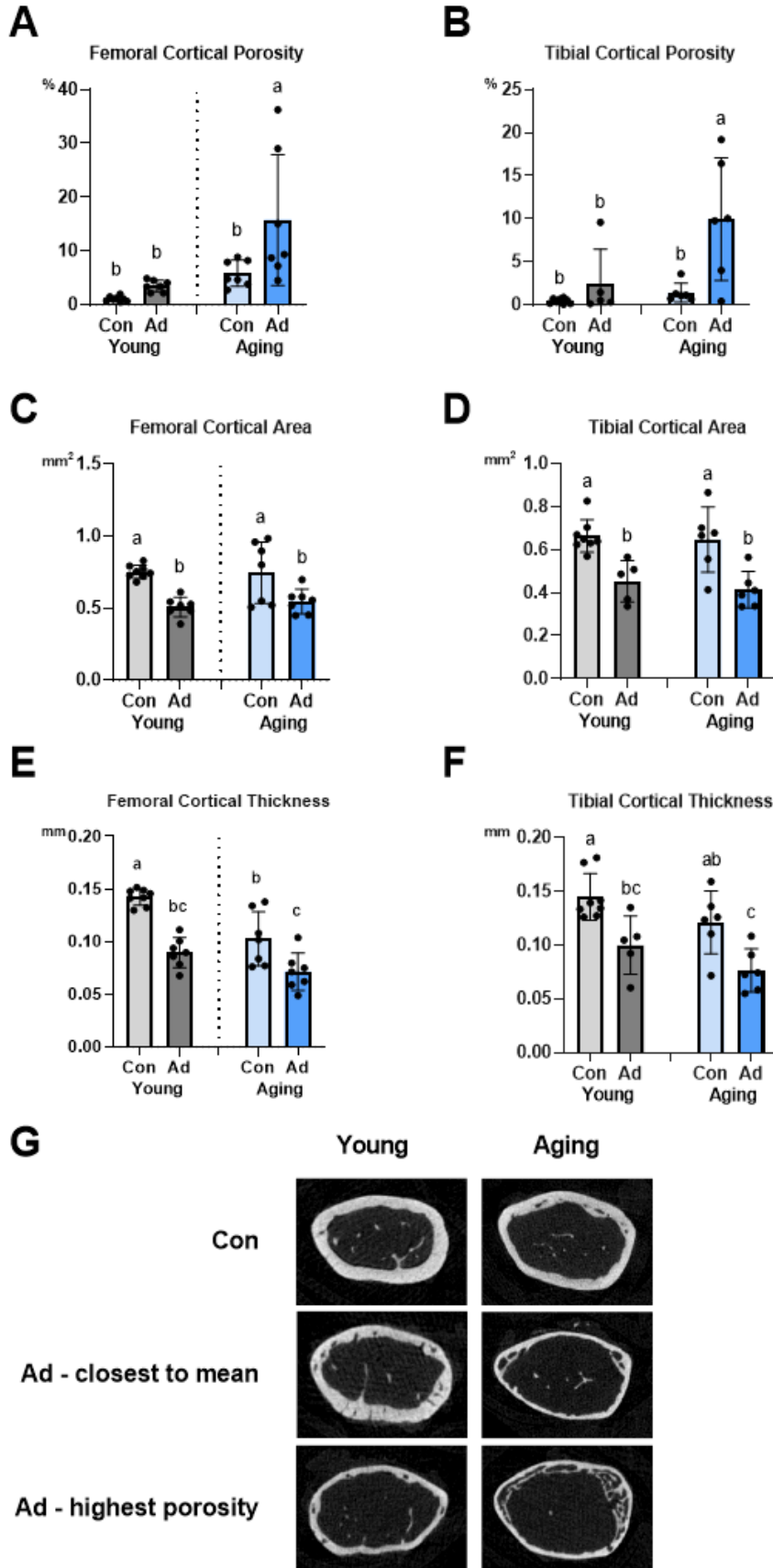
Figure 13: Cortical bone parameters in femur and tibia are compromised with aging and CKD. **A** Femoral cortical porosity was highest in aging AD mice (p=0.001) with an effect of disease (p=0.012) and an interaction effect (p=0.001). **B** Tibial cortical porosity was also highest in aging AD mice (p=0.014) with an effect of diet (p=0.004) but no interaction effect. **C** Regardless of age, AD mice had the lowest femoral cortical bone area (p<0.0001) without an age-by-disease interaction effect. **D** Regardless of age, CON mice had the highest tibial cortical bone area (p<0.0001) without an age-by-disease interaction. **E** Adenine-fed groups exhibited the lower femoral cortical thickness (p<0.0001) with an effect of age (p<0.0001) but no age-by-disease interaction. **F** Tibial cortical thickness was highest in young CON mice (p=0.026) with an effect of disease (p<0.0001) but no interaction effect. **G** Representative μCT images of the femur (CON, AD closest to mean for porosity, and AD highest porosity) for young and aging mice. Data are presented as mean ± standard deviation. Bars with different letter notations are statistically different from each other (p<0.05).

Femoral cortical bone area was affected by diet (p<0.0001), with aging AD mice having -36% lower cortical area and young AD mice having -32% lower cortical area compared to age-matched counterparts (**Figure 13C**). Both age (p<0.0001) and disease (p<0.0001) affected femoral cortical thickness; both young and aging AD mice had roughly 30-38% lower femoral cortical thickness compared to age-matched counterparts (**Figure 13E**). Although there were not differences due to age, both young and aging AD mice had 45-55% lower tibial cortical area and 45-60% lower tibial cortical thickness compared to age-matched counterparts (**Figure 13D and 13F**). There were no differences in distal femur trabecular bone volume across groups but interaction effects existed for both trabecular thickness (p=0.019) and trabecular separation (p<0.0001) (**Table 3**).

Table 3: Trabecular bone architecture and cortical bone mechanical properties.

	Young Con	Young Ad	Aging Con	Aging Ad	Disease p-value	Age p-value	Disease x Age p-value
BV/TV (%)	6.3± 1.1	5.1±1.7	5.4±1.9	4.6±1.9	0.299	0.130	0.706
Tb.Th (mm)	0.04± 0.01^{ab}	0.05± 0.01^{b}	0.04± 0.003^{a}	0.04± 0.003^{ab}	**0.024**	**0.018**	**0.019**
Tb.Sp (mm)	0.25± 0.02^{b}	0.33± 0.04^{b}	0.27± 0.03^{a}	0.34± 0.06^{a}	0.231	**<0.0001**	**<0.0001**
Tb.N (1/mm)	1.49± 0.28	1.10± 0.43	1.45± 0.44	1.09± 0.45	0.882	**0.018**	0.936
Ultimate Force (N)	14.7±1.6^{a}	8.3±1.0^{bc}	10.3±4.0^{b}	5.6±2.0^{c}	**<0.0001**	**0.003**	0.395
Total Displacement (µm)	917± 387^{a}	1075±467^{a}	463±172^{b}	455±211^{b}	0.582	**0.001**	0.544
Stiffness (N/mm)	82.57± 16.83^{a}	40.91± 15.44^{b}	68.73± 20.71^{a}	36.45± 9.44^{b}	**<0.0001**	0.195	0.5
Total Work (mJ)	8.08± 2.62^{a}	5.45± 3.15^{ab}	3.34± 2.01^{bc}	1.48± 1.14^{c}	**0.03**	**<0.0001**	0.696
Ultimate Stress (MPa)	167± 53^{a}	90±22^{b}	98±27^{b}	66±24^{b}	**0.002**	**0.005**	0.153
Modulus (GPa)	11.0±3.8^{a}	4.6±2.1^{b}	7.2±2.2^{b}	4.5±1.2^{b}	0.089	**<0.0001**	0.107
Resilience (MPa)	1.04± 0.57^{a}	0.41± 0.32^{b}	0.51± 0.25^{b}	0.14± 0.05^{b}	**0.004**	**0.018**	0.406
Toughness (MPa)	7.37± 2.12^{a}	5.38± 2.20^{a}	2.94± 1.51^{b}	1.69± 1.41^{b}	**0.045**	**<0.0001**	0.632

Data provided as mean ± standard deviation. Groups with different letter notations are statistically different from each other (p<0.05).

3.3.4   Mechanical properties were negatively affected by both age and disease.

There were no age-by-disease interactions across mechanical properties but several properties had independent age and disease effects. Structural properties of ultimate force, stiffness, and total work and estimated material properties of ultimate stress, resilience, and toughness were all significantly lower in adenine-fed mice compared to controls (**Table 3**). Structural properties of ultimate force, total displacement, and total work and estimated material properties of ultimate stress, modulus, resilience, and toughness were all significantly lower in aging mice compared to young mice (**Table 3**). To assess whether periosteal expansion occurred, total bone area and periosteal perimeter were measured. There were no differences in total bone area (all bone and marrow tissue; p=0.095) or periosteal perimeter (p=0.457). From linear regression models, tibial cortical porosity levels predicted 22% and 15% of the variability in ultimate force and toughness, respectively.

3.4 Discussion

The primary finding of this study is that while both young and aging male C57Bl/6J mice are negatively impacted by adenine-induced CKD, aging mice exhibit a more severe phenotype with greater cortical porosity and higher PTH than young mice. Adenine-induced CKD in both ages led to reduced structural and estimated mechanical properties with no significant interactions between the two conditions (age and disease).

There are multiple animal models that allow researchers to study CKD, two of the most common being 5/6-nephrectomy and oral ingestion of adenine. Surgical methods have several key limitations, including post-surgical mortality, variability in surgical technique, and rapid onset of kidney function decline[84]. Adenine was first utilized in a rat model where higher doses (0.75% adenine) caused rapid, severe kidney alterations that were more consistent with

nephrotoxic disease; however, reductions in dosage to 0.25% adenine produced a milder and more gradual disease more consistent with CKD[113]. Studies from our lab using a casein-based adenine diet for mice have used a 0.2% dose and shown it produces progressive loss of kidney function and recapitulates the biochemical and skeletal effects seen in CKD-MBD[84]. One limitation of the adenine diet is weight loss due to reduced food intake, which could contribute to some, but unlikely all, of the skeletal changes in the model. To our knowledge, the adenine diet has not been utilized to study aging mice, which is a key strength and novelty of the current paper.

It is well-established that cortical porosity increases with age[114,115]. Burghardt et. al (2010) found that cortical porosity was more strongly associated with age compared to other cortical metrics, such as cortical thickness and cortical bone area[116]. Analyses of human iliac crest biopsies have documented that higher cortical porosity with age is more often due to an increase in the size of individual pores rather than areal pore density; additionally, porosity was tied to remodeling of existing canals rather than the generation of new canals[117]. Despite known differences between human and rodent cortical bone structure and physiology, mice develop a skeletal aging phenotype that includes age-related cortical porosity[118]. In this current study, untreated aging mice had lower cortical thickness and cortical area as well as ~6% higher femoral cortical porosity, demonstrating age-induced cortical bone alterations. Although intracortical osteonal remodeling is not part of normal rodent bone physiology, rodents with CKD still develop cortical porosity like humans. We hypothesize there are overlapping mechanisms driving pore development in both species, likely driven though the initiation of resorption by osteoclasts from the endocortical surface that then tunnel through the cortical bone.

In humans and rodents, high circulating PTH is associated with loss of cortical bone and cortical porosity development[33,40,119]. With patients that have declining renal function, serum PTH can be dysregulated and rise uncontrollably[120]. In this current study, our results are

consistent with previous studies that demonstrate that adenine-induced CKD results in elevated PTH[40,65,110]. Importantly, our study shows that aging mice fed adenine had elevations in PTH that were notably higher compared to young AD, specifically 72% higher than young AD mice. The mechanisms leading to more robust PTH response to CKD in aging mice is not known, but it indicates that alterations caused by impaired renal function may be exacerbated by age.

While age-related cortical porosity occurs slowly, CKD-induced cortical porosity in both rodents and humans changes rapidly over time[33,121]. Evaluation of CKD patients demonstrates 4-5% loss of cortical bone density per year[122], illustrating that CKD more rapidly and significantly affects the cortical bone than aging. CKD produces robust cortical porosity, even in younger rodents[40,110], but how this impacts porosity in aging animals is less understood. In the present study, aging AD mice had 78% higher femoral cortical porosity than young AD mice and 63% higher femoral porosity than age-matched counterparts. Previously, Heveran et. al (2019) examined young (12-week) and old (84-week) mice with 5/6-nephrectomy and found that the reduced bone material quality in CKD was distinct from age-related bone quality changes, but no differences in cortical porosity were observed[123]. In our study, adenine-induced CKD caused 4.2-fold higher PTH in young mice and 9-fold higher PTH in aging vs. age-matched counterparts, while the 5/6-nephrectomy in Heveran et. al caused ~2-fold higher PTH across both ages[123]. Since high PTH is associated with cortical porosity in CKD, we hypothesize this difference, namely the higher PTH induced by the adenine model, was largely responsible for the adenine-induced cortical porosity and the heightened porosity development in the aging mice. Unlike our previous study[40], this study did not measure PTH across the experimental timeline, so we can only speculate that the elevated cortical porosity in adenine mice was mediated largely by elevated PTH levels. This result reiterates the importance of PTH in cortical porosity development and certainly supports the clinical approach of controlling PTH levels in CKD patients.

Along with increases in cortical porosity, adenine-induced CKD also resulted in lower cortical thickness and cortical bone area, but no differences between young and aging mice were observed. Because cortical bone is closely linked to the mechanical strength of bone, deterioration of cortical bone, through porosity and cortical thinning, is associated with a decline in mechanical properties. Previously, we demonstrated adenine-induced CKD in male mice reduced structural properties, including ultimate force and stiffness, while estimated material properties, such as toughness, showed no difference between CON and AD[110]. In the current study, there were independent effects of age and disease on both structural and material properties, although no interaction effects were observed. Interestingly, the aging AD mice even with higher cortical porosity did not have greater alterations in mechanical properties vs. the young AD mice. These findings allude to a potential compensatory mechanism that may occur within aging bone to preserve bone mechanical properties despite increasing cortical porosity. Analysis of total bone area and periosteal perimeter of tibiae showed no differences across groups, indicating that periosteal expansion is not a likely compensatory mechanism in this model.

Limitations of the current study include the use of only male mice. We chose to utilize male mice, because we previously showed that with aging, male mice exhibit higher PTH and cortical porosity than aging, female mice without kidney disease[111]. However, this prior study found sex-based differences in regulation of phosphate metabolism in young and aging mice[111], so future studies should assess whether sex-based differences would also be observed in aging mice with CKD. As our focus was on the skeletal manifestations, we used BUN to assess the presence/absence of altered kidney function. We acknowledge that measures, such as GFR or creatinine, can be more specific, and therefore our study is limited in its ability to determine the extent of kidney function or if interactions between aging and CKD occurred with respect to kidney function. The adenine-induced CKD model in mice does cause reduced food intake, which may cause protein malnourishment and lead to metabolic acidosis[124,125]. How each of

these components contributes to disease progression and the skeletal phenotype is not addressed by this work. Finally, our study utilized a relatively small sample size for mechanics, which could have affected our ability to find significant interaction effects.

In conclusion, these data demonstrate that combining aging and CKD leads to an exacerbated cortical porosity phenotype that appears linked to the differential elevations of PTH. This highlights the importance of assessing mechanisms and potential interventions in both young and aged animals to translate to a broader spectrum of CKD patients.

Acknowledgements

3.5 Supplementary Figures

Control Bone   **CKD Bone**
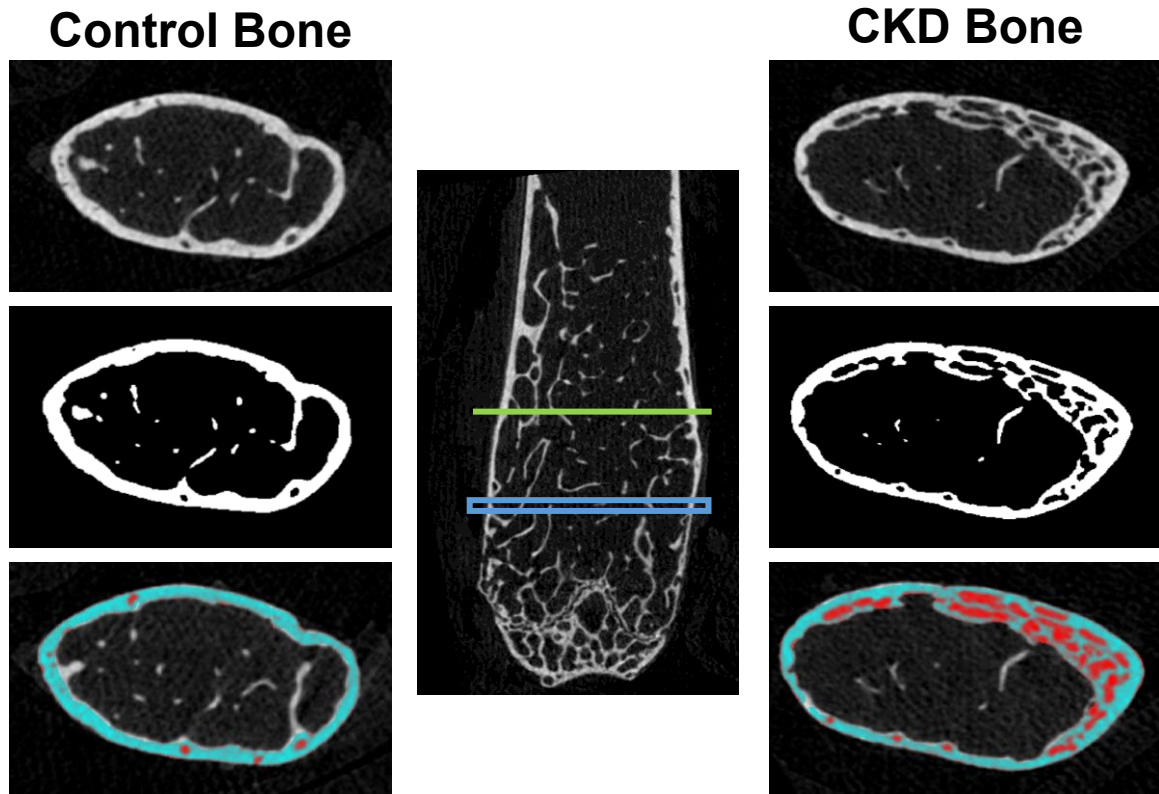
Supplementary Figure 1: MicroCT region of interest for cortical bone of distal femur. Middle image shows anatomical location of femoral analyses (blue box – trabecular ROI and green line – cortical ROI). Representative images for control and CKD bone demonstrate: raw image (top), binary image (middle), and cortical ROI (bottom).

CHAPTER 4

ROMOSOZUMAB TREATMENT IMPROVES TRABECULAR AND CORTICAL BONE IN
HEALTHY YOUNG AND AGING MICE

4.1 Introduction

Osteoporosis is the most common skeletal disorder in the world and is characterized by low bone mass and deterioration of bone microarchitecture[126]. In 2010, 10.2 million people aged 50 and older had osteoporosis and an additional 43.3 million people suffered from low bone mass[7]. Because people are living longer, these numbers will continue to grow, underscoring the importance of finding effective therapies to improve bone quantity and quality.

Modeling is the process by which bones are initially formed and involves uncoupled bone formation and/or bone resorption. However, bone loss associated with osteoporosis is tied to changes in the bone remodeling cycle. In a healthy state, there is a coupling of bone remodeling with bone resorption followed by bone formation at the same spatial location over time, thereby the removal of old bone is replaced with new bone. For this process to be fully coupled, the relative amounts of resorption and formation should be equal (although every remodeling unit is known to have a slight negative bone balance). However, with aging or estrogen deficiency (i.e., menopause), overall resorption is greater than the overall formation (most often due to less activity and/or lower numbers of osteoblasts), which leads to a greater negative bone balance and thus loss of bone with each remodeling cycle[6]. Loss of both trabecular and cortical bone contributes to overall bone loss; trabecular bone loss primarily involves thinning of trabeculae, while cortical bone loss involves an increased number of resorption cavities (called pores)[127].

Osteoporosis therapies fall into one of two broad categories – anti-resorptive and anabolic treatments. Anti-resorptive drugs include bisphosphonates (BPs), which bind to the bone due to high affinity for hydroxyapaptite[128]. BPs inhibit osteoclast activity, thus reducing bone resorption. Denosumab, another anti-resorptive agent, interferes with RANK-RANKL binding, a crucial step in osteoclastogenesis, leading to decreased osteoclast formation and activity. Although anti-resorptives are often the first-line therapy for treating osteoporosis, they are known to blunt the effects of anabolic therapy when used in combination or when administered years later.

Anabolic drugs, including teriparatide and romosozumab, increase bone formation. Teriparatide, intermittently administered parathyroid hormone (PTH), stimulates increased bone turnover, both formation and resorption, but the dosing regimen leads to net gain of bone mass. Romosozumab stimulates the Wnt signaling pathway by inhibiting sclerostin, thereby increasing bone formation[129]. Unlike teriparatide, romosozumab decreases the activation of remodeling while increasing the activation of modeling; therefore, romosozumab treatment results in increased bone formation and decreased bone resorption, which is advantageous for building bone mass rapidly[130].

This study was a pilot study to determine whether romosozumab is an effective anabolic agent in aging versus young mice. Given that the bone formation rate and pool of osteoblasts is lower in aging mice, we sought to determine whether romosozumab is able to effectively stimulate bone formation in aging mice to the same degree as in younger mice. This pilot study was performed prior to exploring the effectiveness of combination treatment in aging mice.

4.2 Materials & Methods

4.2.1   *Animals*: Male C57Bl/6J mice were obtained from Jackson Laboratories (JAX stock #000-664, Bar Harbor, ME, USA) at 15- and 77-weeks of age (n=12/age) and group housed at an institutionally approved animal facility with 12h light/dark cycles. After one week of acclimatization, all mice were fed a grain-based diet (2018SX, Envigo-Teklad Diets, Madison, WI, USA) for four weeks. Once weekly, half of the mice of each age were injected subcutaneously with romosozumab (10mg/kg; Amgen, Thousand Oaks, CA). Body weight was measured weekly, and animals were monitored for health daily. All mice were injected with fluorochrome calcein labels 7 and 2 days prior to euthanasia. Following euthanasia, both femurs of each animal were fixed in 10% neutral buffered saline. All animal procedures were approved by the Indiana University School of Medicine Institutional Animal Care and Use Committee prior to the initiation of experimental protocols, and methods were carried out in accordance with relevant guidelines and regulations.

4.2.2   *Ex Vivo Micro-Computed Tomography of the Femur*: Distal femora were scanned on a SkyScan 1172 system (Bruker, Billerica, MA, USA) with a 0.5 aluminum filter and an 8μm voxel size using a custom holder that allows scanning of 3 bones at a time[112]. Trabecular bone architecture was analyzed from a 1mm region of interest (ROI) just proximal to the distal growth plate as previously described[131]. Measures of trabecular bone included bone volume fraction/total volume, trabecular thickness, trabecular number, and trabecular spacing. Cortical bone geometry was analyzed from five contiguous slices ~2.5mm proximal to the distal growth plate. Measures of cortical bone included cortical bone area, cortical thickness, and cortical porosity. Cortical porosity was determined by assessing void area between the periosteal and endosteal surfaces, presented as a

percentage of overall cortical bone area. All nomenclature followed standard recommendations[87].

4.2.3 *Histomorphometry*: Undemineralized right distal femurs were fixed in neutral buffered formalin, subjected to serial dehydration, and then embedded in methyl methacrylate (Sigma Aldrich, St. Louis, MO). Serial frontal sections (4µm-thick) were cut and left unstained for analysis of fluorochrome calcein labels. Histomorphometric analyses were performed using BIOQUANT (BIOQUANT Image Analysis, Nashville, TN). A standard region of interest of trabecular bone excluding primary spongiosa and endocortical surfaces was utilized. Total bone surface (BS), single-labeled surface (sLS), double-labeled surface (dLS), and interlabel distances were measured at 20X magnification. Mineralized surface to bone surface (MS/BS; [dLS+(sLS/2)]/BS*100), mineral apposition rate (MAR; average interlabel distance/5 days), and bone formation rate (BFR/BS; MS/BS*MAR*3.65) were calculated. All nomenclature for histomorphometry follows standard usage[132].

4.2.4 *Statistical Analyses*: Statistical analyses were completed in SPSS Statistics 27 (IBM, Armonk, NY, USA). Data were analyzed as a 2x2 factorial ANOVA (age-by-treatment) with main effects of treatment (no treatment vs. romosozumab), age (young versus aging), and treatment-by-age interactions and effect sizes (ES) noted. When the 2x2 ANOVA was statistically significant ($p<0.05$), an all-groups Duncan's multiple range test post-hoc analysis was applied to determine individual group differences. All data are presented as mean ± standard deviation.

4.3 RESULTS

4.3.1 *Romosozumab treatment had no effect on body weight in either age.*

Over the course of the study, there was no statistical difference in body weight between treatment groups or between ages (**Figure 14**).
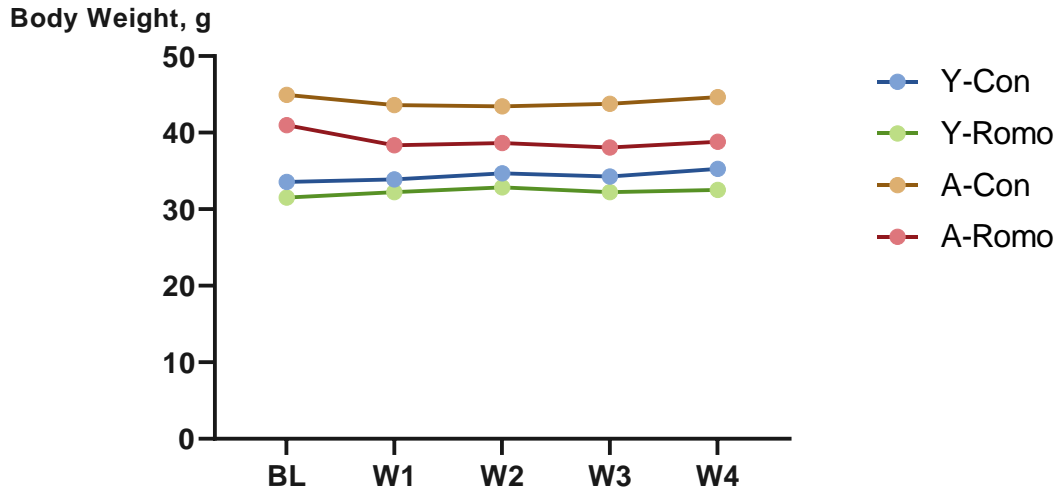
Figure 14: There was no statistical difference in body weight between treatment groups or between ages.

4.3.2   *Both age and treatment influenced trabecular bone parameters.*

Both age (p=0.015, ES=0.263) and treatment (p<0.0001, ES=0.658) affected femoral bone trabecular volume fraction; however, there was no age-by-treatment interaction effect. Aging mice had 62% higher BV/TV when treated with romosozumab than age-matched controls, while young mice had 33% higher BV/TV when treated with romosozumab than age-matched controls (**Figure 15A**).
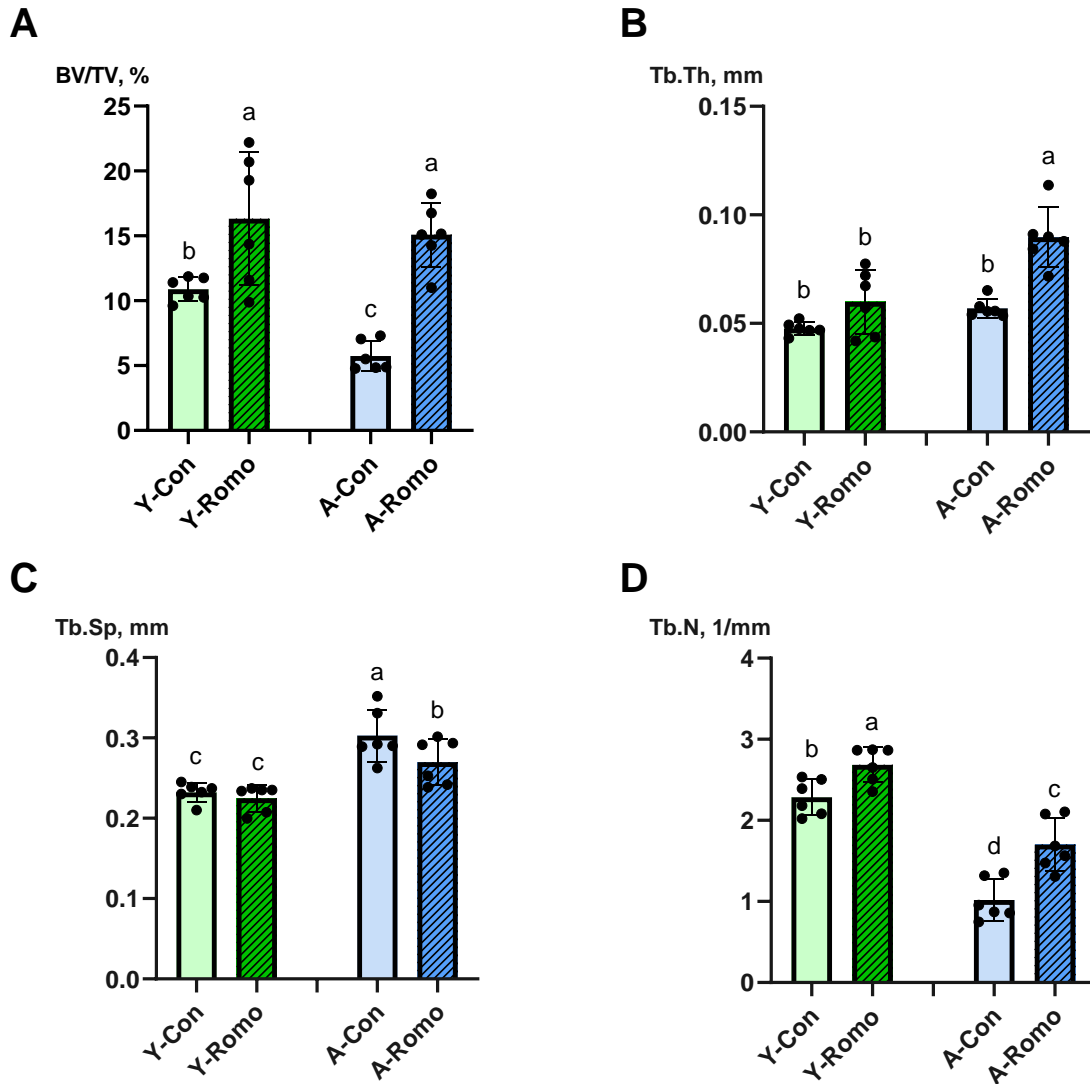
Figure 15: Romosozumab (Romo) treatment improved trabecular bone architecture over control (Con) in young (Y) and aging (A) mice after 4 weeks of treatment. **A** BV/TV was highest in romosozumab-treated animals regardless of age. **B** Trabecular thickness was higher with romosozumab treatment in aging and young animals. **C** Trabecular separation was highest in aging control mice. **D** Romosozumab treatment led to higher trabecular number in both aging and young mice. Data are presented as mean ± standard deviation. Bars with different letter notations are statistically different from each other (p<0.05).

There was an age-by-treatment interaction for femoral trabecular thickness (p=0.026, ES=0.225). With romosozumab treatment, aging mice had 37% thicker trabeculae, and young mice had 20% thicker trabeculae (**Figure 15B**). Aging mice, regardless of treatment, had higher trabecular thickness than young mice; with romosozumab treatment, the aging mice had the highest trabecular thickness of all groups. There was an age effect (p<0.0001, ES=0.636) for femoral trabecular separation, but no treatment or interaction effects (**Figure 15C**). There were age (p<0.0001, ES=0.85) and treatment (p<0.0001, ES=0.569) effects for femoral trabecular number. Regardless of age, romosozumab treatment led to a higher number of trabeculae. With romosozumab treatment, aging mice had 40% higher trabecular number and young mice had 15% higher trabecular number (**Figure 15D**).

4.3.3 *Although cortical porosity was not different across groups, cortical bone area and thickness improved with treatment.*

There were no significant differences between groups for cortical porosity (**Figure 16A**). For cortical bone area, there was an age-by-treatment interaction effect (p=0.005, ES=0.335). Regardless of treatment, the aging mice had higher cortical area (**Figure 16B**). With romosozumab treatment, aging mice exhibited 29% higher cortical bone area than age-matched controls while young mice only had 11% greater cortical bone area than age-matched controls. There was also an age-by-treatment interaction effect (p=0.012, ES=0.275) for cortical thickness. Regardless of age, the romosozumab-treated mice had thicker cortices (**Figure 16C**). Romosozumab treatment resulted in 25% higher cortical thickness in aging

mice and 10% higher cortical thickness in young mice compared to age-matched control groups.
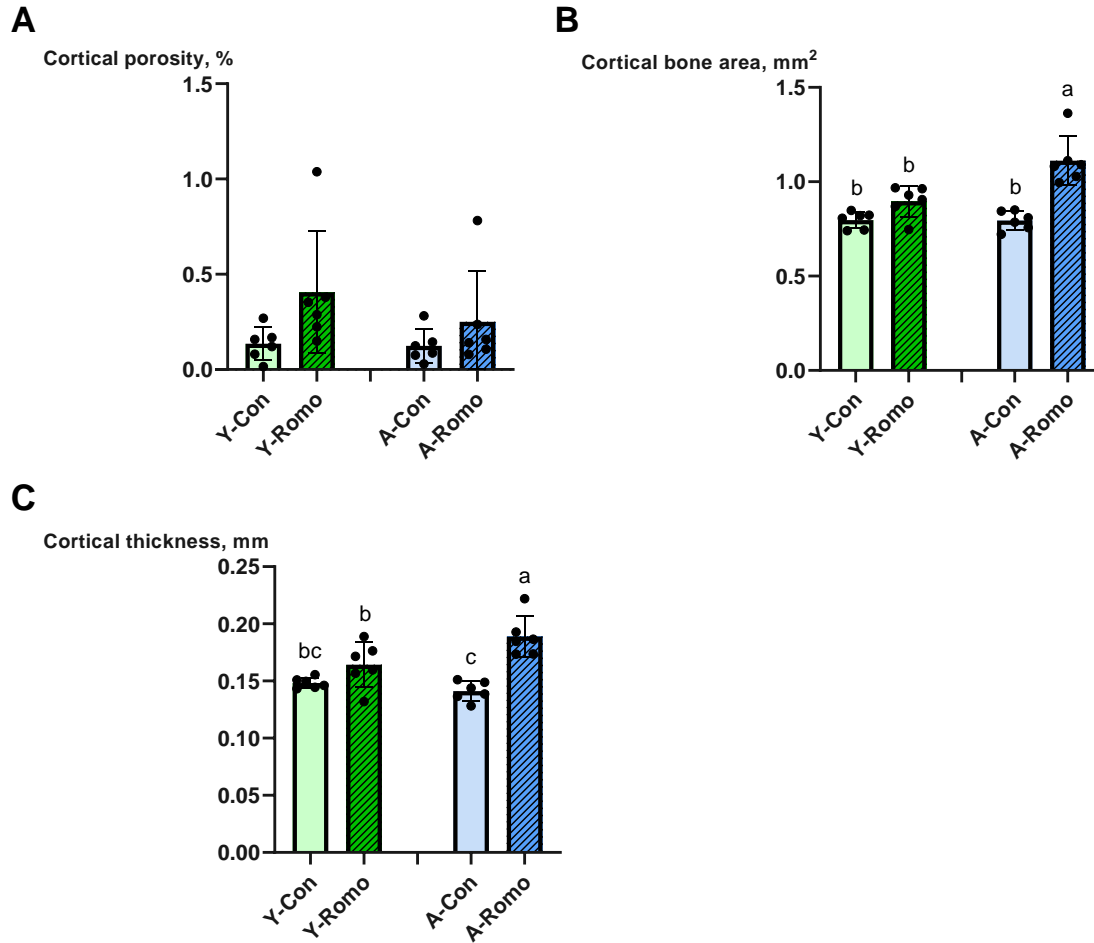
Figure 16: Romosozumab (Romo) treatment improved cortical bone properties over control (Con) in young (Y) and aging (A) mice after 4 weeks of treatment. **A** There were no differences in cortical porosity between ages or treatment groups. **B** Romosozumab treatment led to higher cortical bone area in aging and young mice. **C** There was a main effect of treatment ($p < 0.0001$) and an age-by-treatment interaction ($p = 0.012$) for cortical thickness. Data are presented as mean ± standard deviation. Bars with different letter notations are statistically different from each other ($p < 0.05$).

4.3.4 *There was an influence of age but not treatment on histomorphometry-based bone*

formation.

Although there were no treatment or age-by-treatment interaction effects, there were age effects for all parameters. Mineralizing surface to bone surface (MS/BS) was 30% higher in young mice compared to aging mice regardless of treatment; there were no differences between control and romosozumab-treated animals (**Figure 17A**). Similar patterns were also observed for mineral apposition rate (MAR) and bone formation rate (BFR) (**Figure 17B and 17C**).
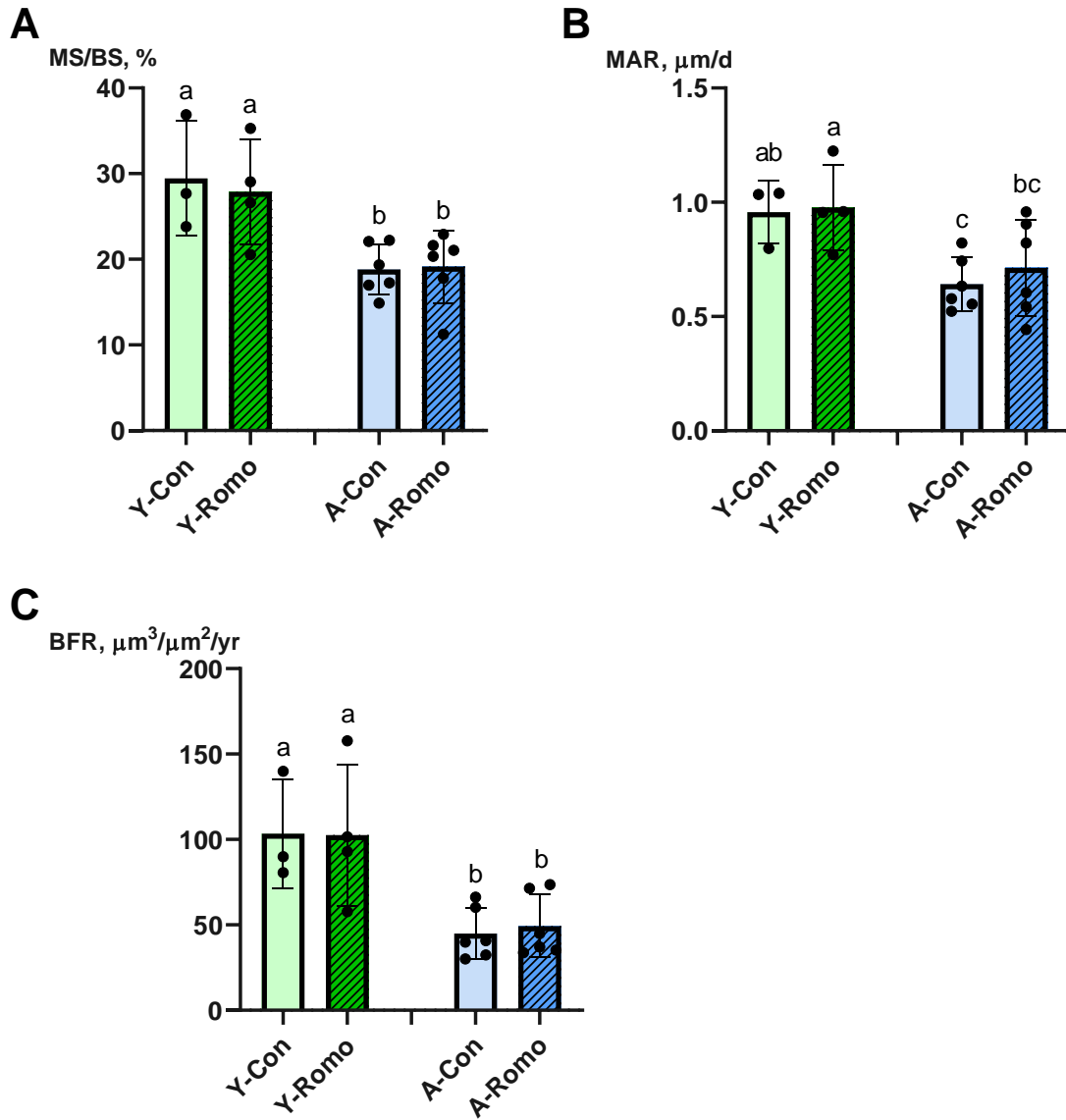
Figure 17: Romosozumab (Romo) treatment had no effect on trabecular bone formation properties compared to control (Con) in young (Y) and aging (A) mice after 4 weeks of treatment. **A** Mineralizing surface per bone surface (MS/BS) was higher in young mice regardless of treatment. **B** Mineral apposition rate (MAR) was higher in young mice regardless of treatment. **C** Bone formation rate (BFR) was higher in young mice compared to aging mice regardless of treatment. Data are presented as mean ± standard deviation. Bars with different letter notations are statistically different from each other (p<0.05).

4.4 DISCUSSION

The primary finding of this study is that romosozumab treatment can improve bone microarchitecture, both trabecular and cortical, in young and aging mice. Although histomorphometric measures demonstrated little change at the time point measured, the structural data for both trabecular and cortical bone illustrates the effectiveness of romosozumab.

Romosozumab has received increasing attention as a potential osteoporosis therapy. Phase I clinical trials utilizing romosozumab have shown stimulation of bone formation and inhibition of bone resorption in healthy men and postmenopausal women[61]. More specifically, healthy men and postmenopausal women demonstrate a dose-dependent increase in bone formation markers, including procollagen 1 intact N-terminal propeptide (P1NP) and bone alkaline phosphatase (BAP), and a dose-dependent decrease in bone resorption markers, including serum C-terminal telopeptide (CTX)[61]. Phase II clinical trials demonstrated that postmenopausal women treated with romosozumab had larger gains in bone mineral density than treatment with alendronate or teriparatide[60]. Phase III clinical trials in men and women with osteoporosis showed increased bone mineral density after 1-year of treatment with romosozumab, indicating that romosozumab is an effective osteoporosis treatment in both men and women[62,133]. Traditional aging studies would typically use mice of at least 2 years of age, while our mice are more consistent with a middle-aged population. In each of the clinical trials previously discussed, the men and women ranged from 40-85 years of age, which is consistent with a mostly middle-age human population and thus the animal ages utilized in the current study.

Research with both ovariectomized rats and gonad-intact female cynomolgus monkeys demonstrate increased trabecular and cortical bone mass and associated gains in bone

mineral density (BMD)[134,135]. Unlike combining parathyroid hormone and bisphosphonates, the effects of romosozumab are not blunted when combined with a bisphosphonate[136], creating the potential for combination anti-resorptive and anabolic therapy. When comparing romosozumab with teriparatide in young rats, romosozumab increased trabecular bone mass in 4 weeks and maintained bone formation rate for over one month superior to teriparatide[137]. Our study builds on previous pre-clinical studies by evaluating the effectiveness of romosozumab in aging mice, data that is surprisingly lacking in the literature.

Our study is consistent with previous studies that demonstrate higher trabecular and cortical bone following treatment in non-aged animals. Most importantly, our study shows that romosozumab treatment had a greater percent difference in trabecular bone volume from age-matched controls in aging mice compared to young mice. Despite the lower basal bone formation rate in aging mice, the romosozumab treatment appeared to stimulate a strong anabolic response in the early treatment phase based on the change in bone volume. An increase in bone formation rate was not detected within the last week of the treatment when fluorochrome labels were given in this study, which suggests the anabolic potential is early in treatment. Although unlikely, an alternate interpretation is that romosozumab suppressed osteoclasts, which could also explain the change in bone mass without a concurrent change in bone formation rate. Additionally, strong increases to cortical bone area and cortical thickness may contribute to reduced fracture risk, which is the key outcome for utilization of romosozumab in patients. This data is promising when aging is overlaid with another disease that negatively affects bone, such as chronic kidney disease.

Limitations of our study include the use of only male mice and the small sample sizes. We chose to utilize male mice, because we previously showed that with aging, male mice exhibit more cortical porosity than aging, female mice in the absence of kidney disease[111]. However, this prior study found sex-based differences in regulation of phosphate metabolism in young and aging mice[111], so future studies should assess whether sex-based differences

would also be observed with romosozumab treatment. The small sample size was due to the overall goal of the study, which was to confirm that romosozumab doses used in young mice were anabolic in aging mice. Another limitation of the current study pertains to histomorphometry. By analyzing the bone at the end of the study, we appear to have missed the window of bone formation following once-weekly romosozumab administration; however, the strong increases in trabecular and cortical bone seen with micro-CT illustrate that the drug was effective and recapitulated previous results.

In conclusion, these data demonstrate that romosozumab treatment effectively increases both trabecular and cortical structural bone properties in young and aging animals. This study highlights the usefulness of romosozumab as a therapy for aging bone.

CHAPTER 5

ROMOSOZUMAB ALONE OR IN COMBINATION WITH PTH SUPPRESSION

IMPROVES TRABECULAR AND CORTICAL BONE MICROARCHITECTURE AND

BONE MECHANICAL PROPERTIES IN AGING MICE WITH CKD

5.1 Introduction

Approximately 15% of adults in the United States have chronic kidney disease (CKD), which leads to a host of comorbidities including increased risk of fractures and greater fracture-related complications. The incidence of CKD increases with age. Those over the age of 65 comprise 38% of the total adult population with CKD[138]. Aging is also commonly associated with osteoporosis, which is recognized as the most common skeletal disorder in the world[10]. Due to deficits in bone quantity and quality, both aging and CKD decrease bone strength and increase in likelihood of fractures. This is due in part to the negative effects of CKD and aging on cortical bone with both leading to cortical thinning and increased cortical porosity[40,110,111,131,139,140]. Cortical porosity is inversely related to bone mechanical properties and fracture[33,34,38,39]. Understanding how aging and CKD interact with respect to cortical bone structure and mechanics has important translational value for designing effective interventions.

Despite the high prevalence of CKD in the aging population, few clinical and pre-clinical studies have assessed these comorbid conditions together. One clinical study found higher 3-year fracture incidence with increasing stages of CKD regardless of age, but an even higher fracture incidence in patients over age 65[30]. Preclinical work in our lab found that aging mice with adenine-induced CKD has altered bone mechanical properties with significantly lower ultimate force and stiffness than aging control mice. Concurrently, femoral and tibial cortical porosity was ~77% higher in aging adenine mice compared to

young adenine mice[131]. These studies point to the negative impact of CKD in the aging skeleton due in part to an exacerbated phenotype of cortical porosity.

Secondary hyperparathyroidism is proposed to be a strong driver of the observed bone deficits in CKD, and many treatment options are aimed at reducing parathyroid hormone (PTH) levels. Patients with early-stage CKD can be given calcimimetics, such as cinacalcet, to mitigate elevations in PTH[50]. Cinacalcet has been shown to reduce fracture risk in patients on hemodialysis (stage 5 CKD) as compared to placebo, yet aging patients on treatment still had a higher risk of fracture than young patients[51]. In pre-clinical models, modulation of PTH through either calcium supplementation or use of calcimimetics[65,141,142] effectively reduces PTH levels and prevents or infills cortical pores depending on the administration period (before or after pore development). However, reducing PTH alone may not be sufficient to mitigate cortical porosity or mechanical fragility, particularly in aging bone where declines in bone formation may hinder the ability to reverse/infill cortical pores. Romosozumab, a humanized monoclonal sclerostin antibody approved for use in osteoporosis, uses PTH-independent mechanisms to increase osteoblast activity, making it an attractive therapeutic for CKD[58]. In post-menopausal women with osteoporosis from both the FRAME and ARCH studies, post-hoc analyses across mild and moderate levels of renal function showed that patients had increased bone mineral density and lower risk of vertebral fractures[58]. The impact in later-stage CKD and how it alters cortical bone is unknown.

The purpose of this study was to assess romosozumab treatment with and without concurrent PTH suppression on bone microarchitecture and mechanical properties in aging mice with adenine-induced CKD. Previously, we demonstrated that calcium suppression through calcium water effectively reduced circulating PTH and reversed cortical porosity in skeletally mature adenine-induced CKD mice[65]. We hypothesized that romosozumab

with concurrent PTH suppression (via calcium water) would most effectively reverse cortical porosity and improve mechanical properties in aging mice with CKD.

5.2 Materials and Methods

5.2.1 *Animals*

Male C57Bl/6J mice were obtained from Jackson Laboratories (JAX stock #000-664, Bar Harbor, ME, USA) at 66 weeks of age (n=154) and group housed at an institutionally approved animal facility with 12h light/dark cycles. After one week of acclimatization, all mice were switched to a casein-based diet with adjusted calcium and phosphorus (0.9% P, 0.6% Ca). Half of the mice were given the same casein-based diet with 0.2% adenine (AD; Envigo-Teklad Diets, Madison, WI, USA) to induce CKD while the remaining mice served as age-matched controls (CON). After six weeks on the adenine diet, the AD mice were switched to the casein diet for the remainder of the study.

At 8 weeks, mice were placed into one of the following treatment groups and received their respective treatment for four weeks: 1) calcium water (Ca), 2) romosozumab (Romo), or 3) combination calcium water and romosozumab (Combo). For calcium water supplementation, 3% calcium gluconate water was provided ad libitum; all other groups remained on standard purified drinking water. For romosozumab treatment, mice were injected subcutaneously with romosozumab once weekly (10mg/kg; Amgen, Thousand Oaks, CA).

Body weight was measured weekly, and animals were monitored for health daily. Animals were euthanized via exsanguination under isoflurane anesthesia, and blood was collected from the heart for biochemical analyses. One femur and one tibia were fixed in 10% neutral buffered formalin, and one tibia and one femur were placed in saline-soaked gauze and frozen. All animal procedures were

73

approved by the Indiana University School of Medicine Institutional Animal Care and Use Committee prior to the initiation of experimental protocols, and methods were carried out in accordance with relevant guidelines and regulations.

The study was completed across two different cohorts. The first cohort was initiated with 71 mice, but 14 mice died or had to be euthanized prior to study endpoint (20% attrition rate). The second cohort was initiated with 83 mice, but 28 mice died or had to be euthanized prior to study endpoint (34% attrition rate). Thus, our final animal number was 113 (n=8-14/group).

5.2.2   Serum Biochemistries

Cardiac blood collected at the time of termination was used to measure serum blood urea nitrogen (BUN) (BioAssay Systems, Hayward, CA, USA) via colorimetric assays. P1NP and CTX (IDS, East Boldon, UK) and serum parathyroid hormone (Immutopics Quidel, San Diego, CA, USA) were measured via ELISA as previously described[40].

5.2.3   Ex Vivo Micro-Computed Tomography of the Femur

Distal femora were scanned on a SkyScan 1172 system (Bruker, Billerica, MA, USA) using a custom holder that allows scanning of 3 bones at a time[112] with the following settings: 60kV, medium camera, 0.5 aluminum filter, frame averaging of 2, 0.7 rotation step, and 8μm voxel size. Trabecular bone architecture was analyzed from a 1mm region of interest (ROI) just proximal to the distal growth plate. Measures of trabecular bone included bone volume/total volume, trabecular thickness, trabecular number, and trabecular spacing. Cortical bone geometry was analyzed from five consecutive slices ~2.5mm proximal to the distal growth plate in a region proximal to the trabecular bone of the distal femur as previously

described[131]. Measures of cortical bone included cortical bone area, cortical thickness, and cortical porosity. Cortical porosity was determined by assessing void area between the periosteal and endosteal surfaces, presented as a percentage of overall cortical bone area. ROIs were hand-drawn with a binary threshold of 100-255. All nomenclature followed standard recommendations[87].

Tibial midshafts were group-scanned using the SkyScan 1176 system (Bruker, Billerica, MA, USA) with a 0.5 aluminum filter and a 9µm voxel size to assess geometric properties (cortical area, cross-sectional moment of inertia) for stress/strain calculations following mechanical testing.

5.2.4 Four-Point Bending of the Tibia

Tibiae underwent four-point bending (TA Instruments, New Castle, DE, USA) as previously described[111]. Briefly, bones were thawed to room temperature soaked in PBS. The anterior surface was placed on two metal supports located ±9mm from the mid-diaphysis testing site, and the upper supports were centered on the bone with a span of ±4mm. Specimens were loaded to failure at a rate of 0.025mm/sec, producing a force-displacement curve for each sample. Structural mechanical properties (yield/ultimate load, pre-yield/post-yield/total displacement, and pre-yield/post-yield/total energy to failure) were obtained directly from the curves using a MATLAB code, while estimated material properties (ultimate stress, elastic modulus, strain, resilience, total toughness) were derived from force-displacement curves and geometric properties noted above using standard beam-bending equations for four-point bending.

Bone resistance to crack propagation was assessed using a linearly elastic fracture toughness testing approach[143]. Right femora were notched at the anterior mid-diaphysis using a low-speed sectioning saw (Buehler, Lake Bluff, IL, USA) not more than halfway through the medullary cavity. The notch was sharpened using a scalpel coated with a 1μm diamond suspension. Femora were loaded in three-point bending with the notched surface in tension, and the crack was advanced until failure. Marrow was removed and femora were dehydrated using a vacuum pump. After gold sputtering, the crack surface was imaged using a scanning electron microscope (JEOL, Akishima, Tokyo, Japan). Stable and unstable crack lines were identified using a custom MATLAB script, and the cortical bone geometry was used to calculate the stress intensity factors for crack initiation and maximum load.

5.2.6 Statistical Analysis

Statistical analyses were completed in SPSS Statistics 27 (IBM, Armonk, NY, USA). Data were analyzed as a 2x2x2 factorial ANOVA (adenine-calcium-romosozumab) with all main and interaction effects noted. When the 2x2x2 ANOVA was statistically significant ($p < 0.05$), an all-groups Duncan post-hoc analysis was applied to determine individual group differences. All data are presented as mean ± standard deviation.

5.3 Results

5.3.1 Animal losses during the study period

During the 8-week CKD induction and maintenance period, 24 adenine mice were found dead and 13 needed to be euthanized, while one control was found dead and

none needed to be euthanized. All mice that were found dead had no changes in body weight or appearance prior to being found dead. During the four-week treatment period, no untreated adenine mice were euthanized and one was found dead, one adenine calcium mouse was euthanized and 3 were found dead, 2 romosozumab mice were euthanized and 2 were found dead, and within the combination treatment group, none were euthanized and 2 were found dead. In the control groups, no mice were euthanized or found dead during the four-week treatment period. The majority of the losses were in the induction phase of CKD and not due to treatment.
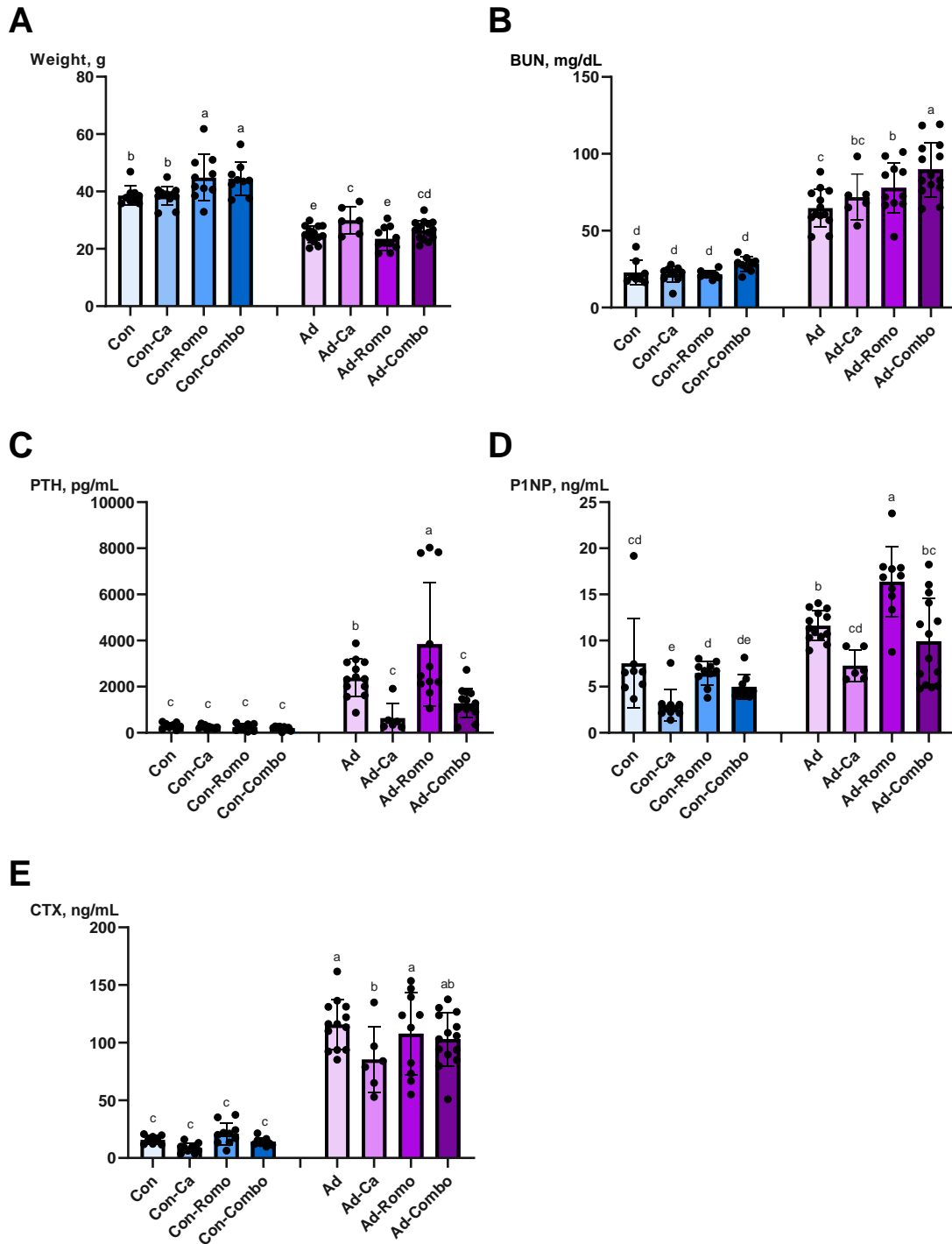
Figure 18: Biochemical parameters reveal interactions between aging and CKD that were altered with PTH suppression and anabolic treatment. **A** Adenine groups (Ad) had lower endpoint body weight (p<0.0001) compared to control (Con) with interaction effects of adenine-calcium

(p=0.044) and adenine-romosozumab (p<0.0001). **B** Blood urea nitrogen (BUN) was highest in adenine groups compared to control (p<0.0001) with an interaction effect of adenine-romosozumab (p=0.023). **C** Parathyroid hormone (PTH) was highest in adenine animals (p<0.0001) with interaction effects of adenine-calcium (p<0.0001) and adenine-romosozumab (p=0.031). **D** Procollagen type I N-terminal propeptide (P1NP) was highest in romosozumab-treated animals (p=0.004) with an interaction effect of adenine-romosozumab (p=0.025). **E** Carboxy-terminal collagen crosslinks (CTX) was highest in adenine animals compared to control (p<0.0001) but no interaction effects. Data are presented as mean ± standard deviation. Bars with different letter notations are statistically different from each other (p<0.05).

5.3.2   *Adenine-fed animals had significantly lower endpoint body weight.*

There was a main effect of adenine (p<0.0001) with animals having lower body weight compared to controls. There were also significant interaction effects of adenine-calcium (p=0.044) and adenine-romosozumab (p<0.0001). The control romosozumab-treated groups had the highest endpoint body weight, and the adenine and adenine-romosozumab animals had the lowest endpoint body weight (**Figure 18A**).

5.3.3   *PTH levels were attenuated with the addition of calcium water while romosozumab treatment led to higher PTH and BUN.*

For blood urea nitrogen (BUN), there were main effects of adenine (p<0.0001), calcium (p=0.03), and romosozumab (p=0.002) and an adenine-romosozumab interaction effect (p=0.023). BUN was higher in all adenine-fed groups compared to control groups (**Figure 18B**). Both romosozumab and combination treatment adenine groups had BUN levels significantly higher than adenine control.

Parathyroid hormone (PTH) levels exhibited main effects of adenine ($p<0.0001$) and calcium ($p<0.0001$), and interaction effects for adenine-calcium ($p<0.0001$) and adenine-romosozumab ($p=0.031$). Overall, the adenine-fed animals had higher PTH levels than controls, with the romosozumab-treated group having the highest levels of all groups (38% higher versus untreated adenine) (**Figure 18C**). Calcium water decreased PTH in both adenine-treated groups, approximately 45-75% lower than untreated adenine and statistically similar to controls.

5.3.4   *Romosozumab treatment led to higher overall bone formation P1NP levels, which were normalized with the addition of calcium water.*

Procollagen type I N-terminal propeptide (P1NP) had main effects of adenine ($p<0.0001$), calcium ($p<0.0001$), and romosozumab ($p=0.004$) and an adenine-romosozumab interaction ($p=0.025$). Adenine-fed animals had higher P1NP levels versus control, with untreated adenine 35% higher than untreated control, and the adenine romosozumab-treated group was 29% higher than untreated adenine (**Figure 18D**). With the addition of calcium water, P1NP levels were 40% and 23% lower in adenine and control animals, respectively.

Carboxy-terminal collagen crosslinks (CTX) had main effects of adenine ($p<0.0001$) and calcium ($p=0.01$). Adenine-fed animals had higher CTX levels regardless of treatment, and the adenine and adenine-romosozumab groups had the highest CTX levels (**Figure 18E**).
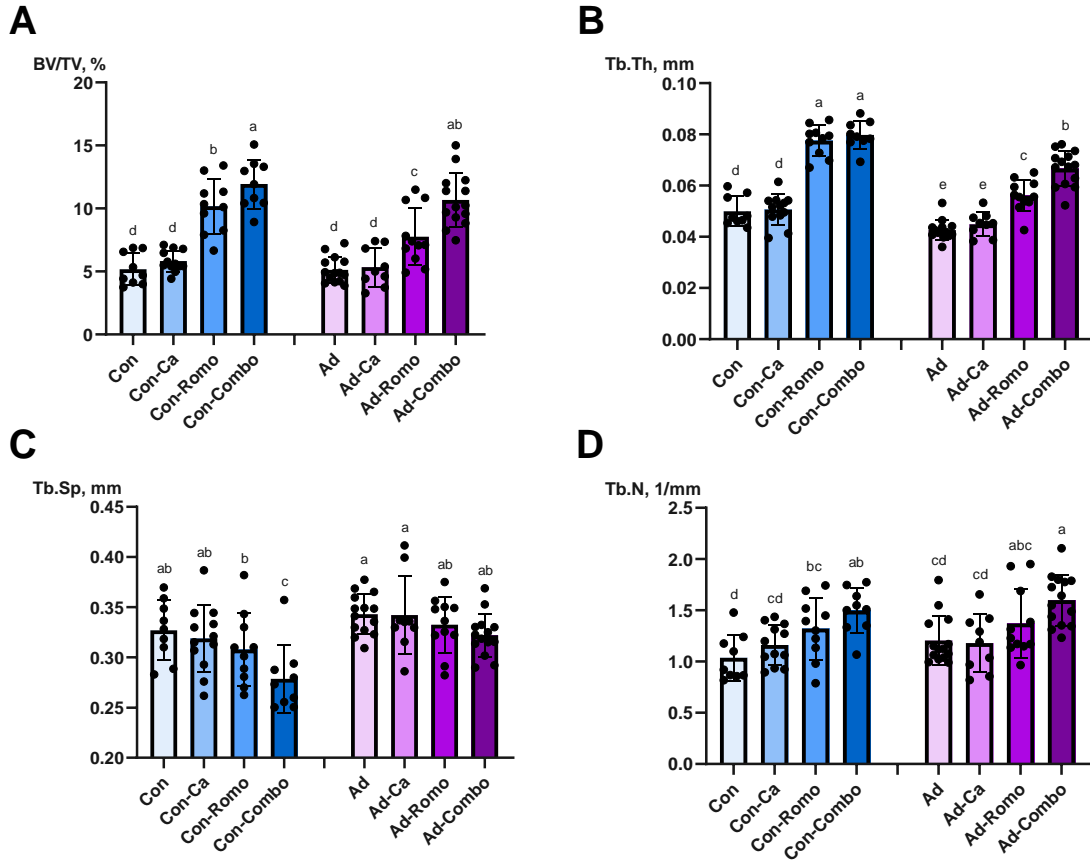
Figure 19: Trabecular microarchitecture is improved with PTH suppression and anabolic treatment in aging and aging-CKD. **A** Trabecular bone volume (BV/TV) was highest in romosozumab-treated groups (p<0.0001) with interaction effects of adenine-romosozumab (p=0.037) and calcium-romosozumab (p=0.012). **B** Trabecular thickness (Tb.Th) was highest in romosozumab-treated groups (p=0.001). **C** There were minimal differences in trabecular separation (Tb.Sp), with romosozumab treatment resulting in the lowest separation between trabeculae (p=0.001). **D** Trabecular number (Tb.N) was highest in animals receiving romosozumab (p<0.0001). Data are presented as mean ± standard deviation. Bars with different letter notations are statistically different from each other (p<0.05).

5.3.5 *Romosozumab treatment improved trabecular microarchitecture in both healthy and adenine-treated animals, and effects were amplified with the addition of calcium water.*

Trabecular bone volume (BV/TV) displayed main effects of adenine ($p=0.006$), calcium ($p<0.0001$), and romosozumab ($p<0.0001$), and interactions between adenine-romosozumab ($p=0.037$) and calcium-romosozumab ($p=0.012$). There were no differences in trabecular BV/TV between adenine and control groups for the untreated and calcium water animals; the addition of romosozumab led to higher BV/TV in both adenine and control mice. Regardless of disease state, the combination treatment resulted in the highest BV/TV, with no difference between the adenine-fed and untreated controls (**Figure 19A**).

For trabecular thickness (Tb.Th), there were main effects of adenine ($p<0.0001$), calcium ($p=0.002$), and romosozumab ($p<0.0001$) and an adenine-romosozumab interaction ($p<0.0001$). Adenine animals had lower trabecular thickness regardless of treatment compared to control animals. Regardless of disease, the combination treatment resulted in the higher trabecular thickness (**Figure 19B**). Although the romosozumab and combination treatments were no different in control animals, the combination treatment resulted in 18% higher trabecular thickness compared to romosozumab alone in adenine-fed animals.

For trabecular separation (Tb.Sp), there were main effects of adenine ($p<0.0001$) and romosozumab ($p=0.001$). Regardless of disease, the combination treatment resulted in the lowest trabecular separation, with romosozumab alone or in combination with calcium water being no different in the adenine-fed groups (**Figure 19C**).

For trabecular number (Tb.N), there were main effects of calcium (p=0.028) and romosozumab (p<0.0001). Trabecular number was highest in the combination treatment groups, with the adenine and control combination treatment groups being no different from one another (**Figure 19D**). Additionally, the combination treatment resulted in significantly higher trabecular number compared to the calcium water and untreated groups.
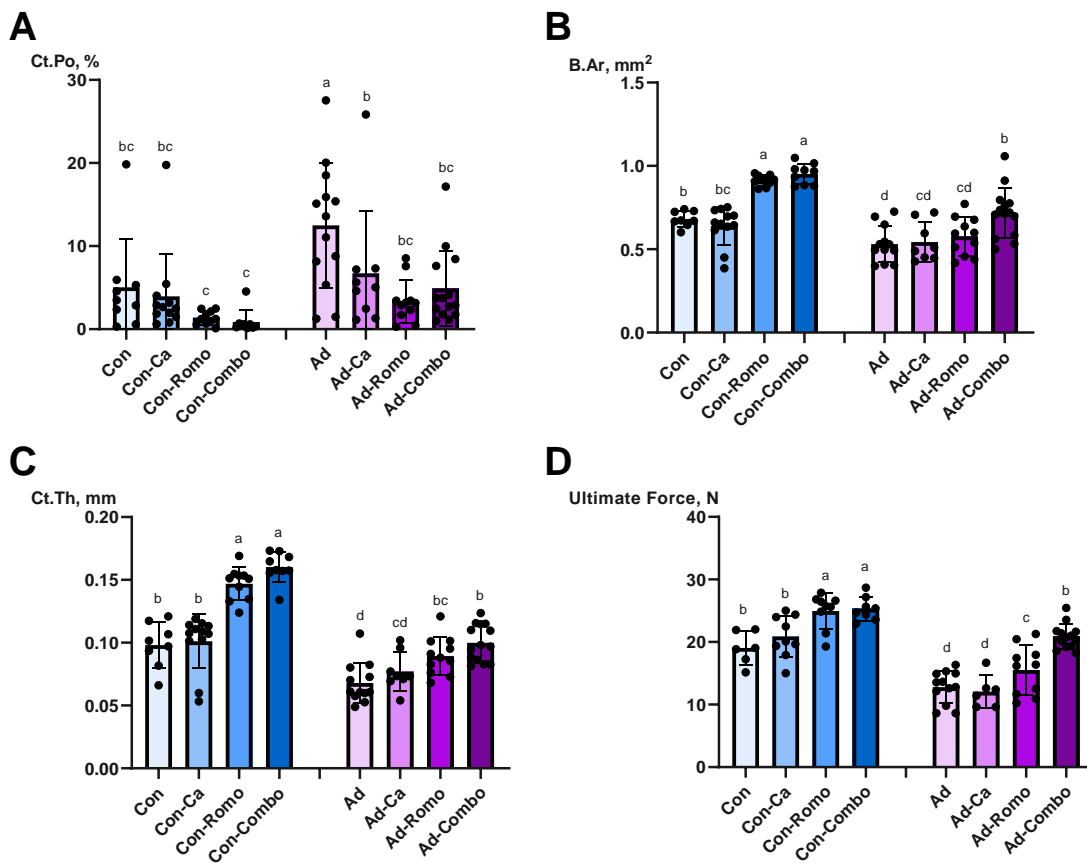
Figure 20: Cortical bone morphology and mechanical properties are improved with PTH suppression and anabolic treatment. **A** Femoral cortical porosity was highest in untreated adenine animals (p<0.0001) and was improved with romosozumab (p<0.0001). **B** Cortical bone area was highest in animals that received romosozumab (p<0.0001) with interaction effects of adenine-romosozumab (p=0.001) and calcium-romosozumab (p=0.027). **C** Cortical thickness was highest

in animals receiving romosozumab (p<0.0001) with an adenine-romosozumab interaction effect (p<0.0001). **D** Ultimate force was compromised with adenine (p<0.0001) but exhibited improvements with calcium (p=0.014) and romosozumab (p<0.0001), demonstrating an adenine-calcium-romosozumab interaction effect (p=0.007). Data are presented as mean ± standard deviation. Bars with different letter notations are statistically different from each other (p<0.05).

5.3.6   *Romosozumab treatment enhanced cortical bone parameters in healthy and adenine-fed animals, and effects were amplified with the addition of calcium water.*

Femoral cortical porosity had main effects of adenine (p<0.0001) and romosozumab (p<0.0001). Porosity was higher in the adenine animals, and all treatments had significantly lower porosity that was comparable with untreated controls (**Figure 20A**). The combination treatment reduced cortical porosity by 61% in adenine animals and 83% in control animals compared to the untreated groups.

Cortical bone area had main effects of adenine (p<0.0001) and romosozumab (p<0.0001) and interaction effects of adenine-romosozumab (p=0.001) and calcium-romosozumab (p=0.027). Cortical bone area was lower in adenine animals compared to control animals regardless of treatment. In adenine-treated animals, the combination treatment group had the highest cortical bone area and was statistically no different from the untreated control group (**Figure 20B**).

Cortical thickness had main effects of adenine (p<0.0001), calcium (p=0.014), and romosozumab (p<0.0001) and an adenine-romosozumab interaction (p<0.0001). Cortical thickness was lower in adenine animals compared to control animals

84

regardless of treatment. The control groups receiving romosozumab and combination treatment had the highest cortical thickness overall, but the same patterns were observed in adenine animals (**Figure 20C**). The adenine animals treated with romosozumab or combination treatment had cortical thickness no different from the control animals.

5.3.7   *Romosozumab treatment enhanced bone structural properties in healthy and adenine-treated animals, and the effect on ultimate force was amplified with the addition of calcium water.*

Ultimate force had main effects of adenine ($p<0.0001$), calcium ($p=0.014$), and romosozumab ($p<0.0001$) and an adenine-calcium-romosozumab interaction effect ($p=0.007$). Adenine-treated animals had lower ultimate force regardless of treatment compared to control animals. The control animals receiving romosozumab or combination treatment had the highest ultimate force; the adenine animals that received the combination treatment were statistically no different than the control animals, 39% higher than the untreated adenine group (**Figure 20D**). With combination treatment, ultimate force was 25% higher in control animals and 39% higher in adenine animals compared to the untreated disease-matched group.

For stiffness, there were main effects of adenine ($p<0.0001$) and romosozumab ($p<0.0001$). Adenine-treated groups had lower stiffness than control animals regardless of treatment. All treated control groups had higher stiffness versus untreated animals (**Table 4**). For the animals that received adenine, the romosozumab and combination treatments resulted in stiffness that was statistically similar to the untreated controls and significantly higher than untreated adenine.

85

For total work, there were main effects of adenine (p<0.0001) and romosozumab (p=0.018). Adenine groups had lower total work compared to control animals. The combination-treated adenine animals were not different from the untreated control animals (**Table 4**). Similar patterns were observed for ultimate stress and toughness.

Table 4: Trabecular bone architecture and bone mechanical and material properties.

	Con	Con-Ca	Con-Romo	Con-Combo	Ad	Ad-Ca	Ad-Romo	Ad-Combo
Trabecular bone volume/tissue volume (%)	5.18 ± 1.28[d]	5.82 ± 0.83[d]	10.18 ± 2.17[b]	11.94 ± 1.94[a]	5.13 ± 1.04[d]	5.34 ± 1.54[d]	7.76 ± 2.27[c]	10.67 ± 2.13[ab]
Trabecular thickness (mm)	0.05 ± 0.006[d]	0.05 ± 0.006[d]	0.08 ± 0.006[a]	0.08 ± 0.005[a]	0.04 ± 0.004[e]	0.04 ± 0.005[e]	0.06 ± 0.006[c]	0.07 ± 0.007[b]
Trabecular spacing (mm)	0.33 ± 0.03[ab]	0.32 ± 0.03[ab]	0.31 ± 0.04[b]	0.28 ± 0.03[c]	0.34 ± 0.02[a]	0.34 ± 0.04[a]	0.33 ± 0.03[ab]	0.32 ± 0.02[ab]
Trabecular number (1/mm)	1.04 ± 0.23[d]	1.16 ± 0.20[cd]	1.32 ± 0.30[bc]	1.50 ± 0.22[ab]	1.21 ± 0.24[cd]	1.18 ± 0.28[cd]	1.37 ± 0.34[abc]	1.60 ± 0.25[a]
Ultimate Force (N)	19.04 ± 2.66[b]	20.88 ± 3.33[b]	24.96 ± 2.81[a]	25.31 ± 1.88[a]	12.78 ± 2.59[d]	12.07 ± 2.61[d]	15.50 ± 3.96[c]	20.88 ± 2.00[b]
Total Displacement (µm)	697.84 ± 488.06	752.25 ± 536.15	835.34 ± 328.35	611.09 ± 233.57	482.30 ± 401.06	743.86 ± 334.87	628.97 ± 343.45	579.63 ± 386.72
Stiffness (N/mm)	97.46 ± 28.54[b]	121.40 ± 17.76[a]	126.94 ± 11.03[a]	128.97 ± 15.46[a]	77.64 ± 12.89[c]	76.00 ± 9.86[c]	95.90 ± 20.85[b]	104.31 ± 19.22[b]
Total Work (mJ)	7.58 ± 5.60[bcd]	9.58 ± 6.12[abc]	13.39 ± 5.15[a]	10.46 ± 3.80[ab]	3.49 ± 2.30[d]	6.45 ± 3.41[bcd]	5.90 ± 2.71[cd]	7.10 ± 3.59[bcd]
Ultimate Stress (MPa)	186.22 ± 42.20[bc]	200.41 ± 46.78[bc]	262.84 ± 69.26[a]	237.20 ± 70.89[ab]	165.06 ± 41.19[c]	151.57 ± 32.76[c]	204.22 ± 56.87[bc]	189.75 ± 56.47[bc]
Total Strain (µε)	76903 ± 49990	81601 ± 56746	87145 ± 35874	72492 ± 27595	50376 ± 47702	76230 ± 35233	59566 ± 27812	63591 ± 39218

Modulus (GPa)	9.07 ± 5.32	10.72 ± 2.52	13.43 ± 5.17	10.67 ± 4.75	11.37 ± 3.13	9.68 ± 3.08	13.22 ± 3.83	8.90 ± 3.89
Resilience (MPa)	1.53 ± 0.83	1.61 ± 0.62	1.62 ± 0.47	1.85 ± 0.65	1.60 ± 0.72	0.99 ± 0.28	1.24 ± 0.54	1.67 ± 0.88
Toughness (MPa)	8.97 ± 7.80[bc]	9.66 ± 5.19[bcd]	14.56 ± 7.03[a]	11.57 ± 4.97[ab]	4.57 ± 2.90[c]	7.94 ± 3.38[bc]	7.40 ± 3.29[bc]	7.04 ± 3.82[bc]
Initiation toughness, K_{init}	79.94 ± 53.00[bcd]	105.78 ± 33.85[ab]	111.38 ± 27.90[ab]	132.07 ± 13.27[a]	7.25 ± 16.49[e]	41.90 ± 44.42[de]	90.29 ± 56.07[abc]	53.15 ± 36.41[cd]
Instability toughness, $K_{max\ load}$	109.55 ± 70.23[ab]	145.69 ± 26.50[a]	120.99 ± 26.57[ab]	146.49 ± 11.29[a]	16.71 ± 40.66[c]	75.63 ± 86.53[bc]	99.31 ± 60.23[ab]	67.23 ± 45.38[bc]

Data provided as mean ± standard deviation. Groups with different letter notations are statistically different from each other (p<0.05).

5.3.8   Romosozumab treatment increased the energy necessary to propagate the initial crack,

while the addition of calcium water mitigated the effect.

Initiation toughness (K init) had main effects of adenine (p<0.0001) and romosozumab (p=0.001). Overall, adenine resulted in lower initiation toughness. In control animals, the combination treatment resulted in higher initiation toughness by 39%; in adenine animals, the romosozumab-treated animals were no different from the control animals and improved initiation toughness by 92% compared to the untreated adenine group (**Table 4**).

For instability toughness at the ultimate load (K max load), there was a main effect of adenine (p<0.0001). Although there were no differences with treatment in control animals, romosozumab and combination treatment improved instability toughness at the ultimate load (**Table 4**). The romosozumab-treated adenine animals were no different from the control animals.

5.4 Discussion

The primary finding of this study is that romosozumab effectively mitigated changes in bone structural and mechanical properties in the setting of aging and CKD. While calcium water supplementation effectively mitigated the high PTH that manifests in adenine-induced CKD, the combination with romosozumab had minimal additive benefit compared to romosozumab alone. Adenine-induced CKD in aging mice led to increased cortical porosity and reduced structural and estimated material mechanical properties, all of which were improved with romosozumab treatment, either alone or in combination with PTH suppression through calcium water.

Clinical studies utilizing romosozumab have shown stimulation of bone formation and inhibition of bone resorption in healthy men and postmenopausal women[51]. This is the result of a dose-dependent increase in bone formation markers, including procollagen I intact N-terminal propeptide (P1NP) and bone alkaline phosphatase (BAP), and a dose-dependent decrease in bone resorption markers, including serum C-terminal telopeptide (CTX)[61]. Phase II clinical trials demonstrated that postmenopausal women treated with romosozumab had larger gains in bone mineral density than treatment with alendronate or teriparatide[30]. Phase III clinical trials in men with osteoporosis showed increased bone mineral density after 1-year treatment with romosozumab, indicating that romosozumab is an effective osteoporosis treatment in both men and women[141]. A phase I clinical trial evaluating the use of single-dose romosozumab in stage 4 and stage 5 CKD patients aged 50 years and older found similar increases in P1NP and decreases in CTX in healthy controls and CKD patients; however, the CKD groups had greater increases in PTH than healthy controls[144]. In our aging mice, we found increased P1NP with romosozumab; intriguingly, we also found higher PTH with romosozumab treatment, like what was found in the previous clinical trial, but whether this has an effect in CKD and CKD-induced bone loss should be assessed further in future studies.

In animal studies using romosozumab, research with both ovariectomized rats and gonad-intact female cynomolgus monkeys demonstrate increased trabecular and cortical bone mass and associated gains in bone mineral density (BMD)[134,135]. When comparing romosozumab with teriparatide in young rats, romosozumab increased trabecular bone mass in 4 weeks and maintained bone formation rate for over one month compared to teriparatide, suggesting that romosozumab increases the maturation of osteoblasts[137]. Our study is consistent

with previous studies that demonstrate higher trabecular and cortical bone and increased P1NP following treatment with romosozumab. Cortical porosity imparted from aging, CKD, and the combination was also significantly lower in romosozumab-treated animals, and this finding likely explains the improved bone mechanical properties with the addition of romosozumab. Most importantly, romosozumab alone and in combination with calcium water, normalized many bone-specific parameters to the levels of the untreated control animals. Our study builds on previous pre-clinical trials by evaluating the effectiveness of romosozumab in both aging mice and aging mice with CKD. Taken together, these findings indicate that romosozumab could be an effective strategy to increase bone mass for aging, CKD patients.

Secondary hyperparathyroidism (SHPT) is a common complication linked to renal function declines in CKD. Elevated PTH increases M-CSF and RANKL expression, which then drive osteoclast differentiation and function[145]. As a result, patients with SHPT are often treated with calcimimetics, which bind to the calcium-sensing receptor (CaSR), decrease PTH secretion, and improve serum calcium and phosphorus levels[146]. Several clinical studies evaluating the use of cinacalcet in stage 3- 5 CKD patients have demonstrated that administration of cinacalcet reduces PTH and improves calcium-phosphorus homeostasis compared to placebo[51,147,148]. Additionally, the use of KP-2326, which is analogous to human etelcalcetide, in the Cy/+ rat model of CKD-MBD found an almost two-fold decrease in PTH compared to untreated CKD animals[142]. Previous studies in that same animal model have shown that suppression of PTH via calcium water supplementation is also effective at reducing cortical porosity in skeletally mature CKD animals[48,65,149]. Our study builds on previous work by demonstrating that calcium water reduces PTH levels in aging mice with adenine-induced CKD. The

aging adenine animals in the current study had more than three-fold higher PTH than the skeletally mature young adenine mice in a previous study performed in our lab[65]. In the current study, even though administration of calcium water reduced PTH by 74% and cortical porosity by 46%, the PTH levels were still 52% higher than untreated control levels. Therefore, effectively reducing PTH in aging animals could require modified treatment (altered dosing). Although calcium water is not a clinically viable treatment due to increased risk of extracellular and vascular calcifications in CKD, these results are promising for the use of PTH-lowering agents (such as calcimimetics) in aging patients with CKD.

Cortical porosity is a central tenet that underlies the skeletal fragility found in CKD and can also be prominent with advanced aging[33–37]. Because the mechanical strength of bone is mostly conferred by the cortex, aggregation of porosity leads to weakened bone and increased fracture risk. In fact, a person with CKD at age 45 has the same fracture risk as a healthy person at 65, while a person aged 65+ has a fracture risk 3-4 times higher than the general population[31]. Increased fracture risk is believed to involve both altered bone quantity and quality. Decreased bone quantity has been frequently shown in pre-clinical studies in form of decreased trabecular volume, increased cortical porosity, and cortical thinning[65,111,131]. Although aging and CKD are both known to negatively affect bone, very few studies have assessed quantity and quality alterations in aging CKD bone. One study performed in aging mice that underwent a 5/6-nephrectomy found significant main effects of aging or CKD for measures of bone quality (via three-point bending, finite element analysis, Raman spectroscopy, and nanoindentation), although interaction effects failed to meet statistical significance[123]. This study highlighted that there are changes in bone quality that are occurring in both aging and CKD, findings that our study builds on by showing that adenine-induced CKD

decreases the energy necessary to move an initial flaw through the bone during fracture toughness tests. However, administration of romosozumab, whether alone or in combination, increased the energy necessary to move the initial flaw and increased the overall toughness at the ultimate load, both of which are promising results for bone mechanical properties.

Limitations of the current study include the use of only male mice and a significant number of animals that did not make it to study endpoint. Because we have previously shown that aging male mice exhibit higher cortical porosity than aging female mice, we chose to use male mice in this first study examining interaction effects[111]. Because sex-based differences have been shown previously in CKD models, future studies should examine the effectiveness of romosozumab and combination treatment in female mice. Overlaying aging and CKD in a pre-clinical model proved difficult as evident by the significant loss of animals. With loss of almost 40% of our animals over the course of the study, the data represented here is likely biased toward animals that were more resilient. However, research investigating the intersection of aging and CKD is extremely relevant and could be useful for developing future therapies. We chose to use BUN as our indictor of altered kidney function, rather than creatinine or glomerular filtration rate (GFR). Therefore, our study is limited in its ability to assess the degree of kidney function and how that was affected by the treatment regimens.

In conclusion, this study demonstrates that romosozumab, whether alone or in combination with PTH-suppressing interventions, is effective at improving trabecular and cortical bone morphology and cortical bone mechanical and material properties when CKD is overlaid with aging. This highlights the importance of testing pharmaceuticals across various ages in disease states to increase the treatment options for multiple patient populations.

Acknowledgements

5.5 Supplementary Tables

Supplementary Table 4. Statistical results from the 2x2x2 ANOVA

	Ad	Ca	Romo	Ad*Ca	Ad*Romo	Ca*Romo	Ad*Ca*Romo
BUN (mg/dL)	**<0.0001**	**0.03**	**0.002**	0.223	**0.023**	0.262	0.785
PTH (pg/mL)	**<0.0001**	**<0.0001**	0.054	**<0.0001**	**0.031**	0.438	0.423
P1NP (ng/mL)	**<0.0001**	**<0.0001**	**0.004**	0.098	**0.025**	0.732	0.072
CTX (ng/mL)	**<0.0001**	**0.01**	0.277	0.265	0.966	0.175	0.177
BV/TV (%)	**0.006**	**<0.0001**	**<0.0001**	0.632	**0.037**	**0.012**	0.288
Tb.Th (mm)	**<0.0001**	**0.002**	**<0.0001**	0.051	**<0.0001**	0.05	0.179
Tb.Sp (mm)	**<0.0001**	0.064	**0.001**	0.319	0.275	0.238	0.662
Tb.N (mm)	0.133	**0.028**	**<0.0001**	0.661	0.87	0.183	0.369
Cortical porosity (%)	**<0.0001**	0.195	**<0.0001**	0.555	0.345	0.079	0.136
Cortical bone area (mm^2)	**<0.0001**	0.113	**<0.0001**	0.095	**0.001**	**0.027**	0.604
Cortical thickness (mm)	**<0.0001**	**0.014**	**<0.0001**	0.805	**<0.0001**	0.413	0.541
Ultimate Force (N)	**<0.0001**	**0.014**	**<0.0001**	0.366	0.665	0.094	**0.007**
Total Displacement (µm)	ND						
Stiffness (N/mm)	**<0.0001**	0.058	**<0.0001**	0.262	0.577	0.487	0.064
Total Work (mJ)	**<0.0001**	0.423	**0.018**	0.208	0.369	0.1	0.431
Ultimate Stress (MPa)	**0.001**	0.457	**0.001**	0.755	0.495	0.441	0.463
Total Strain (µε)	ND						
Modulus (GPa)	ND						
Resilience (MPa)	ND						
Toughness (MPa)	**<0.0001**	0.876	**0.048**	0.261	0.238	0.118	0.992

Initiation toughness, K_{init}	**<0.0001**	0.308	**0.001**	0.257	0.397	0.079	0.126
Instability toughness, $K_{max\ load}$	**<0.0001**	0.138	0.148	0.555	0.296	0.09	0.177

Ad: adenine, Ca: calcium water, Romo: romosozumab

ND: no statistical difference in the model

CHAPTER 6

DISCUSSION

Synthesis

The overarching goals of these studies were to improve our understanding of how aging interacts with CKD to affect bone and evaluate potential therapeutic targets to reduce bone fragility in these comorbid conditions. This dissertation work aimed to answer the following questions: (1) What are the skeletal implications of aging? (2) Does the combination of aging and CKD produce a more severe skeletal phenotype than either alone? (3) Does aging bone have a similar anabolic response to treatment as skeletally mature bone? and (4) Can individual or combined therapies improve bone quantity and quality in aging-CKD?

Little research has assessed the intersection of aging and CKD, leaving questions as to whether these two conditions interact to further accelerate bone loss and how this could influence the response to therapies. Although there are many therapeutic options for treating osteoporosis, treating CKD-associated bone loss is more challenging. Due to reduced renal function, the gold-standard treatment for osteoporosis – bisphosphonates – is contraindicated at later stages of CKD[150,151]. Additionally, CKD patients often experience secondary hyperparathyroidism, meaning that therapies upregulating the PTH pathway, like teriparatide, may not be ideal treatments for CKD patients. In the past five years, a new therapeutic based on the Wnt pathway, known as romosozumab, was developed and approved for the treatment of post-menopausal women at high risk of fracture. This treatment provides an exciting option for the treatment of CKD-associated bone loss.

What are the skeletal implications of aging? In our first study, we aimed to assess the skeletal impact of aging in male and female mice. To answer this question, we placed young and aging mice on a casein diet, which has higher phosphate bioavailability than a traditional rodent diet[84]. Because aging is known to be associated with a normal, mild loss of renal

97

function, our goal was to challenge the mice with an increased phosphate load and examine the effects on both bone microarchitecture and strength. We did find that female mice upregulate FGF23 while male mice upregulate Klotho in response to the casein-based diet as outlined in Chapter 2, but for the purposes of our overarching focus, we were primarily interested in the male and female comparison within the casein-based diet. We found that, in both male and female mice, aging is associated with decreased trabecular bone volume fraction, increased cortical porosity, and decreased cortical thickness compared to younger mice (**Figure 21**). Although architectural changes were observed, there were few changes to bone mechanical properties, with significant differences only being observed in female mice.
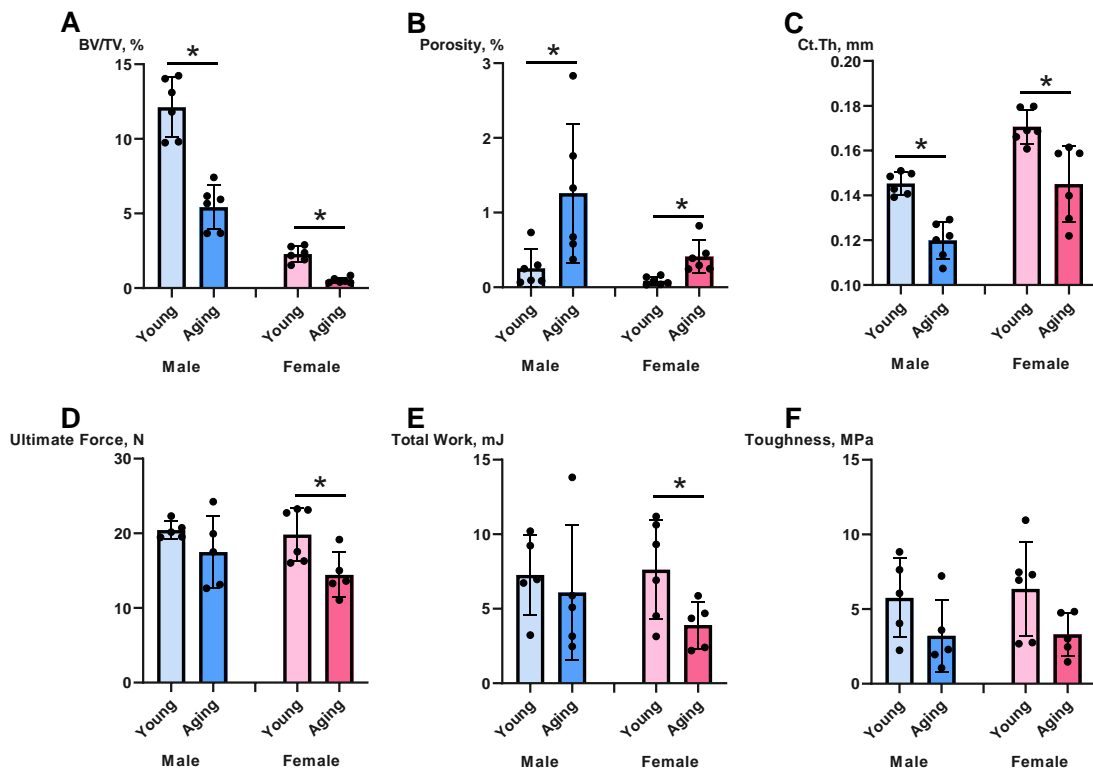
Figure 21: Aging contributes to significant differences in bone microarchitecture and mechanical properties. All data adapted from Chapter 2[111].

This study demonstrated important skeletal effects in an aging mouse model with loss of both trabecular and cortical bone. Most importantly for the studies presented here, this study found that aging males have significantly higher cortical porosity relative to females. Although one of the notable strengths of this study was to include paired sexes, the subsequent studies utilized only male mice due to the high incidence of cortical porosity in those animals. Additionally, the use of the casein diet provided a slight increase in bioavailable phosphate that did not induce CKD and rather mimicked potential increases in phosphate associated with natural aging. Thus, this study allowed us to study the skeletal effects of aging and laid the groundwork for all future studies.

Does the combination of aging and CKD produce a more severe skeletal phenotype than either alone? Nearly 40% of CKD patients are over age 65[138], which underscores the importance of studying a combined model of aging-CKD. However, very few studies have examined this interaction and its effects on bone. In <u>Chapter 3</u>, we studied adenine-induced CKD in young and aging mice. We found that aging mice with adenine-induced CKD had 33% higher BUN and 72% higher PTH compared to young adenine mice. Femoral and tibial cortical porosity were also higher in aging CKD mice versus young, indicating that there was likely higher osteoclast activity and increased cortical pore development in the aging CKD animals. Cortical area and cortical thickness, in both femur and tibia, were also compromised due to adenine-induced CKD but were not impacted by age; therefore, the primary skeletal effect was an exacerbated cortical porosity phenotype in aging CKD mice. Both aging and CKD led to lower mechanical and material bone properties, but interestingly, the mice with the highest cortical porosity did not have greater alterations to mechanical properties, suggesting a potential compensatory mechanism that may occur to preserve overall mechanical strength in conditions of porosity. A potential compensatory mechanism that has been noted in other conditions is periosteal expansion; however, we found that total bone area and periosteal perimeter were no different between groups, indicating that periosteal expansion may not have been the driving factor of this result. Taken together, this study

demonstrated that combining aging and CKD leads to an exacerbated skeletal phenotype that appears to be linked to elevations in PTH.

Does aging bone have a similar anabolic response to treatment as skeletally mature bone? Aging-associated bone loss is due to a reduction in osteoblast-mediated bone formation and an increase in osteoclast-mediated bone resorption. Methods of decreasing resorption, such as utilization of bisphosphonates and denosumab, do not address the low bone formation in aging. Therefore, in Chapter 4, we utilized an anabolic therapy to increase osteoblast activity in aging mice. In both young and aging mice, romosozumab increased trabecular bone volume fraction by both increasing the thickness and number of trabeculae; aging romosozumab-treated mice had 62% higher BV/TV than untreated controls while young romosozumab-treated mice had 33% higher BV/TV than their age-matched controls, indicating a potentially stronger response to romosozumab in the context of aging. Additionally, cortical thickness and cortical bone area were highest in aging animals that received romosozumab, while there were no differences in cortical porosity. This demonstrates that romosozumab can increase bone formation, both in trabecular and cortical bone of young and aging animals. The results from this study are especially promising for aging individuals at high risk of fracture.

Interestingly, in this study, we found no differences in bone formation rate (assessed with dynamic bone histomorphometry) due to romosozumab treatment. These results suggest that the anabolic window is early following romosozumab treatment and that our measurements in the last week of the treatment were not ideal. Regardless of this observation, the bone microarchitecture data are strong, demonstrating that romosozumab effectively increased bone in aging mice. These data build on the work performed in Chapter 2 by providing evidence of romosozumab's application in the context of aging and is promising when considering the work in Chapter 3 and romosozumab's potential utility in aging, CKD patients.

Can individual or combined therapies improve bone quantity and quality in aging-CKD? In Chapter 3, we showed that aging-CKD has a more severe skeletal phenotype than either condition alone. It is known that both aging and CKD increase the risk of fracture, and the risk of hip fracture rises 3-4 fold in CKD patients aged 65+ compared to the general population[31]. However, clear guidelines on treatment options for this patient group are limited. Thus, this study aimed to examine the use of anabolic therapy and PTH suppression in treating aging-CKD bone loss. In Chapter 5, we treated aging mice with adenine-induced CKD with romosozumab, calcium water (to lower PTH), or their combination.

Overall, we found that romosozumab, whether alone or in combination with calcium water, was effective at improving microarchitectural and mechanical properties in aging-CKD mice. As expected, calcium water lowered PTH levels although not to same degree as in young mice[65]; additionally, the combination treatment was less effective at suppressing PTH than calcium water alone. Elevated circulating P1NP levels in romosozumab-treated animals illustrated systemic increases in bone formation, although the anabolic response was blunted when combined with calcium water. Trabecular bone volume fraction (BV/TV) was highest in the combination group and significantly higher than the romosozumab-treated animals. Most significantly, the BV/TV of the adenine combination group was no different than the control groups treated with romosozumab alone or in combination with calcium water. Cortical bone area and thickness were also significantly higher with romosozumab treatment. Additionally, the groups with romosozumab treatment had lower cortical porosity, indicating the anabolic therapy may have prevented the development of more pores or potentially infilled preexisting cortical pores. Coinciding with the improvements to structural parameters were significant improvements to bone mechanical and material properties. These results add to the overall impact of this study by finding dramatic improvements to bone quality and quantity, two features of critical importance in reducing fracture risk.

Although calcium water is an effective method for suppressing PTH in mice, it is not a clinically relevant therapy due to increased risk of extracellular and vascular calcifications in CKD. This series of studies demonstrates that PTH is higher in aging CKD animals than younger animals. Which both points to the need to control PTH levels in the aging population as well as highlights the potential challenges of adequately accomplishing this goal. Approved calcimimetics typically reduce PTH by less than 50%[152], which is not as effective as calcium water that reduces PTH by 75% in the current study. Although the results of this study indicate that PTH suppression is an important therapeutic step preserving bone structure partially through mitigating cortical porosity development, this goal may be challenging. Additionally, we lost approximately 40% of our animals during the course of the study, illustrating the difficulty of studying aging and CKD in a combination model. Although these results are promising, it cannot be overstated that we likely lost data on the most severely affected animals and thus a key portion of the population.

Clinical Implications

The clinical importance of studying the intersection of aging and CKD and its impact on the skeleton is high. With nearly 40% of individuals with CKD being over the age of 65[138], the population of individuals affected is large and continually increasing. Because the overall population is living longer, reducing skeletal fragility in this population would improve the health of our aging society.

Clinical implications of calcimimetics on bone microarchitecture and mechanics.

Secondary hyperparathyroidism is a common complication of CKD and is often associated with bone pain and fractures, key complications of renal osteodystrophy[153,154]. Because PTH directly stimulates receptor activator of nuclear factor kappa-B ligand (RANKL) production, a key osteoclastogenesis regulator[42,43], suppression of PTH can prevent further worsening of bone deficits

by preventing or slowing bone resorption. There are several approved calcimimetics, including cinacalcet and etelcalcetide, which have been utilized in CKD patients. These therapies have been shown to suppress PTH for up to 2-3 years and slow progression of CKD[147,148,152]. Some pre-clinical studies using approved calcimimetics in mice have shown decreased cortical porosity and improved mechanical properties[45,155], while others have found unchanged or increased cortical porosity with calcimimetic treatment[141,142]. The study presented in <u>Chapter 5</u> illustrates proof-of-concept research that in the combination setting of CKD and aging, PTH suppression is effective when used in combination with anabolic therapy to improve structural and mechanical properties of bone. However, the calcium water utilized is not a clinically relevant therapeutic, and thus more research would need to be performed with approved calcimimetics to determine if similar effects are observed.

Clinical implications of anabolic therapy on bone microarchitecture and mechanics.

Several promising anabolic therapies have been approved for the treatment of post-menopausal osteoporosis, including teriparatide and romosozumab. Prior to 2019, teriparatide was the only available anabolic therapy and thus has been highly studied in several disease states affecting bone. Teriparatide has been shown to increase both bone formation and resorption, improving bone mineral density and decreasing fracture incidence in osteoporotic women, and the effects on fracture incidence seem to decrease with duration of treatment[54,156,157]. However, the effects of teriparatide are mitigated when following bisphosphonate treatment[158]. Tied to the increase in bone resorption, administration of teriparatide in a rat model of osteoporosis has also been found to be associated with increased cortical porosity directly proportional to the dosage[159]. These results are concerning when teriparatide is used in CKD patients due to secondary hyperparathyroidism and concurrent increases in osteoclast activity and cortical porosity.

Utilization of romosozumab, a humanized monoclonal antibody against sclerostin, in osteoporotic men and women leads to increased bone mineral density at multiple sites, increased

bone formation markers, and decreased bone resorption markers[60,62,160,161]. The anabolic response of romosozumab is mitigated by 12 months, with P1NP levels returning to pre-treatment levels, although CTX levels remaining low with a two-year treatment duration[162]. Romosozumab decreased fracture incidence by an additional 27% compared to alendronate and by an additional 75% compared to denosumab in osteoporotic women[133,163]. Additionally, there were greater gains to vertebral and femoral strength with romosozumab compared to teriparatide in post-menopausal women with low bone mass[164]. Post-hoc analyses of the ARCH and FRAME studies have shown that patients across mild and moderate levels of renal function had higher bone mineral density and lower risk of vertebral fractures[58]; however, the safety and efficacy of romosozumab in patients with later-stage CKD remains unknown. The study performed in Chapter 5 illustrates the effectiveness of romosozumab, whether alone or in combination with PTH suppression, in improving bone structural and mechanical properties in aging mice with CKD. The research performed in Chapter 5 could potentially lead to clinical trials evaluating the use of romosozumab in combination with approved calcimimetic therapies.

Potential Future Studies

The studies presented herein demonstrate the complexities of aging-CKD and the need for appropriate therapies to mitigate bone loss and reduce fracture risk. Potential future investigations based off the results of these experiments could aid in identifying treatment strategies to alleviate bone loss in aging, CKD patients.

Long-term therapeutic options to preserve bone mass. Our results demonstrate that romosozumab effectively improved bone in an animal model of aging-CKD with or without PTH suppression. However, romosozumab can only be given clinically for a 1-year duration, which leaves the question of how to preserve bone mass after discontinuation of romosozumab. Thus, a

potential future study could sequentially treat aging, CKD mice with romosozumab (as described in Chapter 5) followed by an anti-resorptive (bisphosphonate or denosumab). Alternatively, spacing out the romosozumab dosing through less frequent administration could allow a prolonged duration of active treatment. Considering the results of this dissertation work, this sequential treatment study would potentially result in decreased cortical porosity and increased mechanical properties for a longer period of time.

Study of aging-CKD in a rat model of CKD. One limitation of the adenine-induced CKD mouse model is that *in vivo* micro-CT cannot be performed to monitor the development and progression of cortical porosity throughout the study timeline. The ability to track global changes in porosity as well as monitor individual pore dynamics within the same animal over time would enhance our knowledge of disease progression and the impact of various treatments. Thus, adenine can be used to induce CKD in aged rats[113], which would allow for longitudinal tracking of cortical pores through the course of the disease and with treatment regimens. With the current series of studies, we were unable to assess cortical pore dynamics over time and with different treatments, and this type of model would allow us to expand our understanding of this process.

Evaluation of the skeletal consequences of CKD in the middle-aged population. Previous research in our lab has assessed the skeletal consequences of CKD in skeletally mature young (24-28wk) and aging (86-90wk) mice. However, the period associated with middle age in a rodent model (40-50 weeks) is less understood, and another line of future investigation could examine CKD in this age range. This line of research would broaden our understanding of CKD across ages to determine whether intervention at this stage could be more beneficial than waiting to intervene at the aging timepoint.

Assessment of mineral metabolism in aging-CKD. The study presented in Chapter 2 focused on how mineral metabolism is disturbed in aging in male and female mice. This work demonstrated that males and females utilize different mechanisms to maintain proper FGF23-KL signaling with

a phosphate challenge. Future studies could assess how these factors are altered when CKD is overlaid on top of aging. Furthermore, exploring the sex-specific differences could identify different therapeutic targets for aging CKD.

Evaluation of osteocytes in the context of aging-CKD. Osteocytes are potent regulators of osteoclasts via osteocyte-release of RANKL and factors released during apoptosis or senescence[42,43]. High levels of PTH, like that observed in CKD, directly stimulate osteocytes to release RANKL, which contributes to elevated osteoclastogenesis and increased bone resorption. Intermittent PTH, the basis for the development of teriparatide, has been shown to reduce apoptosis of osteocytes[165,166]. When osteocyte apoptosis is blocked via genetic alterations, cortical porosity increases[167]; adenine-induced CKD is also tied to decreased osteocyte apoptosis[40]. This data could be expanded into a future line of research by examining whether the rate of osteocyte apoptosis is lower in aging-CKD and could that contribute to the elevated porosity seen in this context. Additionally, the effect of a variety of treatments, including antiresorptives and anabolics, on osteocyte apoptosis could be evaluated in the context of aging-CKD. This line of research could expand what is known about osteocytes in contexts where PTH is elevated and identify whether certain treatment regimens have a modifiable impact on these cells.

Conclusion

Discovery of new therapeutic options for the treatment of CKD in the context of aging is critical for improving the health of our society. Little research has been performed at the intersection of aging and CKD, so the current works adds foundational data to the scientific literature. Although clear treatment strategies exist for the treatment of osteoporosis in aging, clear guidelines for aging-CKD are notably lacking. The current series of studies demonstrate that aging

and CKD interact, leading to a more severe skeletal phenotype that compromises the structural integrity of the bone that can be alleviated by PTH suppression and anabolic therapy.

Combination therapy of PTH suppression and anabolic therapy addressed key issues associated with aging and CKD. PTH suppression mitigated the secondary hyperparathyroidism associated with CKD and reduced osteoclast-mediated bone resorption. Anabolic therapy increased aging-associated declines in osteoblast activity and may have stimulated infilling of preexisting cortical pores. Together, these therapies improved both trabecular and cortical bone in aging mice with adenine-induced CKD.

These data demonstrate that romosozumab is an effective anabolic therapy in the context of aging-CKD and improves both structural and mechanical properties of bone. More specifically, combining romosozumab with PTH suppression via calcium water leads to greater improvements to trabecular bone volume fraction, cortical bone area and thickness, and ultimate force. Although we can only speculate whether romosozumab was able to infill cortical pores, it either suppressed their formation or filled them in, which are both positive results. These results support that combination therapy can prevent further bone deterioration observed in aging-CKD. Ideally, skeletal fragility can be improved using an appropriate combination treatment in aging individuals with CKD at high risk of fracture.

CHAPTER 7

REFERENCES

1. Burr, D. B. Bone Morphology and Organization. in *Basic and Applied Bone Biology* 3–26 (2019).

2. Allen, M. R. & Burr, D. B. Bone Growth, Modeling, and Remodeling. in *Basic and Applied Bone Biology* 85–100 (2019).

3. Compston, J. E. Osteoporosis, corticosteroids and inflammatory bowel disease. *Aliment. Pharmacol. Ther.* **9**, 237–250 (1995).

4. Lane, N. E. Epidemiology, etiology, and diagnosis of osteoporosis. *Am. J. Obstet. Gynecol.* **194**, (2006).

5. Leib, E. S., Lewiecki, E. M., Binkley, N. & Hamdy, R. C. Official positions of the International Society for Clinical Densitometry. *J. Clin. Densitom.* **7**, 1–5 (2004).

6. Cosman, F. *et al.* Clinician's Guide to Prevention and Treatment of Osteoporosis. *Osteoporos. Int.* **25**, 2359 (2014).

7. Sarafrazi, N. Osteoporosis or Low Bone Mass in Older Adults: United States, 2017-2018. (2021) doi:10.15620/CDC:103477.

8. Lane, J. M., Russell, L. & Khan, S. N. Osteoporosis. *Clin. Orthop. Relat. Res.* **372**, 139–150 (2000).

9. Arceo-Mendoza, R. M. & Camacho, P. M. Postmenopausal Osteoporosis: Latest Guidelines. *Endocrinol. Metab. Clin. North Am.* **50**, 167–178 (2021).

10. Coughlan, T. & Dockery, F. Osteoporosis and fracture risk in older people. *Clin. Med.* **14**, 187–191 (2014).

11. Weinstein, R. S. & Hutson, M. S. Decreased trabecular width and increased trabecular spacing contribute to bone loss with aging. *Bone* **8**, 137–142 (1987).

12. Russo, C. R. *et al.* Structural adaptations to bone loss in aging men and women. *Bone* **38**, 112–118 (2006).

13. Chandra, A. & Rajawat, J. Skeletal Aging and Osteoporosis: Mechanisms and Therapeutics. *Int. J. Mol. Sci.* **22**, (2021).

14. Zimmermann, E. A. & Ritchie, R. O. Bone as a Structural Material. *Advanced Healthcare Materials* vol. 4 1287–1304 (2015).

15. Boskey, A. L. & Coleman, R. Critical reviews in oral biology & medicine: Aging and bone. *Journal of Dental Research* vol. 89 1333–1348 (2010).

16. Thomas, C. D. L. *et al.* Femoral Neck Trabecular Bone: Loss With Aging and Role in Preventing Fracture. *J. Bone Miner. Res.* **24**, 1808–1818 (2009).

17. Panula, J. *et al.* Mortality and cause of death in hip fracture patients aged 65 or older - A population-based study. *BMC Musculoskelet. Disord.* **12**, 105 (2011).

18. Vestergaard, P., Rejnmark, L. & Mosekilde, L. Increased mortality in patients with a hip fracture-effect of pre-morbid conditions and post-fracture complications. *Osteoporos. Int.* **18**, 1583–1593 (2007).

19. Armas, L. A. G. & Recker, R. R. Pathophysiology of osteoporosis: new mechanistic insights. *Endocrinol. Metab. Clin. North Am.* **41**, 475–486 (2012).

20. Surowiec, R. K., Allen, M. R. & Wallace, J. M. Bone hydration: How we can evaluate it, what can it tell us, and is it an effective therapeutic target? *Bone reports* **16**, (2021).

21. Wang, X. *et al.* Age-related deterioration of bone toughness is related to diminishing amount

of matrix glycosaminoglycans (GAGs). *JBMR plus* **2**, 164–173 (2018).

22. Creecy, A. *et al.* The age-related decrease in material properties of BALB/c mouse long bones involves alterations to the extracellular matrix. *Bone* **130**, (2020).

23. CDC. Chronic Kidney Disease in the United States. cdc.gov/kidneydisease/publications-resources/2019-national-facts.html (2019).

24. Moe, S. *et al.* Definition, evaluation, and classification of renal osteodystrophy: A position statement from Kidney Disease: Improving Global Outcomes (KDIGO). *Kidney International* vol. 69 1945–1953 (2006).

25. Alem, A. M. *et al.* Increased risk of hip fracture among patients with end-stage renal disease. *Kidney Int.* **58**, 396–399 (2000).

26. Maravic, M., Ostertag, A., Torres, P. U. & Cohen-Solal, M. Incidence and risk factors for hip fractures in dialysis patients. *Osteoporos. Int.* **25**, 159–165 (2014).

27. Kazama, J. J. Chronic kidney disease and fragility fracture. *Clin. Exp. Nephrol.* **21**, 46–52 (2017).

28. Seiler, S., Heine, G. H. & Fliser, D. Clinical relevance of FGF-23 in chronic kidney disease. *Kidney Int.* **76**, (2009).

29. Kim, S. M., Long, J., Montez-Rath, M., Leonard, M. & Chertow, G. M. Hip Fracture in Patients With Non-Dialysis-Requiring Chronic Kidney Disease. *J. Bone Miner. Res.* **31**, 1803–1809 (2016).

30. Naylor, K. L. *et al.* The three-year incidence of fracture in chronic kidney disease. *Kidney Int.* **86**, 810–818 (2014).

31. Moe, S. M. & Nickolas, T. L. Fractures in patients with CKD: Time for action. *Clinical*

Journal of the American Society of Nephrology vol. 11 1929–1931 (2016).

32.   Burr, D. B. Cortical bone: a target for fracture prevention? *Lancet* **375**, 1672–1673 (2010).

33.   Nickolas, T. L. *et al.* Rapid cortical bone loss in patients with chronic kidney disease. *J. Bone Miner. Res.* **28**, 1811–1820 (2013).

34.   Nishiyama, K. K. *et al.* Longitudinal HR-pQCT and image registration detects endocortical bone loss in kidney transplantation patients. *J. Bone Miner. Res.* **30**, 554–61 (2015).

35.   Araujo, M. J. C. L. N. *et al.* The pitfall of treating low bone turnover: Effects on cortical porosity. *Bone* **91**, 75–80 (2016).

36.   Sharma, A. K. *et al.* Deterioration of Cortical Bone Microarchitecture: Critical Component of Renal Osteodystrophy Evaluation. *Am. J. Nephrol.* **47**, 376–384 (2018).

37.   McNerny, E. M. B. & Nickolas, T. L. Bone Quality in Chronic Kidney Disease: Definitions and Diagnostics. *Current Osteoporosis Reports* vol. 15 207–213 (2017).

38.   Nickolas, T. L. *et al.* Bone mass and microarchitecture in CKD patients with fracture. *J. Am. Soc. Nephrol.* **21**, 1371–80 (2010).

39.   Seeman, E. Overview of bone microstructure, and treatment of bone fragility in chronic kidney disease. *Nephrology* **22**, 34–35 (2017).

40.   Metzger, C. E., Swallow, E. A. & Allen, M. R. Elevations in Cortical Porosity Occur Prior to Significant Rise in Serum Parathyroid Hormone in Young Female Mice with Adenine-Induced CKD. *Calcif. Tissue Int.* **106**, 392–400 (2020).

41.   Moe, S. M. *et al.* A rat model of chronic kidney disease-mineral bone disorder. *Kidney Int.* **75**, 176–184 (2009).

42.   Bellido, T., Saini, V. & Pajevic, P. D. Effects of PTH on osteocyte function. *Bone* vol. 54

250–257 (2013).

43.   Wein, M. N. Parathyroid Hormone Signaling in Osteocytes. *JBMR Plus* **2**, 22–30 (2018).

44.   Cusano, N. E. *et al.* Skeletal Microstructure and Estimated Bone Strength Improve Following Parathyroidectomy in Primary Hyperparathyroidism. *J. Clin. Endocrinol. Metab.* **103**, 196–205 (2018).

45.   Zheng, C.-M. *et al.* Osteoclast-Released Wnt-10b Underlies Cinacalcet Related Bone Improvement in Chronic Kidney Disease. *Int. J. Mol. Sci.* **20**, 2800 (2019).

46.   Aref, M. W. *et al.* Parathyroid suppression therapy normalizes chronic kidney disease-induced elevations in cortical bone vascular perfusion: a pilot study. *Osteoporos. Int.* **30**, 1693–1698 (2019).

47.   Li, X. *et al.* Etelcalcetide (AMG 416), a peptide agonist of the calcium-sensing receptor, preserved cortical bone structure and bone strength in subtotal nephrectomized rats with established secondary hyperparathyroidism. *Bone* **105**, 163–172 (2017).

48.   Moe, S. M. *et al.* A Comparison of Calcium to Zoledronic Acid for Improvement of Cortical Bone in an Animal Model of CKD. *J. Bone Miner. Res.* **29**, 902–910 (2014).

49.   Moe, S. *et al.* Definition, evaluation, and classification of renal osteodystrophy: A position statement from Kidney Disease: Improving Global Outcomes (KDIGO). *Kidney International* vol. 69 1945–1953 (2006).

50.   Waziri, B., Duarte, R. & Naicker, S. Chronic kidney disease–mineral and bone disorder (CKD-MBD): Current perspectives. *International Journal of Nephrology and Renovascular Disease* vol. 12 263–276 (2019).

51.   Moe, S. M. *et al.* Effects of cinacalcet on fracture events in patients receiving hemodialysis: The EVOLVE trial. *J. Am. Soc. Nephrol.* **26**, 1466–1475 (2015).

52. Yang, W. C. *et al.* An open-label, crossover study of a new phosphate-binding agent in haemodialysis patients: Ferric citrate. *Nephrol. Dial. Transplant.* **17**, 265–270 (2002).

53. Cohen-Solal, M., Funck-Brentano, T. & Torres, P. U. Bone fragility in patients with chronic kidney disease. *Endocr. Connect.* **9**, R93–R101 (2020).

54. Nishikawa, A., Ishida, T., Taketsuna, M., Yoshiki, F. & Enomoto, H. Safety and effectiveness of daily teriparatide in a prospective observational study in patients with osteoporosis at high risk of fracture in Japan: final report. *Clin. Interv. Aging* **11**, 913 (2016).

55. Broadwell, A. *et al.* Denosumab Safety and Efficacy Among Participants in the FREEDOM Extension Study With Mild to Moderate Chronic Kidney Disease. *J. Clin. Endocrinol. Metab.* **106**, 397–409 (2021).

56. Pimentel, A., Ureña-Torres, P., Zillikens, M. C., Bover, J. & Cohen-Solal, M. Fractures in patients with CKD—diagnosis, treatment, and prevention: a review by members of the European Calcified Tissue Society and the European Renal Association of Nephrology Dialysis and Transplantation. *Kidney International* vol. 92 1343–1355 (2017).

57. Robinson, D. E. *et al.* Safety of Oral Bisphosphonates in Moderate-to-Severe Chronic Kidney Disease: A Binational Cohort Analysis. *J. Bone Miner. Res.* **36**, 820–832 (2021).

58. Miller, P. D. *et al.* Efficacy and Safety of Romosozumab Among Postmenopausal Women With Osteoporosis and Mild-to-Moderate Chronic Kidney Disease. *J. Bone Miner. Res.* (2022) doi:10.1002/JBMR.4563.

59. Lewiecki, E. M. Role of sclerostin in bone and cartilage and its potential as a therapeutic target in bone diseases. *Therapeutic Advances in Musculoskeletal Disease* vol. 6 48–57 (2014).

60. McClung, M. *et al.* Romosozumab in postmenopausal women with low bone mineral

density. *N. Engl. J. Med.* **370**, 248–259 (2014).

61. Padhi, D., Jang, G., Stouch, B., Fang, L. & Posvar, E. Single-dose, placebo-controlled, randomized study of AMG 785, a sclerostin monoclonal antibody. *J. Bone Miner. Res.* **26**, 19–26 (2011).

62. Michael Lewiecki, E. *et al.* A Phase III Randomized Placebo-Controlled Trial to Evaluate Efficacy and Safety of Romosozumab in Men With Osteoporosis. *J. Clin. Endocrinol. Metab.* **103**, 3183–3193 (2018).

63. Schuit, S. C. E. *et al.* Fracture incidence and association with bone mineral density in elderly men and women: The Rotterdam Study. *Bone* **34**, 195–202 (2004).

64. Black, D. M. *et al.* Axial and appendicular bone density predict fractures in older women. *J. Bone Miner. Res.* **7**, 633–638 (2009).

65. Metzger, C. E. *et al.* Reversing cortical porosity: Cortical pore infilling in preclinical models of chronic kidney disease. *Bone* **143**, (2021).

66. Chen, G. *et al.* α-Klotho is a non-enzymatic molecular scaffold for FGF23 hormone signalling. *Nature* **553**, 461–466 (2018).

67. Shimada, T. *et al.* Targeted ablation of Fgf23 demonstrates an essential physiological role of FGF23 in phosphate and vitamin D metabolism. *J. Clin. Invest.* **113**, 561–568 (2004).

68. Shimada, T. *et al.* FGF-23 Is a Potent Regulator of Vitamin D Metabolism and Phosphate Homeostasis. *J. Bone Miner. Res.* **19**, 429–435 (2003).

69. Shimada, T. *et al.* Vitamin D receptor-independent FGF23 actions in regulating phosphate and vitamin D metabolism. *Am. J. Physiol. - Ren. Physiol.* **289**, (2005).

70. Choi, N. W. Kidney and phosphate metabolism. *Electrolyte Blood Press.* **6**, 77–85 (2008).

71. Beck, L. *et al.* Targeted inactivation of Npt2 in mice leads to severe renal phosphate wasting, hypercalciuria, and skeletal abnormalities. *Proc. Natl. Acad. Sci. U. S. A.* **95**, 5372–5377 (1998).

72. Erben, R. G. & Andrukhova, O. FGF23-Klotho signaling axis in the kidney. *Bone* **100**, 62–68 (2017).

73. Lanske, B. & Razzaque, M. S. Premature aging in klotho mutant mice: Cause or consequence? *Ageing Res. Rev.* **6**, 73–79 (2007).

74. Mirza, M. A. *et al.* Serum fibroblast growth factor-23 (FGF-23) and fracture risk in elderly men. *J. Bone Miner. Res.* **26**, 857–864 (2011).

75. Yamazaki, Y. *et al.* Establishment of sandwich ELISA for soluble alpha-Klotho measurement: Age-dependent change of soluble alpha-Klotho levels in healthy subjects. *Biochem. Biophys. Res. Commun.* **398**, 513–518 (2010).

76. Pedersen, L., Pedersen, S. M., Brasen, C. L. & Rasmussen, L. M. Soluble serum Klotho levels in healthy subjects. Comparison of two different immunoassays. *Clin. Biochem.* **46**, 1079–1083 (2013).

77. Zuo, Z. *et al.* Aging-related kidney damage is associated with a decrease in klotho expressionand an increase in superoxide production. *Age (Omaha).* **33**, 261–274 (2011).

78. Cirillo, M., Ciacci, C. & De Santo, N. G. Age, Renal Tubular Phosphate Reabsorption, and Serum Phosphate Levels in Adults. *N. Engl. J. Med.* **359**, 864–866 (2008).

79. Webster, R. *et al.* Klotho/fibroblast growth factor 23- and PTH-independent estrogen receptor-α-mediated direct downregulation of NaPi-IIa by estrogen in the mouse kidney. *Am. J. Physiol. - Ren. Physiol.* **311**, F249–F259 (2016).

80. Carrillo-López, N. *et al.* Indirect regulation of PTH by estrogens may require FGF23. *J. Am.*

Soc. Nephrol. **20**, 2009–2017 (2009).

81. Koh, N. *et al.* Severely reduced production of klotho in human chronic renal failure kidney. *Biochem. Biophys. Res. Commun.* **280**, 1015–1020 (2001).

82. Ix, J. H., Chonchol, M., Laughlin, G. A., Shlipak, M. G. & Whooley, M. A. Relation of sex and estrogen therapy to serum fibroblast growth factor 23, serum phosphorus, and urine phosphorus: The heart and soul study. *Am. J. Kidney Dis.* **58**, 737–745 (2011).

83. Dalal, M. *et al.* Relationship of serum fibroblast growth factor 23 with cardiovascular disease in older community-dwelling women. *Eur. J. Endocrinol.* **165**, 797–803 (2011).

84. Jia, T. *et al.* A novel model of adenine-induced tubulointerstitial nephropathy in mice. *BMC Nephrol.* **14**, 116 (2013).

85. Livak, K. J. & Schmittgen, T. D. Analysis of relative gene expression data using real-time quantitative PCR and the 2-ΔΔCT method. *Methods* **25**, 402–408 (2001).

86. Chen, N. X. *et al.* Effect of Advanced Glycation End-Products (AGE) Lowering Drug ALT-711 on Biochemical, Vascular, and Bone Parameters in a Rat Model of CKD-MBD. *J. Bone Miner. Res.* (2019) doi:10.1002/jbmr.3925.

87. Bouxsein, M. L. *et al.* Guidelines for assessment of bone microstructure in rodents using micro-computed tomography. *J. Bone Miner. Res.* **25**, 1468–1486 (2010).

88. Wallace, J. M., Golcuk, K., Morris, M. D. & Kohn, D. H. Inbred Strain-Specific Response to Biglycan Deficiency in the Cortical Bone of C57BL6/129 and C3H/He Mice. *J. Bone Miner. Res.* **24**, 1002–1012 (2009).

89. Allen, M. R. *et al.* Skeletal effects of zoledronic acid in an animal model of chronic kidney disease. *Osteoporos. Int.* **24**, 1471–1481 (2013).

90. Turner, C. H. & Burr, D. B. Basic biomechanical measurements of bone: A tutorial. *Bone* **14**, 595–608 (1993).

91. Prideaux, M. *et al.* Generation of two Multipotent Mesenchymal Progenitor Cell Lines Capable of Osteogenic, 1 Mature Osteocyte, Adipogenic, and Chondrogenic Differentiation 2 3 1. *bioRxiv* 2020.11.19.385138 (2020) doi:10.1101/2020.11.19.385138.

92. Chen, B., Liu, Z., Zhang, J., Wang, H. & Yu, B. RNA sequencing identifies gene expression profile changes associated with β-estradiol treatment in U2OS osteosarcoma cells. *Onco. Targets. Ther.* **10**, 3421–3427 (2017).

93. GREENBLATT, R. B., OETTINGER, M. & BOHLER, C. S. -. Estrogen-Androgen Levels in Aging Men and Women: Therapeutic Considerations. *J. Am. Geriatr. Soc.* **24**, 173–178 (1976).

94. Thompson, W. R. *et al.* Osteocyte specific responses to soluble and mechanical stimuli in a stem cell derived culture model. *Sci. Rep.* **5**, (2015).

95. Kurosu, H. *et al.* Suppression of Aging in Mice by the Hormone Klotho. *Science (80-.).* **309**, 1829–1833 (2005).

96. Kim, H. R. *et al.* Circulating α-klotho levels in CKD and relationship to progression. *Am. J. Kidney Dis.* **61**, 899–909 (2013).

97. Wan, M. *et al.* Fibroblast growth factor 23 and soluble klotho in children with chronic kidney disease. *Nephrol. Dial. Transplant.* **28**, 153–161 (2013).

98. Rotondi, S. *et al.* Soluble α -Klotho serum levels in chronic kidney disease. *Int. J. Endocrinol.* **2015**, (2015).

99. Yang, W. *et al.* Association of kidney disease outcomes with risk Factors for CKD: Findings from the Chronic Renal Insufficiency Cohort (CRIC) study. *Am. J. Kidney Dis.* **63**, 236–

243 (2014).

100.   Lane, N. E. *et al.* Association of serum fibroblast growth factor 23 (FGF23) and incident fractures in older men: The Osteoporotic Fractures in Men (MrOS) study. *J. Bone Miner. Res.* **28**, 2325–2332 (2013).

101.   Chudek, J. *et al.* Fibroblast growth factor 23 (FGF23) and early chronic kidney disease in the elderly. *Nephrol. Dial. Transplant.* **29**, 1757–1763 (2014).

102.   Finch, C. E., Mobbs, C. V., Felicio, L. S. & Nelson, J. F. Ovarian and steroidal influences on neuroendocrine aging processes in female rodents. *Endocr. Rev.* **5**, 467–497 (1984).

103.   Diaz Brinton, R. Minireview: translational animal models of human menopause: challenges and emerging opportunities. *Endocrinology* **153**, 3571–3578 (2012).

104.   Bruce, H. M. & Callow, R. K. Cereals and rickets. The rôle of inositolhexaphosphoric acid. *Biochem. J.* **28**, 517–528 (1934).

105.   Grases, F. & Costa-Bauza, A. Key aspects of myo-inositol hexaphosphate (phytate) and pathological calcifications. *Molecules* vol. 24 (2019).

106.   Buades Fuster, J. M., Sanchís Cortés, P., Perelló Bestard, J. & Grases Freixedas, F. Fosfatos de origen vegetal, fitato y calcificaciones patológicas en la enfermedad renal crónica. *Nefrología* **37**, 20–28 (2017).

107.   Kamao, M. *et al.* Absorption of calcium, magnesium, phosphorus, iron and zinc in growing male rats fed diets containing either phytate-free soybean protein or soybean protein isolate or casein. *J. Nutr. Sci. Vitaminol. (Tokyo).* **46**, 34–41 (2000).

108.   Brink, E. J., Dekker, P. R., Van Beresteijn, E. C. H. & Beynen, A. C. Inhibitory effect of dietary soybean protein vs. casein on magnesium absorption in rats. *J. Nutr.* **121**, 1374–1381 (1991).

109. Bala, Y. *et al.* Cortical porosity identifies women with osteopenia at increased risk for forearm fractures. *J. Bone Miner. Res.* **29**, 1356–1362 (2014).

110. Metzger, C. E., Swallow, E. A., Stacy, A. J. & Allen, M. R. Adenine-induced chronic kidney disease induces a similar skeletal phenotype in male and female C57BL/6 mice with more severe deficits in cortical bone properties of male mice. *PLoS One* **16**, (2021).

111. Tippen, S. P. *et al.* Age and sex effects on FGF23-mediated response to mild phosphate challenge. *Bone* **146**, (2021).

112. Kohler, R. *et al.* The Effect of Single Versus Group μCT on the Detection of Trabecular and Cortical Disease Phenotypes in Mouse Bones. *JBMR Plus* e10473 (2021) doi:10.1002/jbm4.10473.

113. Diwan, V., Brown, L. & Gobe, G. C. Adenine-induced chronic kidney disease in rats. *Nephrology* vol. 23 5–11 (2018).

114. Atkinson, P. J. Changes in resorption spaces in femoral cortical bone with age. *J. Pathol. Bacteriol.* **89**, 173–178 (1965).

115. Jowsey, J. Age changes in human bone. *Clin. Orthop. Relat. Res.* **17**, 210–7 (1960).

116. Burghardt, A. J., Kazakia, G. J., Ramachandran, S., Link, T. M. & Majumdar, S. Age- and gender-related differences in the geometric properties and biomechanical significance of intracortical porosity in the distal radius and tibia. *J. Bone Miner. Res.* **25**, 983–993 (2010).

117. Andreasen, C. M. *et al.* Understanding age-induced cortical porosity in women: Is a negative BMU balance in quiescent osteons a major contributor? *Bone* **117**, 70–82 (2018).

118. Jilka, R. L. *et al.* Decreased oxidative stress and greater bone anabolism in the aged, when compared to the young, murine skeleton with parathyroid hormone administration. *Aging Cell* **9**, 851–867 (2010).

119. Newman, C. L. *et al.* Cortical bone mechanical properties are altered in an animal model of progressive chronic kidney disease. *PLoS One* **9**, (2014).

120. Niculescu, D. A. *et al.* Combined Effects of Vitamin D Status, Renal Function and Age on Serum Parathyroid Hormone Levels. *Front. Endocrinol. (Lausanne).* **12**, 1 (2021).

121. McNerny, E. M. B. *et al.* Time course of rapid bone loss and cortical porosity formation observed by longitudinal μCT in a rat model of CKD. *Bone* **125**, 16–24 (2019).

122. Costa, L. R., Carvalho, A. B., Bittencourt, A. L., Rochitte, C. E. & Canziani, M. E. F. Cortical unlike trabecular bone loss is not associated with vascular calcification progression in CKD patients. *BMC Nephrol.* **21**, 1–7 (2020).

123. Heveran, C. M. *et al.* Chronic kidney disease and aging differentially diminish bone material and microarchitecture in C57Bl/6 mice. *Bone* **127**, 91–103 (2019).

124. Zha, Y. & Qian, Q. Protein nutrition and malnutrition in CKD and ESRD. *Nutrients* **9**, (2017).

125. Laboux, T. & Azar, R. Dietary control of metabolic acidosis in chronic kidney disease. *Nephrol. Ther.* **15**, 491–497 (2019).

126. Kanis, J. A., Melton, L. J., Christiansen, C., Johnston, C. C. & Khaltaev, N. The diagnosis of osteoporosis. *J. Bone Miner. Res.* **9**, 1137–1141 (1994).

127. Chen, H., Zhou, X., Fujita, H., Onozuka, M. & Kubo, K. Y. Age-related changes in trabecular and cortical bone microstructure. *Int. J. Endocrinol.* **2013**, (2013).

128. Stapleton, M. *et al.* Development of bone targeting drugs. *International Journal of Molecular Sciences* vol. 18 (2017).

129. Bandeira, L., Lewiecki, E. M. & Bilezikian, J. P. Romosozumab for the treatment of

osteoporosis. *Expert Opin. Biol. Ther.* **17**, 255–263 (2017).

130. Ominsky, M. S., Niu, Q. T., Li, C., Li, X. & Ke, H. Z. Tissue-level mechanisms responsible for the increase in bone formation and bone volume by sclerostin antibody. *J. Bone Miner. Res.* **29**, 1424–1430 (2014).

131. Tippen, S. P. *et al.* The combination of aging and chronic kidney disease leads to an exacerbated cortical porosity phenotype. *Bone* **154**, (2022).

132. Dempster, D. W. *et al.* Standardized nomenclature, symbols, and units for bone histomorphometry: A 2012 update of the report of the ASBMR Histomorphometry Nomenclature Committee. *J. Bone Miner. Res.* **28**, 2–17 (2013).

133. Cosman, F. *et al.* Romosozumab Treatment in Postmenopausal Women with Osteoporosis. *N. Engl. J. Med.* **375**, 1532–1543 (2016).

134. Li, X. *et al.* Sclerostin antibody treatment increases bone formation, bone mass, and bone strength in a rat model of postmenopausal osteoporosis. *J. Bone Miner. Res.* **24**, 578–588 (2009).

135. Ominsky, M. S. *et al.* Two doses of sclerostin antibody in cynomolgus monkeys increases bone formation, bone mineral density, and bone strength. *J. Bone Miner. Res.* **25**, 948–959 (2010).

136. Li, X. *et al.* Increased bone formation and bone mass induced by sclerostin antibody is not affected by pretreatment or cotreatment with alendronate in osteopenic, ovariectomized rats. *Endocrinology* **152**, 3312–3322 (2011).

137. Ominsky, M. S. *et al.* Differential temporal effects of sclerostin antibody and parathyroid hormone on cancellous and cortical bone and quantitative differences in effects on the osteoblast lineage in young intact rats. *Bone* **81**, 380–391 (2015).

138. CDC. Chronic Kidney Disease in the United States, 2021. https://www.cdc.gov/kidneydisease/publications-resources/ckd-national-facts.html (2021).

139. Khosla, S. Pathogenesis of age-related bone loss in humans. *J. Gerontol. A. Biol. Sci. Med. Sci.* **68**, 1226–35 (2013).

140. Chan, G. K. & Duque, G. Age-related bone loss: Old bone, new facts. *Gerontology* vol. 48 62–71 (2002).

141. Swallow, E. A. *et al.* Cortical porosity development and progression is mitigated after etelcalcetide treatment in an animal model of chronic kidney disease. *Bone* **157**, (2022).

142. Damrath, J. G. *et al.* Non-Additive Effects of Combined NOX1/4 Inhibition and Calcimimetic Treatment on a Rat Model of Chronic Kidney Disease-Mineral and Bone Disorder (CKD-MBD). *JBMR plus* **6**, (2022).

143. Damrath, J. G., Metzger, C. E., Allen, M. R. & Wallace, J. M. A novel murine model of combined insulin-dependent diabetes and chronic kidney disease has greater skeletal detriments than either disease individually. *Bone* **165**, (2022).

144. Hsu, C. P., Maddox, J., Block, G., Bartley, Y. & Yu, Z. Influence of Renal Function on Pharmacokinetics, Pharmacodynamics, and Safety of a Single Dose of Romosozumab. *J. Clin. Pharmacol.* **62**, 1132–1141 (2022).

145. Wein, M. N. & Kronenberg, H. M. Regulation of bone remodeling by parathyroid hormone. *Cold Spring Harb. Perspect. Med.* **8**, (2018).

146. Andress, D. L. *et al.* Management of secondary hyperparathyroidism in stages 3 and 4 chronic kidney disease. *Endocr. Pract.* **14**, 18–27 (2008).

147. Block, G. A. *et al.* Cinacalcet for secondary hyperparathyroidism in patients receiving hemodialysis. *N. Engl. J. Med.* **350**, 1516–1525 (2004).

148. Charytan, C. *et al.* Cinacalcet hydrochloride is an effective treatment for secondary hyperparathyroidism in patients with CKD not receiving dialysis. *Am. J. Kidney Dis.* **46**, 58–67 (2005).

149. Moe, S. M. *et al.* Anti-Sclerostin Antibody Treatment in a Rat Model of Progressive Renal Osteodystrophy. *J. Bone Miner. Res.* **30**, 499–509 (2015).

150. Burr, D. B. & Allen, M. R. Bisphosphonates and PTH for Preventing Fractures. *Stud. Mechanobiol. Tissue Eng. Biomater.* **5**, 151–176 (2013).

151. Eastell, R., Walsh, J. S., Watts, N. B. & Siris, E. Bisphosphonates for postmenopausal osteoporosis. *Bone* **49**, 82–88 (2011).

152. Moe, S. M. *et al.* Long-term treatment of secondary hyperparathyroidism with the calcimimetic cinacalcet HCl. *Nephrol. Dial. Transplant* **20**, 2186–2193 (2005).

153. Salem, M. M. Hyperparathyroidism in the hemodialysis population: a survey of 612 patients. *Am. J. Kidney Dis.* **29**, 862–865 (1997).

154. Owda, A., Elhwairis, H., Narra, S., Towery, H. & Osama, S. Secondary hyperparathyroidism in chronic hemodialysis patients: prevalence and race. *Ren. Fail.* **25**, 595–602 (2003).

155. Li, X. *et al.* Etelcalcetide (AMG 416), a peptide agonist of the calcium-sensing receptor, preserved cortical bone structure and bone strength in subtotal nephrectomized rats with established secondary hyperparathyroidism. *Bone* **105**, 163–172 (2017).

156. Lindsay, R. *et al.* A novel tetracycline labeling schedule for longitudinal evaluation of the short-term effects of anabolic therapy with a single iliac crest bone biopsy: early actions of teriparatide. *J. Bone Miner. Res.* **21**, 366–73 (2006).

157. Lindsay, R., Krege, J. H., Marin, F., Jin, L. & Stepan, J. J. Teriparatide for osteoporosis:

Importance of the full course. *Osteoporos. Int.* **27**, 2395–2410 (2016).

158. Langdahl, B. L. *et al.* Romosozumab (sclerostin monoclonal antibody) versus teriparatide in postmenopausal women with osteoporosis transitioning from oral bisphosphonate therapy: a randomised, open-label, phase 3 trial. *Lancet* **390**, 1585–1594 (2017).

159. Takakura, A. *et al.* Administration frequency as well as dosage of PTH are associated with development of cortical porosity in ovariectomized rats. *Bone Res.* **5**, 17002 (2017).

160. Cosman, F. *et al.* FRAME Study: The Foundation Effect of Building Bone With 1 Year of Romosozumab Leads to Continued Lower Fracture Risk After Transition to Denosumab. *J. Bone Miner. Res.* **33**, 1219–1226 (2018).

161. Inose, H. *et al.* The Real-World Effect of 12 Months of Romosozumab Treatment on Patients With Osteoporosis With a High Risk of Fracture and Factors Predicting the Rate of Bone Mass Increase: A Multicenter Retrospective Study. *JBMR Plus* e10637 (2022) doi:10.1002/JBM4.10637.

162. McClung, M. R. *et al.* Effects of 24 Months of Treatment With Romosozumab Followed by 12 Months of Denosumab or Placebo in Postmenopausal Women With Low Bone Mineral Density: A Randomized, Double-Blind, Phase 2, Parallel Group Study. *J. Bone Miner. Res.* **33**, 1397–1406 (2018).

163. Saag, K. G. *et al.* Romosozumab or Alendronate for Fracture Prevention in Women with Osteoporosis. *N. Engl. J. Med.* **377**, 1417–1427 (2017).

164. Keaveny, T. M. *et al.* Greater Gains in Spine and Hip Strength for Romosozumab Compared With Teriparatide in Postmenopausal Women With Low Bone Mass. *J. Bone Miner. Res.* **32**, 1956–1962 (2017).

165. Jilka, R. L. *et al.* Increased bone formation by prevention of osteoblast apoptosis with

parathyroid hormone. *J. Clin. Invest.* **104**, 439–446 (1999).

166. Weinstein, R. S., Jilka, R. L., Almeida, M., Roberson, P. K. & Manolagas, S. C. Intermittent parathyroid hormone administration counteracts the adverse effects of glucocorticoids on osteoblast and osteocyte viability, bone formation, and strength in mice. *Endocrinology* **151**, 2641–2648 (2010).

167. Jilka, R. L. *et al.* Dysapoptosis of osteoblasts and osteocytes increases cancellous bone formation but exaggerates cortical porosity with age. *J. Bone Miner. Res.* **29**, 103–117 (2014).

Samantha P. Tippen

EDUCATION

May 2023	**PhD**, Anatomy and Cell Biology	
	Indiana University, earned at IUPUI	Indianapolis, IN, USA
May 2014	**M.S.**, Forensic Science	
	Sam Houston State University	Huntsville, TX, USA
May 2012	**B.S.**, Chemistry; **B.A.**, Anthropology	
	University of North Texas	Denton, TX, USA

RESEARCH EXPERIENCE

2018 – 2023   Graduate Research Assistant

Institution: Indiana University School of Medicine

Mentor: Matthew R. Allen, PhD

Dissertation Title: Interactions between aging and chronic kidney disease on the skeleton

2012-2014   Graduate Research Assistant

Institution: Sam Houston State University

Mentor: Sheree Hughes-Stamm, PhD

Thesis Title: Tissue damage, STR profiling success, and DNA extraction efficiencies for incinerated human teeth

TEACHING EXPERIENCE

Professional Courses

Course: GRDM-G717, Biomedical Science III: Cellular Basis of Systems Biology

Role: Lecturer / Teaching Assistant

Terms: 2019 – 2022

Course: ANAT-D528, Anatomy for Health Care Professionals

Role: Teaching Assistant

Terms: 2021-2022

Course: MEDX-620, Human Structure

Role: Prosector

Term: 2021

Course: ANAT-D853, Human Developmental Anatomy

Role: Teaching Assistant

Term: 2022

Course: ANAT-D520, Basic Histology

Role: Associate Instructor

Terms: 2021-2022

Course: GRDM-G819, Basic Bone Biology

Role: Co-Instructor

Term: 2022

Course: MSHS-B842, Musculoskeletal Disease & Injury

Role: Lecturer & TBL Facilitator

Term: 2022

Undergraduate Courses

Course: BIOL-N461, Cadaveric Human Anatomy

Role: Laboratory Instructor

Terms: 2022-2023

GRANTS & FELLOWSHIPS

Granting Agency: National Institutes of Health (NIDDK); F31 Predoctoral Fellowship

Title: Chronic kidney disease effects on cortical bone porosity and mechanics with age (F31-DK130603)

Role: Principal Investigator

Dates: 2021-2023

Granting Agency: National Institutes of Health (NHLBI); T32 Training Grant

Title: Comprehensive Training Program in Musculoskeletal Research, Department of Anatomy, Cell Biology, & Physiology, Indiana University School of Medicine

Role: Predoctoral Trainee (PI: A. Robling)

Dates: 2019-2021

INSTITUTIONAL SERVICE & OUTREACH

University Service

Data & Climate Task Force	Member	2020-2021
Graduate Curriculum Committee	Student Representative	2020-2022
BGSAA^	Representative, ACBP^	2020-2022

^Biomedical Graduate Student Advocacy Association is formed by student representatives from each department. I represented the Anatomy, Cell Biology, & Physiology department.

Outreach

Northside Middle School	Gross Anatomy Lab Tour	2023
Mississinewa High School	Gross Anatomy Lab Tour	2022
North Decatur High School	Gross Anatomy Lab Tour	2022
Lafayette Jefferson High School	Gross Anatomy Lab Tour	2022
Westfield High School	Advanced Gross Anatomy Lab Tour	2022
Livonia High School	Advanced Gross Anatomy Lab Tour	2022
Central 9 Career Center	Gross Anatomy Lab Tour	2022
University College	Field Trip Friday: Behind the Scenes	2021
Central 9 Career Center	Gross Anatomy Lab Tour	2021

PUBLICATIONS

* 2022 Metzger CE, Newman CL, **Tippen SP**, Golemme NT, Chen NX, Moe SM, Allen MR. (2022) "Cortical porosity occurs at varying degrees throughout the skeleton in rats with chronic kidney disease." Bone Reports 101612. https://doi.org/10.1016/j.bonr.2022.101612

* 2022 Swallow EA, Metzger CE, Chen NX, Wallace JM, **Tippen SP**, Kohler R, Moe SM, Allen MR. (2022) "Cortical porosity is elevated after a single dose of zoledronate in two rodent models of chronic kidney disease." Bone Reports 101174. https://doi.org/10.1016/j.bonr.2022.101174

* 2021 **Tippen SP**, Metzger CE, Swallow EA, Sacks SA, Wallace JM, Allen MR. (2021) "The combination of aging and chronic kidney disease leads to an exacerbated cortical porosity phenotype." Bone 154:116228. https://doi.org/10.1016/j.bone.2021.116228

*   2021   **Tippen SP**, Noonan ML, Ni P, Metzger CE, Swallow EA, Sacks SA, Chen NX, Thompson WR, Prideaux M, Atkins GA, Moe SM, Allen MR, White KE. (2021) "Age and sex effects on FGF23-mediated response to mild phosphate challenge." Bone 146:115885. https://doi.org/10.1016/j.bone.2021.115885

*   2021   Metzger C, Swallow EA, Stacey AJ, **Tippen SP**, Hammond M, Chen N, Moe SM, Allen ME. (2021) "Reversing cortical porosity: Cortical pore infilling in preclinical models of chronic kidney disease." Bone 143:115632. https://doi.org/10.1016/j.bone.2020.115632

         2021   Kim ST, Sheshadri A, Shannon V, Kontoyiannis DP, Kantarjian H, Garcia-Manero G, Ravandi F, Im JS, Boddu P, Bashoura L, Balachandran DD, Evans SE, Faiz S, Ruiz Vazquez W, Divenko M, Mathur R, **Tippen SP**, Gumbs C, Neelapu SS, Naing A, Wang L, Diab A, Futreal A, Nurieva R, Daver N. (2021) "Distinct immunophenotypes of T cells in bronchoalveolar lavage fluid from leukemia patients with immune checkpoint inhibitors-related pulmonary complications." Front Immunol 11:590494. https://doi.org/10.3389/fimmu.2020.590494

*   2020   Noonan ML, Clinkenbeard EL, Ni P, Swallow EA, Agoro R, **Tippen SP**, Allen MR, White KE. (2020) "Erythropoietin and a hypoxia-inducible factor prolyl hydroxylase inhibitor (HIF-PHDi) lowers FGF23 in a model of chronic kidney disease (CKD)." Physiol Rep 8(11):e14434. https://doi.org/10.14814/phy2.14434

         2020   Reuben A, Zhang J, Chiou SH, Gittelman RM, Li J, Lee WC, Fujimoto J, Behrens C, Liu X, Wang F, Quek K, Wang C, Kheradmand F, Chen R, Chow CW, Lin H, Bernatchez C, Jalali A, Hu X, Wu CJ, Eterovic AK, Parra ER, Yusko E, Emerson R, Benzeno S, Vignali M, Wu X, Ye Y, Little LD, Gumbs C, Mao X, Song X, **Tippen S**, Thornton RL, Cascone

T, Snyder A, Wargo JA, Herbst R, Swisher S, Kadara H, Moran C, Kalhor N, Zhang J, Scheet P, Vaporciyan AA, Sepesi B, Gibbons DL, Robins H, Hwu P, Heymach JV, Sharma P, Allison JP, Baladandayuthapani V, Lee JJ, Davis MM, Wistuba II, Futreal PA, Zhang J. (2020) "Comprehensive T cell repertoire characterization of non-small cell lung cancer." Nat Commun (2020) 11(1):603. https://doi.org/10.1038/s41467-019-14273-0

2020   Mitra A, Andrews MC, Roh W, Petaccia De Macedo M, Hudgens CW, Carapeto F, Reuben A, Wang F, Mao X, Song X, Wani K, **Tippen S**, Ng K, Schalck A, Sakellariou-Thompson DA, Chen E, Reddy SM, Spencer C, Weisnoski D, Little LD, Gumbs C, Cooper ZA, Burton EM, Hwu P, Davies MA, Zhang Z, Bernatchez C, Navin N, Sharma P, Allison JP, Tetzlaff M, Wargo JA, Hwu W, Lazar AJ, Futreal PA. (2020) "Spatially-resolved analyses link genomic and immune diversity and reveal unfavorable neutrophil activation in melanoma." Nat Commun 11:1839. https://doi.org/10.1038/s41467-020-15538-9

2019   Hu X, Fujimoto J, Ying L, Fukuoka J, Ashizawa K, Sun W, Reuben A, Chow CW, McGranahan N, Chen R, Hu J, Godoy MC, Tabata K, Kuroda K, Shi L, Li J, Behrens C, Parra ER, Little LD, Gumbs C, Mao X, Song X, **Tippen S**, Thornton RL, Kadara H, Scheet P, Roarty E, Ostrin EJ, Wang X, Carter BW, Antonoff MB, Zhang J, Vaporciyan AA, Pass H, Swisher SG, Heymach JV, Lee JJ, Wistuba II, Hong WK, Futreal PA, Su D, Zhang J. (2019) "Multi-region exome sequencing reveals genomic evolution from preneoplasia to lung adenocarcinoma." Nat Commun 10(1):2978. https://doi.org/10.1038/s41467-019-10877-8

2018   Hillman RT, Celestino J, Terranova C, Beird HC, Gumbs C, Little L, Nguyen T, Thornton R, **Tippen S**, Zhang J, Lu KH, Gershenson DM, Rai K, Broaddus RR, Futreal PA. (2018) "KMT2D/MLL2 inactivation is associated with recurrence in adult-type granulosa cell tumors of the ovary." Nat Commun 9:2496. https://doi.org/10.1038/s41467-018-04950-x

2018   Takahashi K, Wang F, Morita K, Yan Y, Hu P, Zhao P, Zhar AA, Wu C, Gumbs C, Little L, **Tippen S**, Thornton R, Coyle M, Mendoza M, Thompson E, Zhang J, DiNardo C, Jain N, Ravandi F, Cortes J, Garcia-Manero G, Kornblau S, Andreeff M, Jabbour E, Bueso-Ramos C, Takaori-Kondo A, Patel K, Konopleva M, Kantarjian H, Futreal A. (2018) "Integrative genomic analysis of adult mixed phenotype acute leukemia (MPAL) delineates lineage associated molecular subtypes." Nat Commun 9:2670. https://doi.org/10.1038/s41467-018-04924-z

2018   Morita K, Wang F, Yan Y, Burks J, Gumbs C, Little L, **Tippen S**, Thornton R, Coyle M, Zhang J, Song X, DiNardo C, Jabbour E, Andreeff M, Cortes J, Konopleva M, Patel K, Garcia-Manero G, Kantarjian H, Bueso-Ramos C, Futreal PA, Takahashi K. (2018) "The landscape of genotype-phenotype correlation in AML." Cl Lymph Myelom Leuk 18:S209-10. https://doi.org/10.1016/j.clml.2018.07.066

2018   Morita K, Kantarjian H, Wang F, Yan Y, Bueso-Ramos C, Sasaki K, Issa GC, Wang S, Jorgensen J, Song X, Zhang J, **Tippen S**, Thornton R, Coyle M, Little L, Gumbs C, Pemmaraju N, Daver N, DiNardo C, Konopleva M, Andreef M, Ravandi F, Cortes J, Kadia T, Jabbour E, Garcia-Manero G, Patel K, Futreal A, Takahashi K. (2018) "Clearance of somatic mutations at remission and the risk of relapse in acute myeloid leukemia." J Clin Oncol 36(18):1788-97. https://doi.org/10.1200/jco.2017.77.6757

2018   Takahashi K, Hu B, Wang F, Yan Y, Kim E, Vitale C, Patel KP, Strati P, Gumbs C, Little L, **Tippen S**, Song X, Zhang J, Jain N, Thompson P, Garcia-Manero G, Kantarjian H, Estrov Z, Do K-A, Keating M, Burger JA, Ferrajoli A, Futreal PA, Wierda WG. (2018) "Clinical implications of cancer gene mutations in patients with chronic lymphocytic leukemia treated with lenalidomide." Blood 131(16):1820-1832. https://doi.org/10.1182/blood-2017-11-817296

2017   Morita K, Wang F, Patel K, Bueso-Ramos C, Zhar AA, Gumbs C, Little L, **Tippen S**, Thornton R, Coyle M, Zhang J, Song X, Mendoza M, Wu C-J, Kornblau S, DiNardo C, Ravandi F, Garcia-Manero G, Jabbour E, Andreeff M, Kantarjian H, Cortes J, Konopleva M, Futreal A, Takahashi K. (2017) "Genomic landscape of mixed phenotype acute leukemia (MPAL)." Cl Lymph Myelom Leuk 17:S273-274. https://doi.org/10.1016/j.clml.2017.07.050

2017   Takahashi K, Wang F, Kantarjian H, Song X, Patel K, Neelapu S, Gumbs C, Little L, **Tippen S**, Thornton R, DiNardo CD, Ravandi F, Bueso-Ramos C, Zhang J, Wu X, Garcia-Manero G, Futreal PA. (2017) "Copy number alterations detected as clonal hematopoiesis of indeterminate potential." Blood Advances 1:1031-1036. https://doi.org/10.1182/bloodadvances.2017007922

2017   Takahashi K, Wang F, Patel K, Bueso-Ramos CE, Issa GC, Song X, Zhang J, **Tippen S**, Little L, Gumbs C, Ravandi F, Kadia TM, Daver NG, Dinardo CD, Konopleva M, Andreeff M, Cortes JE, Jabbour E, Futreal A, Kantarjian HM. (2017) "Distinct patterns of somatic mutation clearance and association with clinical outcome in patients with AML." J Clin Oncol 35 (15-suppl):7005-7005. https://doi.org/10.1200/jco.2017.35.15_suppl.7005

INSTITUTIONAL SERVICE & OUTREACH

National

"PTH suppression improves cortical bone parameters in aging mice with CKD"

2021

Poster, American Society of Nephrology (presented virtually due to COVID)

"Chronic kidney disease and aging interact to promote cortical porosity"

2021

Poster, American Society for Bone & Mineral Research (presented virtually due to COVID)

Regional

"Presentation of a Successful F31 Grant"

2022

Informal discussion for the School of Health & Human Sciences at Indiana University Purdue University Indianapolis (IUPUI)

"Making the Most of Guest Lecturing Experiences"

2021

Webinar panel discussion for Indiana University Purdue University Indianapolis (IUPUI) and Indiana University School of Medicine

Local

"A phosphate and calcium-enriched diet promotes progression of 5/6-nephrectomy-induced chronic kidney disease in C57Bl/6 mice"

2021

Presenter, Indiana Center for Musculoskeletal Health Journal Club

"Chronic kidney disease and aging differentially diminish bone material and microarchitecture in C57Bl/6 mice"

2020

Presenter, Indiana Center for Musculoskeletal Health Journal Club